1997

Hydration metamorphism and diabase-granophyre relations in a thick basaltic sill emplaced into wet sediments western Montana

Michael A. Poage
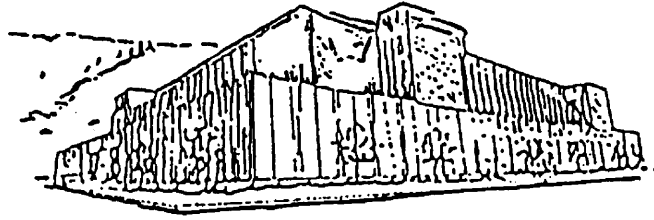*The University of Montana*

Maureen and Mike
MANSFIELD LIBRARY

The University of **MONTANA**

Permission is granted by the author to reproduce this material in its entirety, provided that this material is used for scholarly purposes and is properly cited in published works and reports.

*** Please check "Yes" or "No" and provide signature ***

Yes, I grant permission   _X_

No, I do not grant permission   _____

Author's Signature _____

Date _____1/27/97_____

Any copying for commercial purposes or financial gain may be undertaken only with the author's explicit consent.

Hydration, Metamorphism and Diabase-Granophyre Relations in a Thick Basaltic Sill Emplaced into Wet Sediments, Western Montana

by

Michael A. Poage

A. B., Dartmouth College, 1991
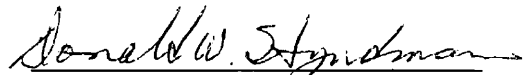
Presented in partial fulfillment of the requirements for the degree of

Master of Science

University of Montana

1997

Approved by:

Donald W. Hyndman
Chairman, Board of Examiners

[signature]
Dean, Graduate School

2-7-97
Date

UMI Number: EP37951

UMI°

Dissertation Publishing

UMI EP37951

ProQuest°

Poage, Michael A.,   M.S.,   February 1997   Geology

Hydration, Metamorphism and Diabase-Granophyre Relations in a Thick Basaltic Sill Emplaced into Wet Sediments, Western Montana

Director: Donald W. Hyndman   *ДшҔН*

The Plains Sill is a 150-300 meter-thick diabase-granophyre body exposed near the towns of Plains and Perma in western Montana. It intruded into the wet sediments of the Middle Proterozoic Prichard Formation during deposition of the Belt / Purcell Supergroup. Hydrothermal activity, driven by heat from the sill, resulted in metamorphism of the diabase as well as pervasive alteration and local reconstitution of overlying sediments.

The diabase portion of the sill has the composition of a high-iron tholeiite with mixed continental to oceanic affinities. It shows weak upward differentiation trends of increasing iron, sodium, potassium, and titanium, and decreasing magnesium and calcium. An upward trend of increasing metamorphism in a thicker section of the diabase, indicates that the metamorphic event affecting the sill is local and likely retrograde. Higher-temperature hornblende underwent partial retrogradation to form overgrowths and ragged aggregates of lower-temperature blue-green hornblende during cooling. Plagioclase is variably altered to epidote.

There is no evidence that primary clinopyroxene ever crystallized out of the magma, an indication that the magma may have incorporated sufficient water during emplacement under hydrous conditions to crystallize primary hornblende.

A miarolitic granophyre layer, 0-150 meters thick, caps the diabase. Field relations suggest that the granophyre is of magmatic origin and was formed during crystallization of the diabase. Separation of granophyric material from the diabase resulted from either filter-pressing of a late-stage felsic magma fraction, or dissolution of granitic constituents into a high-temperature water-rich fluid derived from the enclosing wet sediments. This fluid may have then migrated up-dip where the Plains Sill cut up-section from the Prichard D to E, and accumulated to produce the anomalous thicknesses of granophyre.

Regionally, the Plains Sill is one of at least sixteen mafic sills intruded into the lower Belt/Purcell Supergroup. A parallel is drawn with sill-sediment complex models as applied to presently active rift systems, specifically the Guaymas Basin in the Gulf of California. Successively younger sills are thought to intrude above older sills in the sediment column, controlled by the lower lithostatic loads and reduced resistance to lateral intrusion imposed by less lithified, nearer surface sediments.

Table of Contents

Acknowledgments

List of Tables

List of Figures

Introduction

The Plains Sill is a 150-300 meter-thick diabase-granophyre body exposed near the towns of Plains and Perma in western Montana. Locally, it is one of three thick basaltic sills exposed in the Middle Proterozoic Prichard Formation of the Belt/Purcell Supergroup (Figure 1). Regionally, it is one in a suite of stratigraphically equivalent sills which extend as far north as the Sullivan Mine area in southeastern British Columbia (Moyie Sills) and as far west as Crossport, Idaho (Purcell Sills). The Moyie and Purcell Sills are thought to have played an important role in the dynamics of early Belt sedimentation (Sears and Buckley 1992) and to be consistent with an intracratonic rift environment (Höy 1989; Sears et al. 1994). They comprise approximately 25% of the total section through the lower and middle Prichard Formation in the Crossport, Idaho area (Bishop 1974), 21% of the Prichard section encountered in the Arco 1 Paul Gibbs borehole in northwest Montana, 30% of a typical lower and lower-middle Aldridge (Prichard equivalent) section in southeastern British Columbia (Höy 1989) and ~10% in this study area (Cressman 1985). The sills appear to reflect basin-wide magmatic events, perhaps akin to flood basalts such as the Keweenawan basalts accompanying continental rifts (Sears et al. 1994).

Buckley and Sears (1992, 1993) presented evidence that the Plains Sill was emplaced at shallow levels into the wet sediments of the lower Prichard Formation, and Höy (1989) showed similar evidence for several of the Moyie Sills. Thus, the Plains Sill provides the opportunity to study the dynamics of sill emplacement into wet sediments, as well as magma-water interaction, metamorphism of basaltic rocks, diabase-granophyre relations and the origin of granophyre. I present a model whereby emplacement of the thick basaltic sill into wet sediments resulted in possible initial hydration of the basaltic magma followed by variable retrograde metamorphism.

1

Differentiation of the initial magma followed by migration and local accumulation of the separated felsic phase, resulted in anomalously thick granophyre zones at the top of the sill. Hydrothermal activity, driven by heat from the sill, caused pervasive alteration and local reconstitution of overlying sediments as well as homogenization of initial strontium ratios. In addition, the suite of Purcell Sills is considered in light of sill-sediment complex models as applied to rift systems such as the Guaymas Basin in the Gulf of California (Einsele 1985). In the course of discussion of the Plains Sill, comparisons are drawn with the underlying and likely co-magmatic Paradise Sill, as well as the numerous sills of the Arco 1 Paul Gibbs borehole.
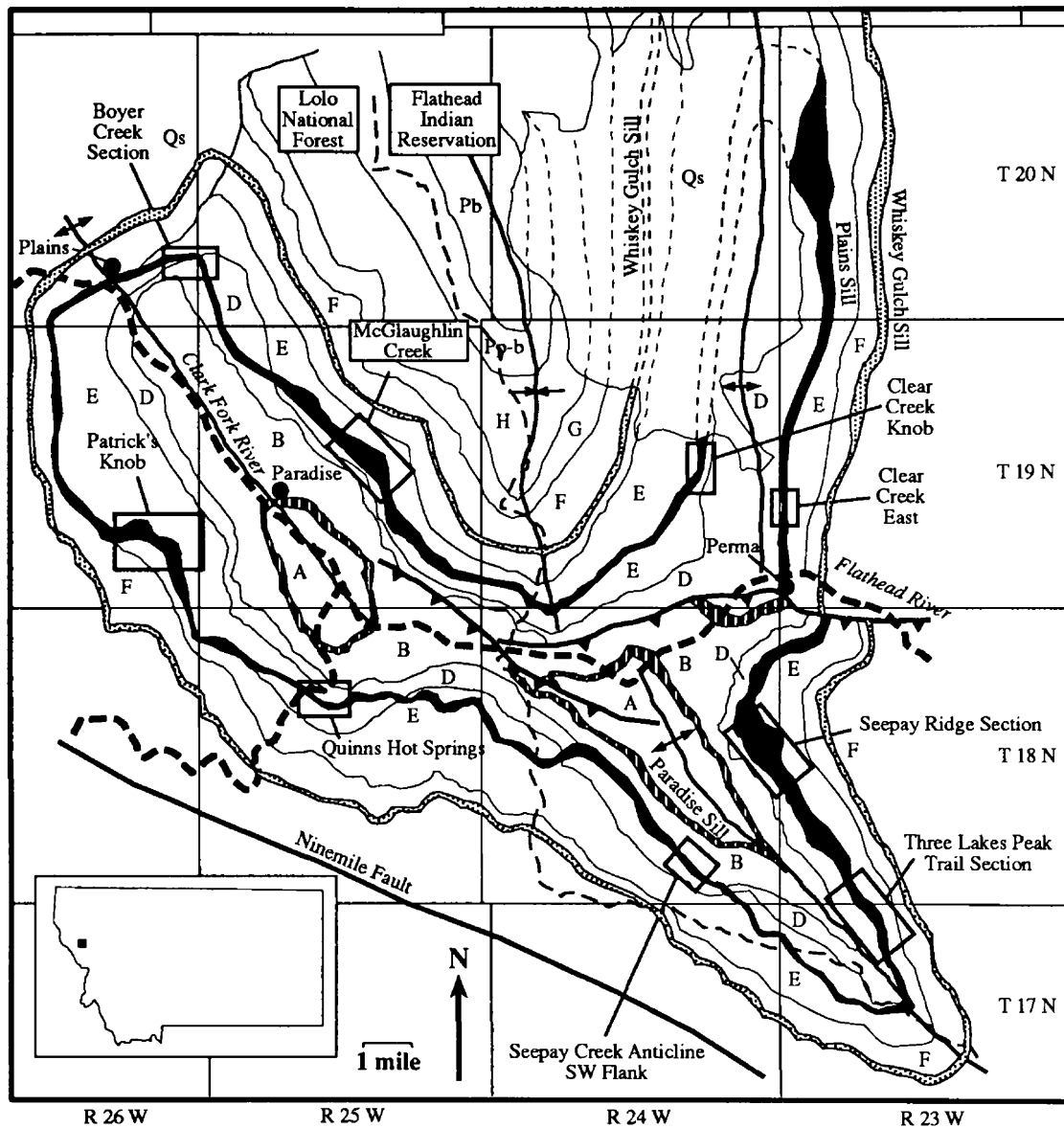
Figure 1. Simplified geologic map of the Plains-Paradise-Perma area showing the Plains, Paradise and Whiskey Gulch sills intruding the Prichard Formation of the lower Belt Supergroup (after Sears, 1992). Figure 2 contains a simplifed section through the Prichard Formation. Labeled sections are shown in detail in Figure 3.
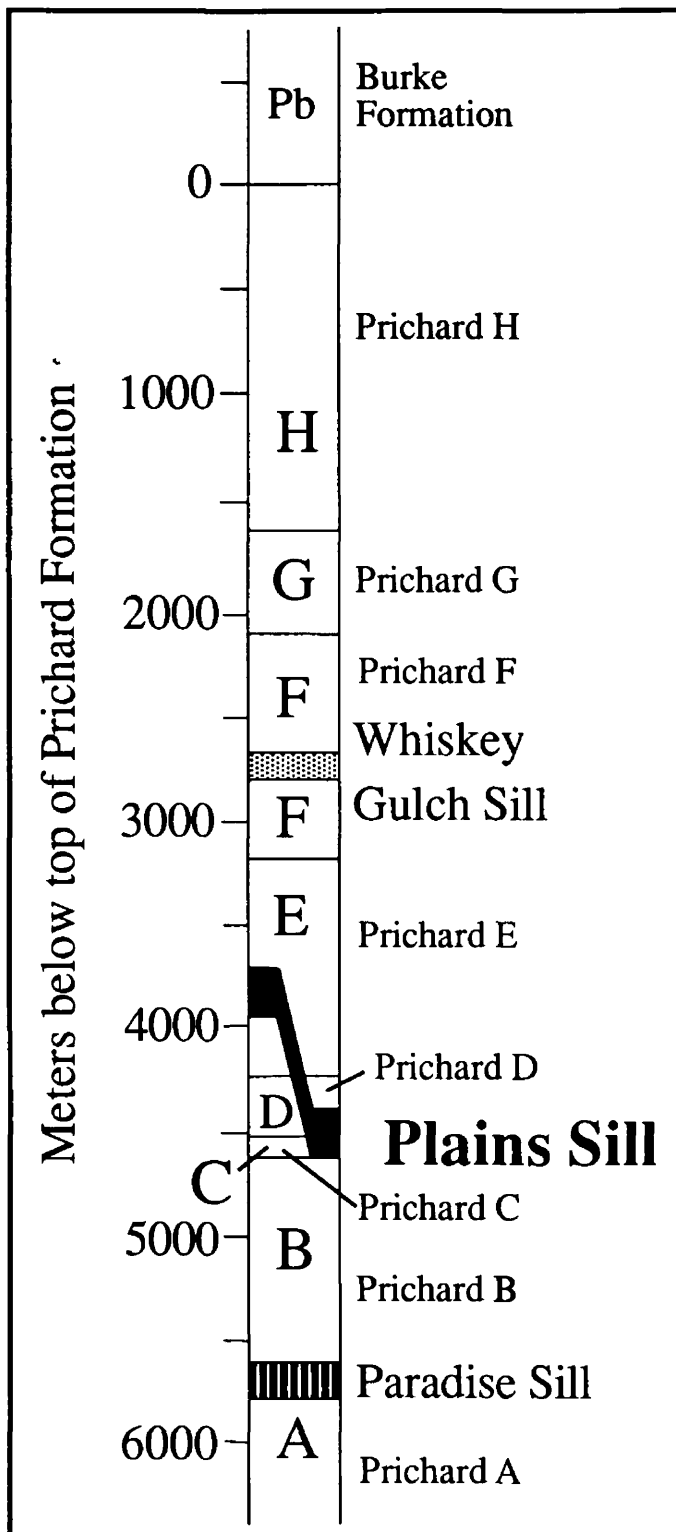
Figure 2. Simplified section through the Prichard
Formation showing thicknesses of each member
and the position of the three mafic sills (after
Cressman 1985).
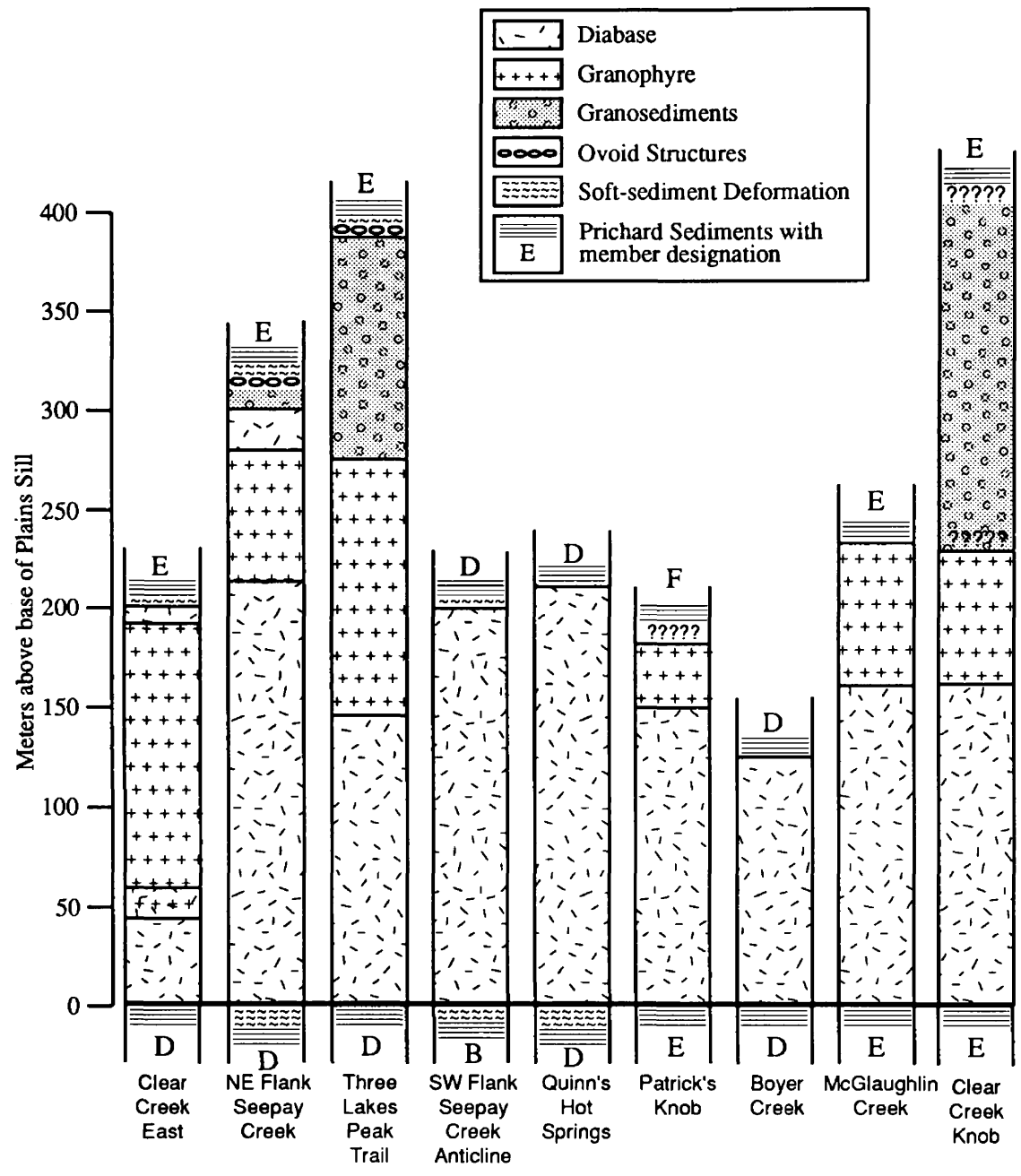
Figure 3. Nine sections through the Plains Sill showing variations in the occurrence and thickness of lithologies and emplacement related features. The thicknesses of the granophyre and granosediments at Clear Creek Knob and the granophyre at Patrick's Knob are not well constrained due to poor exposure.

Summary of Samples and Analytical Methods

Table 1 lists all samples relevant to this paper, their location, position with respect to the sill and rock type. Samples from the Plains Sill at the Clear Creek and the Three Lakes Peak Trail section and four samples from the Paradise Sill were analyzed by x-ray fluorescence at Washington State University's GeoAnalytical laboratory. Normalized major-oxide and trace-element data are presented in Tables 4-7 and Table 12. ICP analysis on samples from the Seepay Ridge section through the Plains Sill and a nearby section through the Paradise Sill were performed by Bondar-Clegg. ICP data were generously furnished by the Confederated Salish-Kootenai Tribes and are presented in Tables 8-11.

Strontium isotope analyses were provided by Dr. Kurtis Kyser of the University of Saskatchewan. Data are presented in Table 2.

I analyzed specific mineral phases using the Cameca MBX Microprobe at Washington State University's GeoAnalytical Laboratory. Beam width was set at 5 microns, beam current at 10.8 nA and excitation voltage at 20 kV. Microprobe data are presented in Table 3.

Sample	Rock Type	Comments:
Plains Sill at the Clear Creek Section:		
71501-71502	Sediment	Sediment below Plains Sill
71503-71509	Diabase	Plains Sill diabase sampled at 6m intervals
71901	Diabase	Plains Sill diabase sampled at 6m intervals
71902-71904	Transition	Transitional between diabase and granophyre
71905-71910	Granophyre	Plains Sill granophyre sampled at 6m intervals
72001-72016	Granophyre	Plains Sill granophyre sampled at 6m intervals
72017	Diabase	Plains Sill upper diabase - some chicken track
72018	Diabase	Fine-grained possible chill zone
72019-72020	Sediment	Sediments above Plains Sill
Plains Sill at the Three Lakes Peak Trail Sction:		
Base Seds II	Sediment	Sediments 7-14 meters below Plains Sill
Base Seds I	Sediment	Sediments 0-7 meters below Plains Sill
72701-72722	Diabase	Plains Sill diabase sampled at 7m intervals
72723-72739	Granophyre	Plains Sill granophyre sampled at 7m intervals
72740-72754	Granosediment	Granosediment above Plains Sill taken at 7m intervals
72755-72756	Sediment	Sediment above Plains Sill sampled at 7m intervals
Four Samples from the Bottom of the Paradise Sill:		
60227	Diabase	Paradise Sill diabase
60228	Diabase	Paradise Sill diabase
60229	Diabase	Paradise Sill diabase
60230	Diabase	Paradise Sill diabase
Plains Sill at the Seepay Ridge Section:		
F92-583 - 599	Diabase	Plains Sill diabase sampled at ~4m intervals
F92-2000 - 2044	Diabase	Plains Sill diabase sampled at ~4m intervals
F92-2045 - 2066	Granophyre	Plains Sill granophyre sampled at ~4m intervals
F92-2067 - 2068	Diabase	Plains Sill upper diabase - chicken-track texture
Paradise Sill at the Seepay Ridge Section:		
F92-550 - 581	Diabase	Differentiated Paradise Sill at the Seepay Ridge section - samples taken at ~6m intervals
Other samples:		
BLEB II	Granosediment	Bleb of granophyre within granoseds (microprobed)
BLEB III	Granophyre	Granophyre inclusion in diabase (microprobed)

Table 1. Sample numbers, rock type and location of samples relevant to this paper.

Local Geology

Figure 1 shows the simplified geology of the field area, including the trace of the Plains, Paradise and Whiskey Gulch Sills as exposed in the Seepay Creek, Camas Prairie and Plains Anticlines of the Purcell Anticlinorium. The stratigraphic position of the Plains Sill varies locally from the Prichard Member D (i.e. Quinns Hot Springs, Boyer Creek) through the boundary between Prichard Members D and E along the eastern portion of the map area, to its highest position at the Prichard E-F boundary near Patrick's Knob. The majority of the local exposures show the Plains Sill intruding the Prichard E or at the D-E boundary. The Paradise Sill, lower in the section, intrudes at the Prichard A-B boundary, whereas the stratigraphically higher Whiskey Gulch Sill intrudes the Prichard F. Prichard units are defined by Cressman (1985; 1989). Thickness of Prichard units as well as positions of the sills are shown in Figure 2.

Plains Sill outcrop is generally poor, with the majority of exposure occurring on steep talus slopes, heavily vegetated forest, and grass-covered prairie. Nine sections though the Plains Sill and enclosing sediments are labeled on the map and presented in varying detail in Figure 3. Four distinct rock units make up the sill-sediment package: diabase (lower and upper), granophyre, granosediment, and sediment and are discussed individually.

Diabase [Samples 71503-9, 71901; F92-582 - 599, F92-2000 - 2028; 72701-22]

The lower diabase portion of the sill varies in thickness from 40- >200 meters and comprises the bulk of the mafic rocks of the Plains Sill. There is no apparent correlation between diabase thickness and stratigraphic position of intrusion. In hand specimen, the rock appears dark green to nearly black in color, and consists of about 60% medium-grained intergrown subhedral amphibole laths set in a groundmass of

finer-grained plagioclase with some discernible free quartz (Figure 4). Variable

amounts of epidote, biotite, ilmenite, sphene, apatite, and rutile are also present but can

only be seen in thin section. Abundances vary relative to the degree of metamorphism

(see section on Metamorphism of the Plains Sill). No metamorphic fabric is apparent.

A number of textural variations are readily observed in the field. Fine-grained

chill margins are found only at the top and bottom of the Clear Creek East section and at

the bottom of the Three Lakes Peak Trail section. A coarser-grained variation with

highly elongate amphibole crystals, up to 10 centimeters, arranged in sheafs (termed

chicken-track diabase; Buckley and Sears 1993) is present toward the top of most

diabase sections and is very common in the upper diabase unit of the Clear Creek East

and Seepay Ridge sections (Figure 5). The origin of the chicken-track texture is

unknown but may result from inhibition of nucleation in the presence of abundant water

during the latest stages of crystallization. Another coarser-grained variant shows the

amphibole crystals adopting a more equidimensional form with a distinctly mottled

overall appearance (Figure 6). Diabase showing this texture is found as float in several

sections and forms a laterally persistent lens approximately 20 meters thick in the

middle of the Three Lakes Peak Trail section. A fourth textural variant shows coarser

grained diabase adopting an irregular vein-like form, up to 15 centimeters wide, within

medium-grained diabase (Figure 7). Contacts are diffuse over approximately one

centimeter; this texture may have resulted from pore water streaming through the sill

during cooling and crystallization. This textural variant was first noticed by D. W.

Hyndman in a Moyie Sill in British Columbia, and was subsequently found at the

Seepay Ridge and Quinn's Hot Springs sections

Sharply bounded felsic veinlets up to 5 centimeters wide (Figure 8) as well as

felsic segregations up to 10 centimeters (Figure 9) showing more diffuse contacts are

present within the diabase. Both the veinlets and segregations consist primarily of

quartz, plagioclase and granophyric quartz-plagioclase intergrowths. Microprobe data show the composition of the feldspars in one such segregation (BLEB III) to be An_{25} to An_{31} (Table 3, Nos. 25-28), significantly less calcic than the An_{35-77} between different grains of plagioclase in the diabase (Table 3, Nos. 1-11). Though volumetrically insignificant, these occurrences provide evidence that the diabasic magma was capable of producing and transporting at least some felsic magma during the course of crystallization and cooling. Similar veinlets are found in the stratigraphically equivalent sills in Boundary County, Idaho (Bishop 1974) This is discussed in more detail below, in the section entitled "Origin of the Granophyre."

Granophyre [Samples 72723-39; 71905-72016; F92-2047 - 2064]

A biotite-quartz-plagioclase granophyre layer, 0-150 meters thick, caps the diabase. The following discussion presumes that the granophyre is of igneous origin. This presumption will be discussed in more detail in the section entitled "Origin of the Granophyre." Its origin is one of the foci of this paper. In hand specimen, the granophyre appears to be approximately 20% fine-grained biotite, roughly equal parts anhedral quartz, plagioclase and fine-grained quartz-plagioclase intergrowths, with minor white mica (Figure 10). In thin section, the biotite is seen forming mostly fine-grained patchy aggregates with sparse intergrown muscovite. Sodic plagioclase (An_{0-11}) occurs as both euhedral-subhedral crystals and as quartz-albite intergrowths showing a variety of granophyric intergrowth textures (Figure 11). Development of cuneiform and vermicular granophyric quartz-plagioclase intergrowths varies from section to section. They are best developed and most abundant at the Seepay Ridge section and far less abundant and pronounced in the Clear Creek and Three Lakes Peak Trail sections. There is no immediate explanation for this difference. Plagioclase within the quartz-feldspar intergrowths is variably altered to fine-grained white mica.

At all localities, the granophyre contains abundant miarolitic cavities into some of which have grown euhedral quartz and feldspar crystal faces. Cavities are often stained a light brick-red to limonite-orange color, presumably from the later oxidation of iron-bearing sulfide or oxide minerals by fluids migrating through the cavities. These miarolitic cavities are similar to those found in some epizonal felsic plutons and are taken as evidence that the granophyric rocks are of igneous origin.

In the Clear Creek section, the granophyre is weakly to strongly mylonitized, showing parallel orientation of biotite crystals and weakly developed but distinct layers of biotite and quartz plus plagioclase. The mylonitic fabric is roughly parallel to bedding in the enclosing sediments. A very weak fabric defined by sub-parallel orientation of biotite crystals is also seen in the granophyric rocks at the Seepay Ridge section. The origin of this fabric is not clear. Since only the granophyre and neither the underlying diabase or the enclosing sediments show a fabric, it is likely that mylonitization took place while the granophyre was still hot but after the diabase had already cooled enough to remain unaffected. It has been suggested (S. N. Buckley, personal communication 1994) that perhaps the basin was, at least locally, subsiding under the weight of the sill while the granophyre was still hot enough to behave plastically.

The diabase-granophyre contact, though not seen exposed in this study, is inferred to be generally sharp as intermediate composition rocks are absent in most localities. The exception is the Clear Creek East section where the contact with the lower granophyre is compositionally gradational over approximately 18 meters of section (Table 6, Samples 71902-71904). It is not clear whether this compositional gradation results from mixing of diabase and granophyric magmas, from fine-scale mingling or by some differentiation process.

There is no apparent correlation between the thickness of diabase and the thickness of granophyre. The extreme case in the Clear Creek section shows approximately 150 meters of granophyre overlying 40 meters of diabase, whereas the Seepay Ridge section shows about 90 meters of granophyre overlying 200 meters of diabase. The granophyre layer is absent in the Quinns Hot Springs and Boyer Creek sections, as well as along the southwest flank of Seepay Creek Anticline where the sill intrudes the Prichard Member D. This suggests that stratigraphic level of intrusion may impose some control on the presence or absence of granophyre.

Granophyre is common in the Crossport Sills (Bishop 1974) though does not commonly occur in thicknesses disproportionate to that of the diabase. A single 25 meter thick, but discontinuous, granophyre overlying one of the Crossport C Sill is interpreted to have formed by filter pressing and injection into an overlying low-pressure zone where the sill moves from being concordant to Prichard sediments, to being discordant (Bishop 1974). An anomalously thick granophyric body also overlies the Moyie Sill beneath the stratiform sediment-hosted Sullivan base-metal deposit in southeastern British Columbia (Turner et al. 1992). No granophyric rocks are associated with the lower Paradise Sill, though it shows much stronger internal differentiation trends (see Origin of the Granophyre).

Upper Diabase [Samples 72017-18; F92-2067-68]

The upper diabase unit is present at the Clear Creek and the Seepay Ridge sections. It is generally less than fifteen meters thick and directly overlies the granophyre with sharp contacts. In both sections, the upper diabase shows both the typical medium-grained texture and the more distinctive chicken-track texture, characterized by highly elongate amphibole crystals. At the Clear Creek section, a narrow fine-grained chill margin is present at the upper diabase-sediment contact.

Amphiboles in the upper diabase from the Clear Creek East section show deformation textures (Figure 12) and were probably deformed by the same process that mylonitized the underlying granophyre.

At the Three Lakes Peak Trail section, the upper diabase is absent along the line of sampling (72701-72756) but is present overlying the granosediments nearby. This is the only case where the upper diabase does not directly overlie the granophyre and may have implications for the disturbance and homogenization of such a thick section of sediments (see below).

Granosediments [Samples 72740-54]

A distinctive layer of reconstituted sediment (granosediment) up to 125 meters thick overlies the sill. The rocks are fine- to medium-grained and internally massive, showing no relict sedimentary structure. In hand specimen, they appear to consist of approximately 20% fine-grained biotite and 40% quartz and plagioclase set a fine-grained groundmass. In thin section, they show similarities to the granophyre with ragged aggregates of biotite, euhedral-subhedral albite crystals and larger optically continuous patches of undulose quartz (Figure 13). Granophyric textures are generally absent, though small patches of very fine-grained white mica distributed throughout larger quartz patches, may represent alteration of plagioclase. The groundmass of the granosediments is pervasively altered to fine-grained white mica, a feature that easily distinguishes them from the granophyre. The white mica-rich matrix may represent altered clay.

The granosediment layer varies dramatically in thickness. It is generally absent where the Plains Sill intrudes the Prichard D, though present in the transition where the sill cuts up-section from the Prichard D to the Prichard E between the Boyer Creek and McGlaughlin Creek sections. At the Seepay Ridge section, the granosediment layer is

restricted to several meters above the upper diabase and is completely absent in several places along the ridge. It thickens rapidly to over 100 meters approaching the Three Lakes Peak Trail section, where the upper diabase unit is only variably present and in some places overlies the granosediment layer. A thick granosediment layer is also present at the Clear Creek Knob and McGlaughlin Creek sections.

At the top of the granosediment layer, ovoid structures, up to 10 centimeters in length, consist of an inner core of meta-sediment often preserving relict bedding, surrounded by concentric growth or reaction rings (Figure 14). They are most abundant along the Seepay Ridge section, with a few being found at the granosediment-sediment interface at the Three Lakes Peak Trail section. They are absent at all other localities. These were first reported in this area by Buckley and Sears (1992) and are similar to those reported adjacent to Moyie sills in British Columbia (Höy 1989) as well as mafic sills in Antarctica (Krynauw et al. 1988). Krynauw et al. (1988) interpret ovoids to be the product of sill emplacement into partly consolidated, wet sediments. In the case of the Plains Sill, it appears that partially lithified fragments of sediment retained internal coherence as sediment layers around them were reconstituted. These fragments then reacted with fluids during metamorphism to produce the typically concentric reaction rings.

Above the ovoids, the granosediments grade upward into complexly folded metasediments, which, on the scale of meters, give way to undeformed hornfelsed sediments. Figure 15 shows the transition from completely massive granosediments showing no relict sedimentary textures to deformed metasediments with primary bedding preserved.

Concentrated toward the top of the thicker section of granosediments along the Three Lakes Peak Trail are inclusions of coarser-grained felsic material, closely resembling the underlying granophyre (Figure 16a). A single diabase inclusion was

found. Ranging in size from less than 1 centimeter to over 15 centimeters in diameter, most are distinctly rounded, though a few are more amoeboid in shape. There are no angular inclusions. They are highly visible against the granosediments, being significantly coarser-grained and much lighter in color. Most show a thin approximately 2 millimeter rind, presumably resulting from interaction with the surrounding granosediments during reconstitution and alteration. In thin section, cuneiform and vermicular granophyric quartz-plagioclase intergrowths, as well as intergrowths assuming the morphology of euhedral plagioclase, are very well developed (Figure 16b).

I interpret these to have been injected into the overlying soupy granosediments during the course granophyre emplacement and crystallization. The granosediments were likely unable to hold the fluid in a vein or dike form and consequently the pegmatite-like "blebs" assumed a rounded form as they were transported upward either by density contrast or by convection within the granosediments. It is not clear what controls the thickness of the granosediment layer above the sill, but it appears to be thickest where the upper diabase is absent and the granophyre contacts the sediments directly, as is the case at the Three Lakes Peak Trail, Clear Creek Knob, and McGlaughlin Creek sections. It is possible that the upper diabase, where present, solidified very quickly and limited sediment reconstitution by acting as a relatively impermeable seal between the underlying granophyre and overlying sediments.

Enclosing Sediments [Samples 71501-2, 72019-20, B.S.I, B.S.II, 72755-6]

The enclosing meta-sediments, Prichard Members D and E, are fine-grained laminated siltites and argillites (Cressman 1985) largely composed biotite, muscovite, quartz and plagioclase with variable, but usually minor, amounts of chlorite, tourmaline, hornblende, garnet and opaque minerals. Contact metamorphic effects,

though not carefully documented in this study, are generally limited to less than 25 meters from the contact. This observation is in accord with a maximum thickness of 23.3 meters observed by Meglen (1975). Contact rocks are often bleached relative to the rest of the Prichard, perhaps due to albitization. Spotted hornfels is common along the upper contact of the sill, with most spots being fine- to medium-grained aggregates of biotite. A common contact metamorphic assemblage along the bottom of the sill includes coarse chlorite books, rare hornblende and garnet porphyroblasts, and abundant fine-grained biotite and muscovite.

Evidence of soft-sediment deformation is seen on the upper and lower contacts at several sections, in both the Prichard Members D and E. Along the Seepay Ridge and Three Lakes Peak Trail sections, the overlying granosediments grade upward into a complexly folded zone of Prichard E sediments. Local, small-scale isoclinal folds in the sediments above the upper diabase at the Clear Creek East section may represent soft-sediment deformation resulting from sill emplacement. The Prichard D sediments below the sill at the Quinns Hot Springs section show similarly contorted bedding.

Figure 4. Plains Sill Diabase. Sample is ~7 centimeters across.
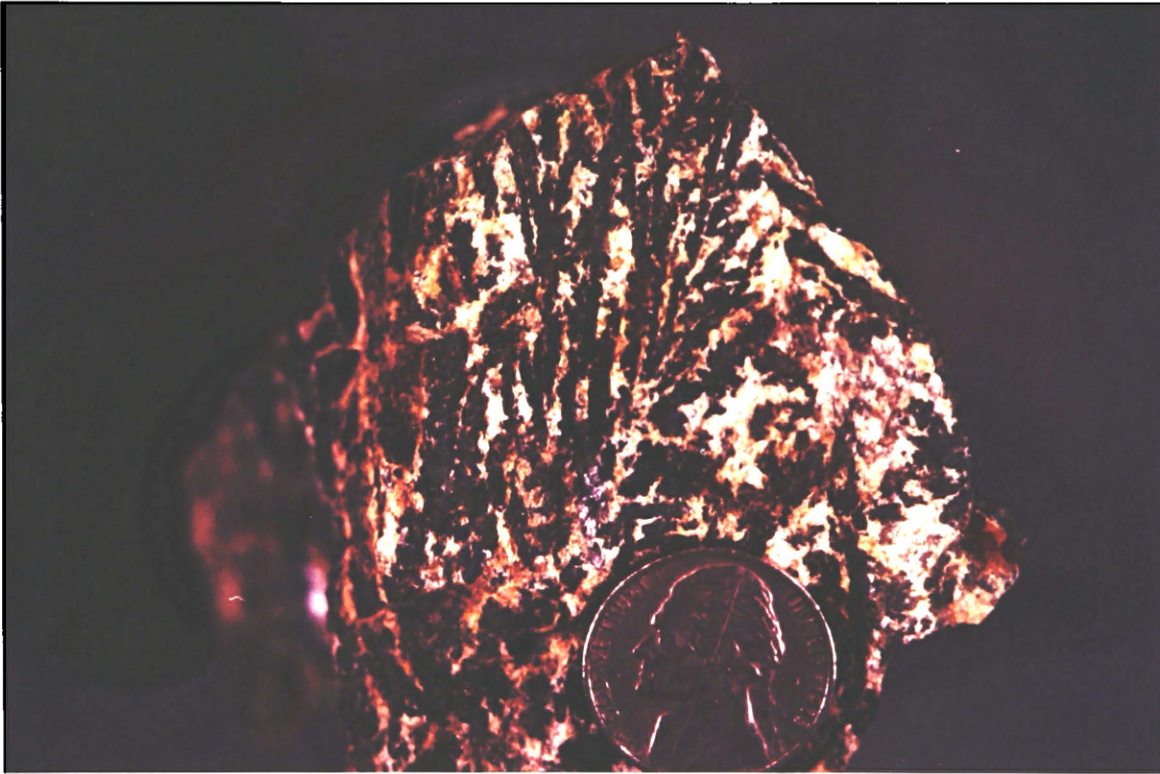
Figure 5. Chicken-track diabase texture from Seepay Ridge area.

Figure 6. Coarse-grained diabase showing more equidimensional hornblende.
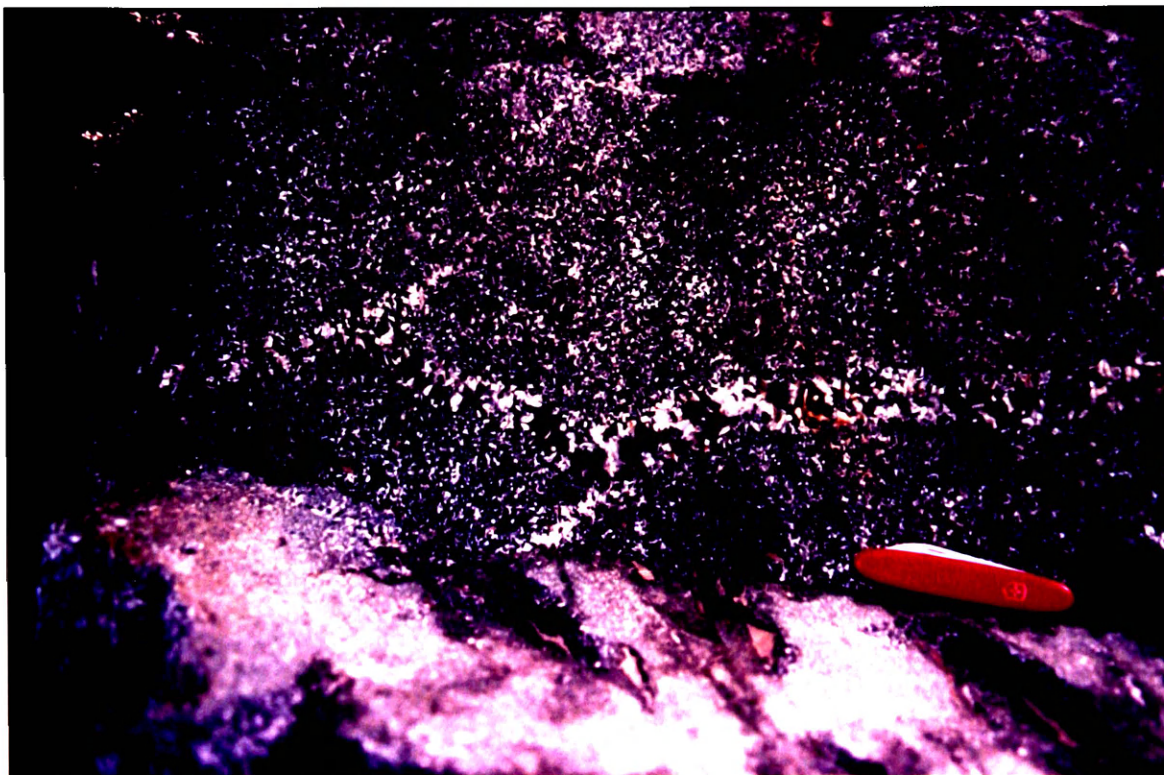
Figure 7. Irregular vein-like coarse-grained diabase within medium-grained diabase.

Figure 8. Granophyre veinlet within diabase.
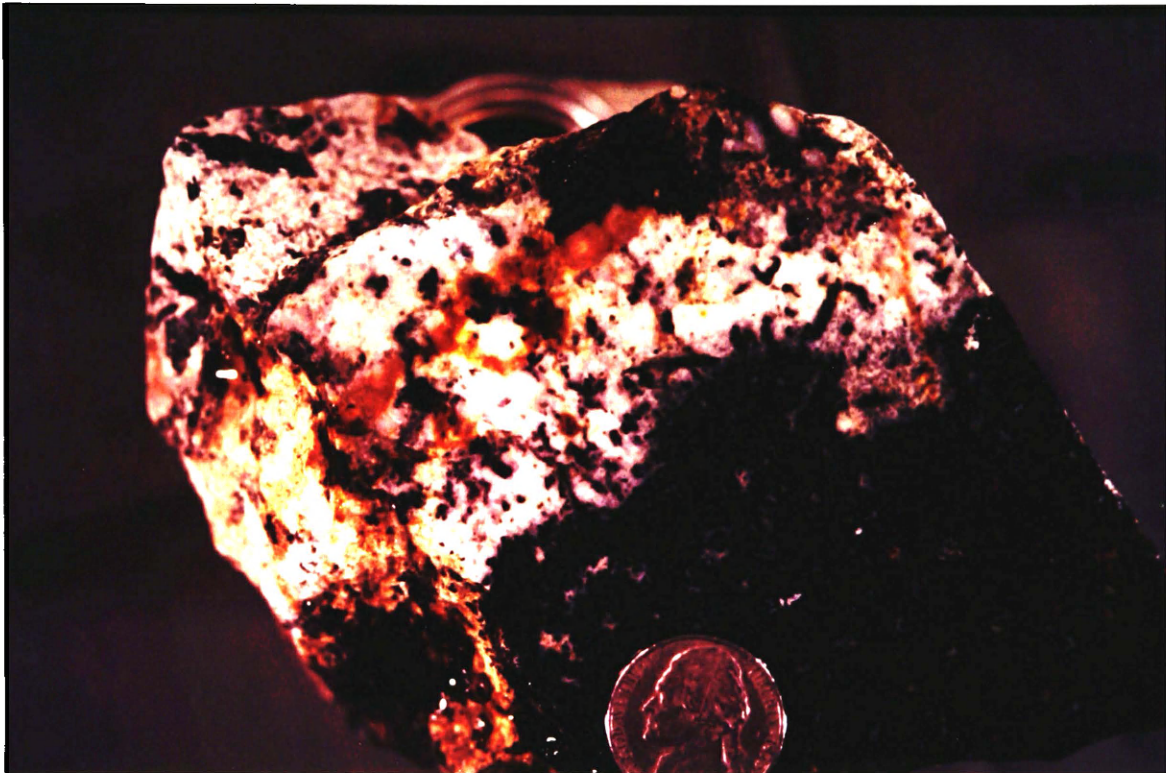
Figure 9. Granophyre segregation within diabase.
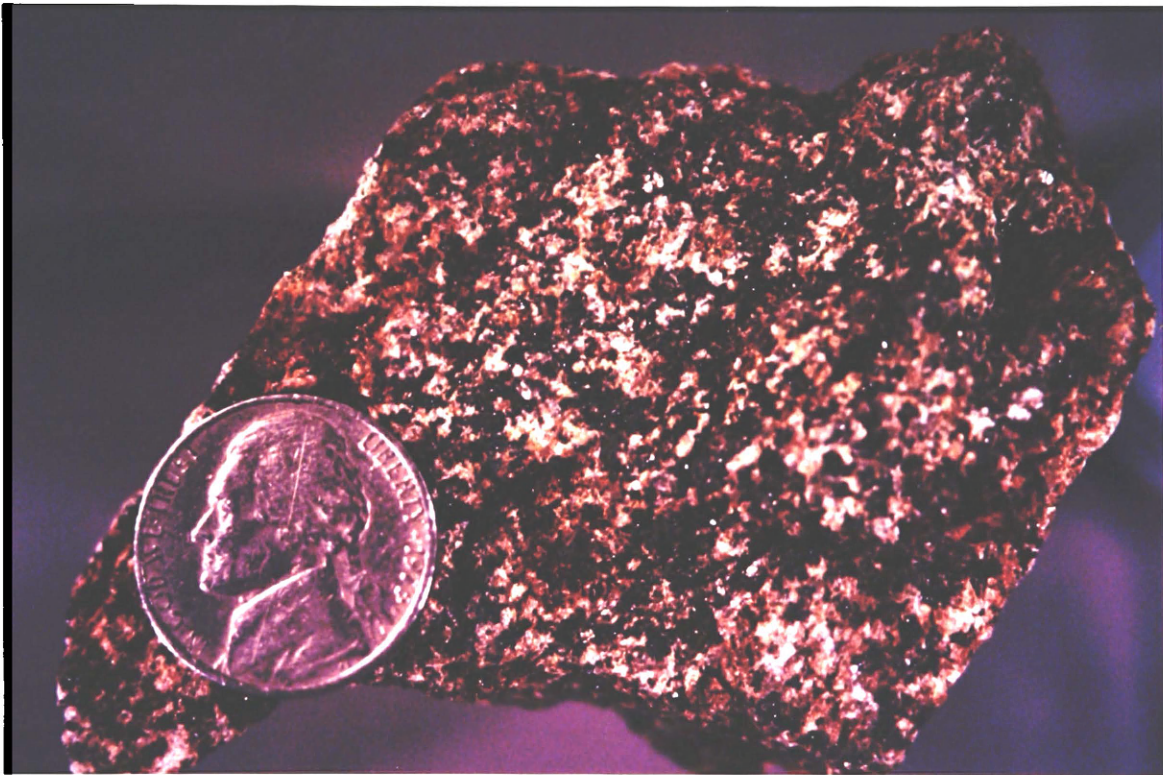
Figure 10. Plains Sill granophyre.
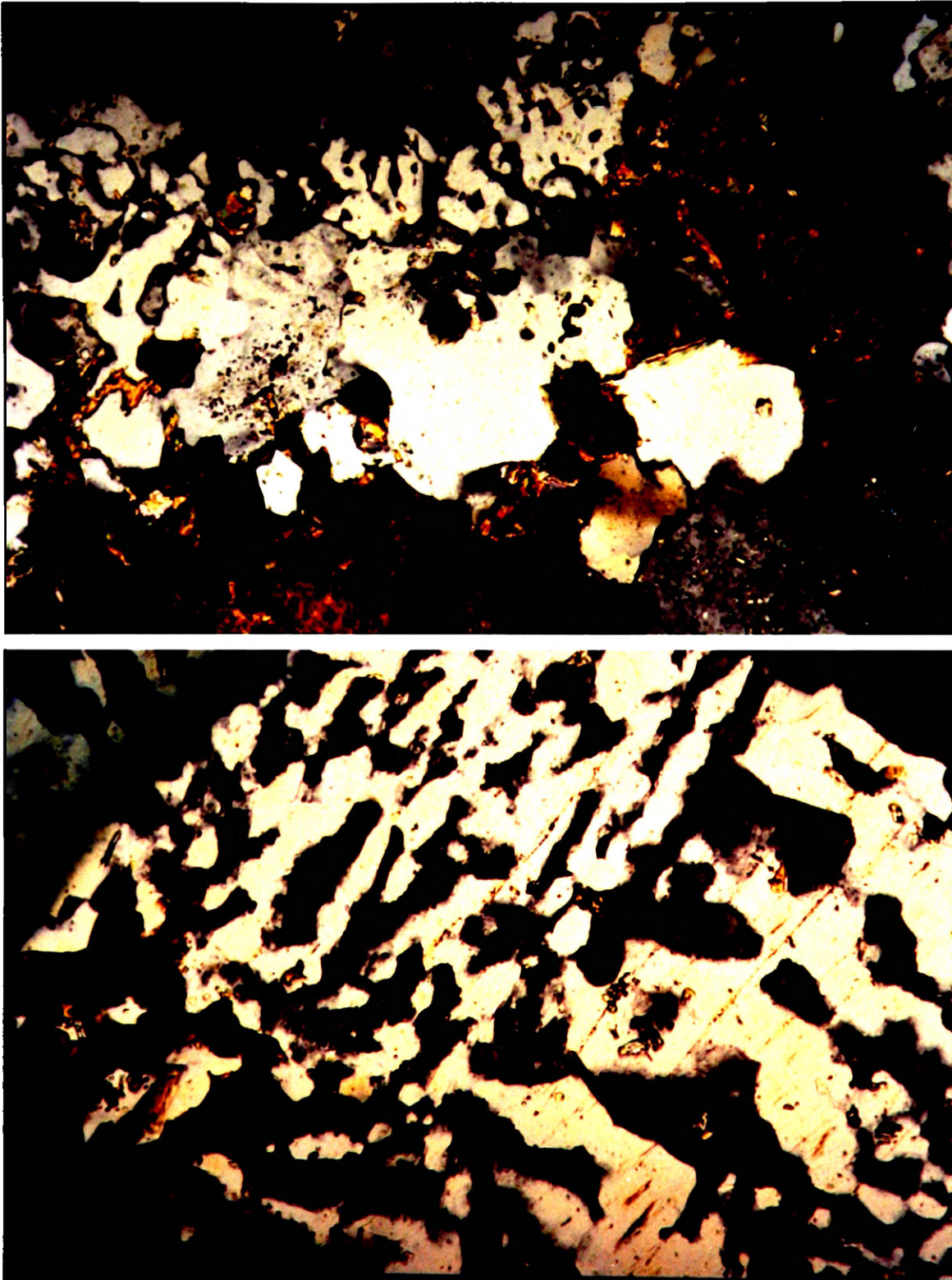
Figure 11. Symplectic textures within the granophyre. 3.5 and 1mm FOV for top and bottom photomicrographs respectively.
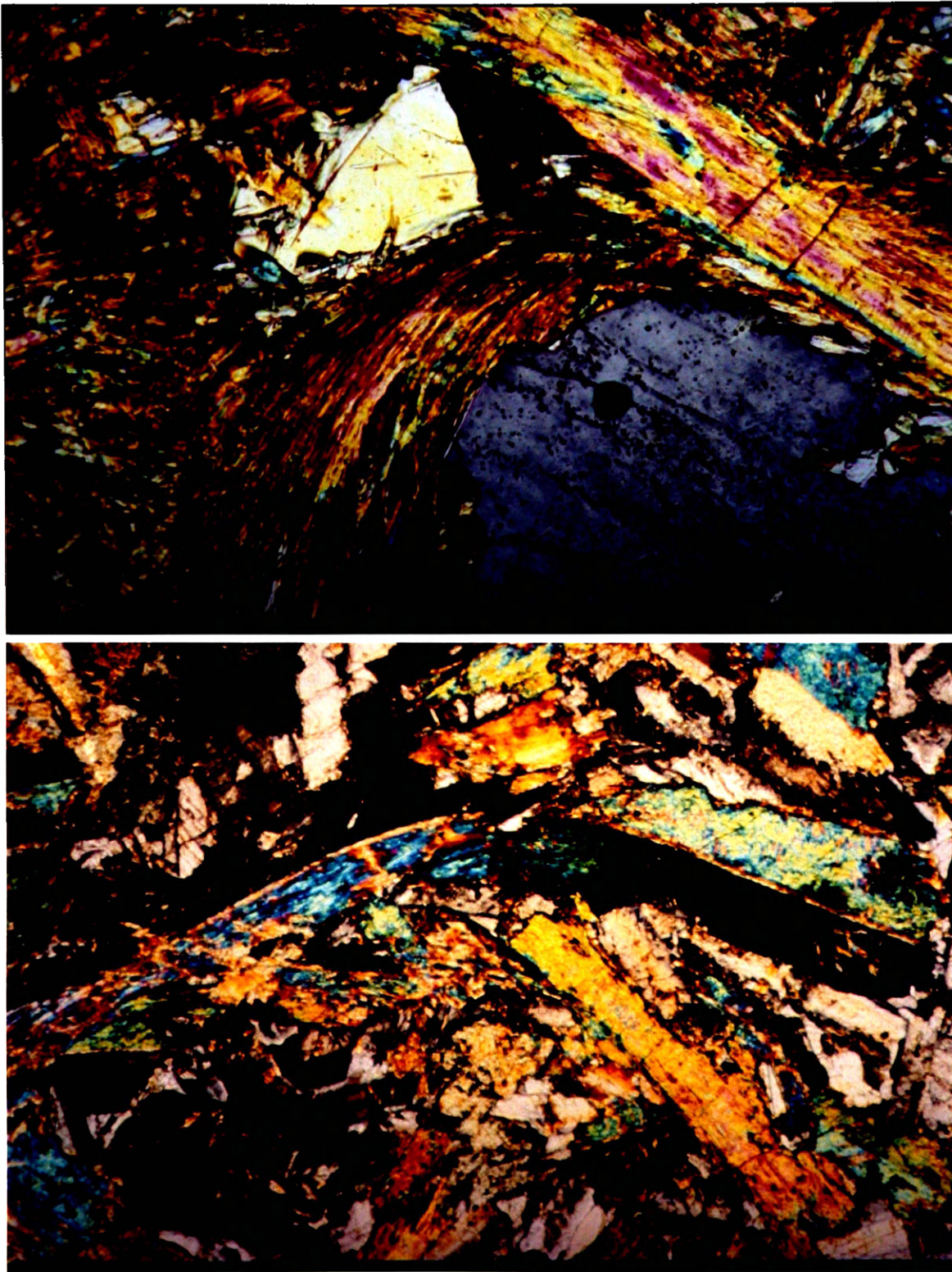
Figure 12. Deformation textures within the upper diabase at Clear Creek. Top and bottom FOV are 1 and 3.5mm respectively.
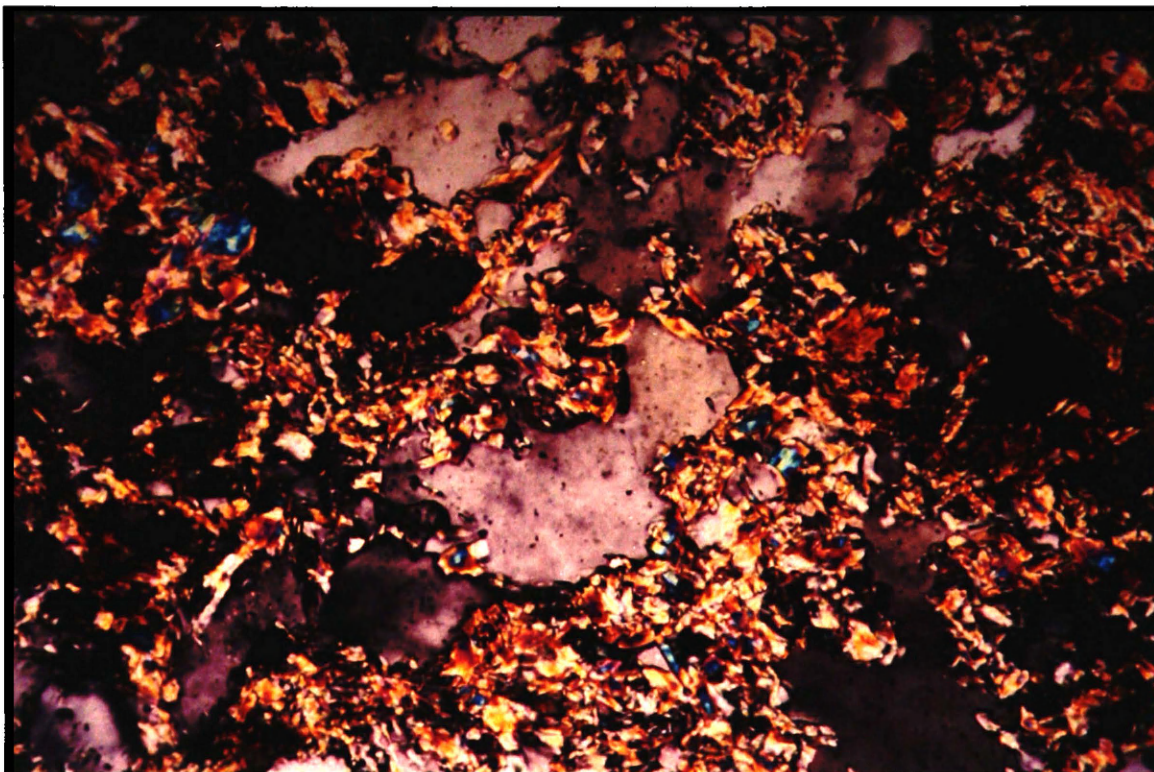
Figure 13. Photomicrograph of granosediment (1mm FOV).

Figure 14. Ovoid structures toward the top of the granosediment.
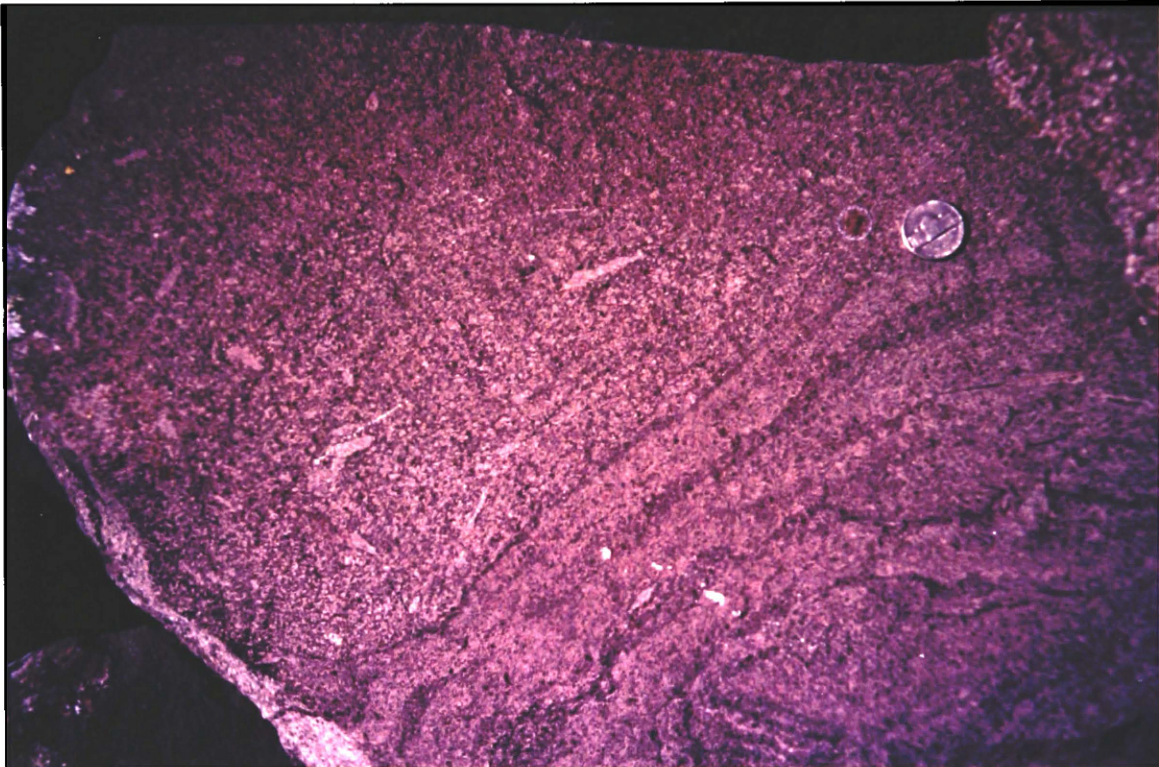
Figure 15. Transition from granosediment into complexly folded sediment.

Figure 16a. Granophyre inclusion within the granosediment.
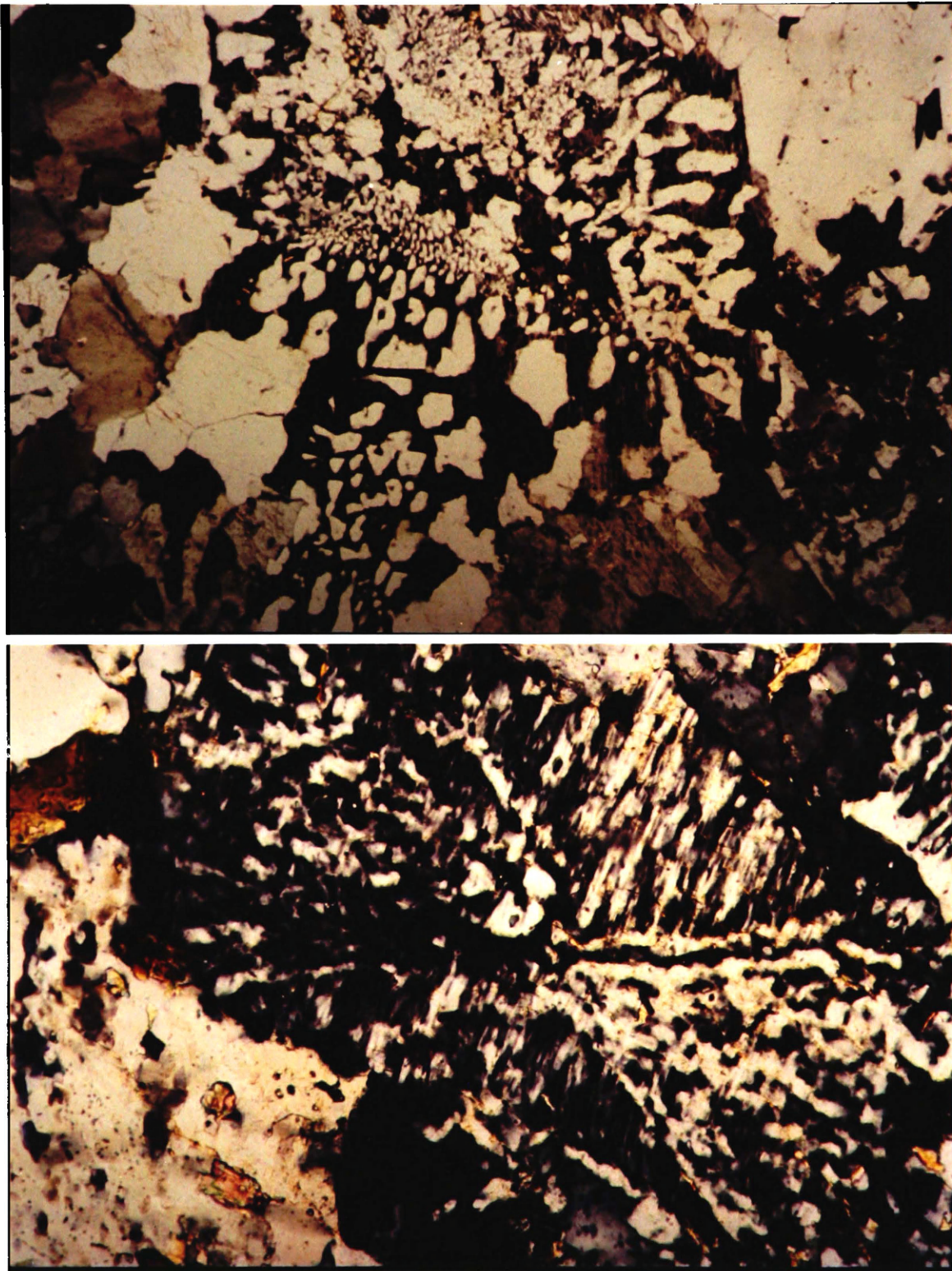
Figure 16b. Intergrowth textures within the granophyre inclusion. 3.5, 1mm FOV for top and bottom photomicrographs respectively.

Metamorphism of the Plains Sill

Twenty-two thin sections (samples 72701-72722) were examined to characterize the metamorphism of the Plains Sill at the Three Lakes Peak Trail section. Additional thin sections from the Clear Creek and Seepay Ridge sections show no major differences in metamorphic style. I analyzed, using the microprobe, four samples at the Three Lakes Peak Trail section in an attempt to quantify metamorphic reactions (Table 3) and assess whether constituents were added or subtracted during metamorphism.

The present mineral assemblage consists of two generations of hornblende (green and blue-green), plagioclase, epidote, quartz, biotite, ilmenite, sphene and chlorite in approximate order of decreasing abundance. It is consistent with the epidote-amphibolite metamorphic facies or the transition from lower-amphibolite to epidote-amphibolite facies of basalt composition rocks (Miyashiro 1968).

Since it is not clear whether primary clinopyroxene ever crystallized from the melt (see section entitled Hydration of the Plains Sill), it is omitted from the discussion except to say that if it ever did exist, all evidence has been completely removed. This also makes it impossible to attach primary or secondary status to hornblende. Igneous hornblende is typically brown or green-brown colored. No brownish hornblende is now present in the Plains Sill though there may have been originally. It is clear in thin sections that the deeper blue-green hornblende came later than the paler green hornblende. Thus, I refer to the two variants as earlier- and later-formed hornblende, rather than assume that one is primary and one is secondary. Indeed, it is likely that both are secondary, with the green hornblende either altering from primary brown hornblende or from primary clinopyroxene.

Blue-green hornblende and epidote dominate the retrograde metamorphic assemblage. Petrographic evidence suggests that metamorphism followed two parallel reaction sequences. Green, earlier formed, hornblende altered either to deeper green or blue-green hornblende and in some cases is partially altered to biotite. The timing of biotite formation is difficult to ascertain as sometimes significant biotite is present while green hornblendes still appear fairly unaltered. The second sequence shows plagioclase altering to epidote; in some cases it appears that epidote is further altered to white mica. The green to blue-green transition in hornblende can progress fairly far before plagioclase starts altering to epidote as is apparent in the samples from the Clear Creek section where hornblende alteration is extensive inboard of the fine-grained chill zones and plagioclase is virtually unaltered. Free quartz appears to increase with more advanced metamorphism. It is likely a product of the green to blue-green hornblende reaction as it increases irrespective of plagioclase alteration in the Clear Creek section. These two reaction sequences are discussed below. An additional reaction is the alteration of ilmenite to sphene (Figure 20), which occurs at all degrees of metamorphism in the diabase.

The diabase shows considerable variation in the degree of metamorphism. The lower chill zone and several medium-grained samples above it (72701-72704) contain approximately 60% green hornblende, 25% plagioclase (An_{53-77}), 7-10% quartz, up to 3% epidote, and trace amounts of chlorite, apatite, ilmenite, and sphene. These samples show relatively little alteration of green hornblende and plagioclase (Figure 17). Degree of metamorphism increases upwards and peaks about 28 meters from the top of the sill (Figure 18). Samples there contain approximately 60% green to blue-green amphibole, up to 20% epidote, 15-20% quartz, minor amounts of discernible plagioclase (though some may be obscured by abundant fine-grained epidote), 1% ilmenite often enclosed in sphene, and small but variable amounts of biotite, muscovite,

and apatite. The upper-most four samples (72719-72722) are decidedly more metamorphosed than those at the base but are less so than those in the middle (72705-72718). At the Clear Creek section, plagioclase remains virtually unaltered through the 42 meters of diabase whereas hornblende shows considerable alteration from green to blue-green hornblende and sometimes biotite. The chill margins at the bottom and top of the sill (71503, 72018) show little alteration of green hornblende.

A later regional metamorphic event would likely alter the sill more uniformly from bottom to top, as well as between sections of the sill. Since this is not the case, the primary metamorphic event affecting the sill is probably local. The general increase toward the top of the sill may reflect proximity to the still-hot overlying granophyre. An alternative possibility is that intrusion of another nearby sill (i.e. the Paradise Sill) may have driven metamorphism, but this seems unlikely given the narrow nature of the contact metamorphic zones of the Plains and Paradise sills and the few discernible hornfels zones from the Arco 1 Paul Gibbs borehole cuttings. In the absence of another suitable and local heat source, metamorphism of the diabase is likely retrograde, driven by it own heat. Degree of metamorphism was likely dependent upon local cooling rates within the sill, with slower rates toward the top of the diabase allowing reactions to proceed further than at the chilled base of the sill. In some capacity, fluid migration through the sill aided metamorphism as quartz-epidote veinlets are common and are flanked by selvages of advanced alteration to epidote, blue-green hornblende, and biotite (Figure 19).

Green Hornblende - Blue-Green Hornblende - Biotite Reaction Sequence

Larger, more robust hornblende crystals are generally green and form the dominant fabric of the rock. Their compositions are somewhat variable with no apparent systematic variation from bottom to top of the sill (Table 3). Larger crystals

generally contain abundant inclusions of quartz. In the more altered-appearing samples, larger hornblende crystals are often very ragged with biotite intergrown parallel to the c-axis of the hornblende.

Later-formed hornblende occurs as reaction rims or overgrowths on the larger crystals (Figure 21), as smaller more elongate crystals often (though not always) nucleating on larger crystals (Figure 22), or as fine-grained mats of elongate crystals. Some larger crystals also show deeper green to blue-green pleochroic streaks parallel to the c-axis, though there is no apparent compositional change between these and the host crystal (Table 3, nos. 33-34, 35-36). Reaction rims or overgrowths and some of the elongate needle-shaped crystals, show deeper blue-green pleochroism characteristic of lower-temperature metamorphic hornblende (Miyashiro 1968, p. 799-834).

Microprobe data show a systematic compositional change of increased Al_2O_3 (up to 9.23 weight percent change), total iron-oxide (up to 3%), Na_2O and K_2O (approximately 0.5% each) and substantial decreases in MgO (up to 5.3%) and SiO_2 (up to 8.5%) between complementary cores and rims of the larger crystals showing blue-green or overgrowths (Table 3, Nos. 38-41). In cases where smaller needle-shaped crystals nucleate on larger hornblende crystals, there is a similar compositional shift but, in some instances, is less pronounced. It is not clear whether the later-formed hornblende is formed by modification of earlier-formed hornblende grains, or whether it is simply using earlier-formed hornblende as a nucleation surface and deriving its constituents from the destruction of plagioclase, from reaction with a late-stage magmatic fraction, or from reaction with a pore-water derived fluid high in dissolved major elements. A combination of all of these seems likely. Without knowing the source of the constituents of the later-formed hornblende, it is impossible to reasonably assess whether or not constituents were gained or lost during this reaction.

Contrary to the observation that the blue-green pleochroism is indicative of lower temperature metamorphic hornblende, is the fact that these compositional shifts, specifically the increase in aluminum, tend to suggest higher temperatures of formation (Liou et al. 1974; Spear 1981). A primitive aluminum in hornblende geothermometer derived from the data of Liou et al. (1974), Spear (1981) and Helz (1973) and used by Lytwyn and Casey (1995) shows an increasing temperature of formation with increasing Al(IV), or aluminum substitution for silicon in the tetrahedral sites. Although I realize that this geothermometer is not likely to directly apply to the Plains Sill, it is still worth making the point that the abundance of Al(IV) in the later-formed hornblendes puts their temperature of formation up into granulite facies and well out of reach of the upper temperature limits of co-existing epidote. Thus it is not likely that formation temperatures so much dictated the abundance of Al(IV) as did the locally available constituents.

Biotite abundance varies throughout the sill though is never more than several percent of the total rock. In general, it is more abundant in the more altered samples and is often seen intergrown with altered-appearing hornblende, though not always in blue-green hornblende (Figure 23). It is probably a further alteration product of hornblende involving the liberation of calcium and the consumption of potassium, presumably from interaction with a late-stage potassic magma fraction or circulating hydrothermal fluids.

Plagioclase-Epidote-White Mica Sequence

Destruction of plagioclase and its alteration to clinozoisite is the other highly visible aspect of the retrograde metamorphism affecting the sill. In the lower chill zone and for several samples above that, plagioclase is relatively unaffected and is seen as more pristine twinned and, in some cases, zoned crystals. In the more altered samples,

epidote is seen altering from plagioclase in varying degrees. Cores of plagioclase crystals are most often altered before their respective rims (Figure 24). Though higher calcium and aluminum contents of the cores are likely responsible for preferential alteration of plagioclase cores, there is insufficient evidence from the microprobe data to conclude this. Epidote alteration is also seen "invading" plagioclase crystals along fractures and even along twin planes.

Simplified mass-balance calculations using microprobe data from two plagioclase-epidote pairs (Table 3, nos. 4, 74; 10, 77) suggest that the plagioclase to epidote reaction requires input of external calcium, ferric iron and aluminum, and removal of sodium and silica. The following plagioclase-epidote reaction assumes 1) that plagioclase crystal volume does not change significantly during alteration, 2) the volume of epidote present in the core of a crystal is equal to the volume of plagioclase digested and 3) the densities of plagioclase and epidote are 2.7 and 3.35 respectively. As there are no cracks in the rims of plagioclase altering to epidote, an isovolumetric assumption seems valid. Since it is impossible to ascertain with certainty what other phases (if any) are also present with the epidote in the plagioclase cores, it is also impossible to determine whether or not one unit volume of plagioclase alters to one unit volume of epidote. In any case, using these assumptions, a plagioclase-to-epidote reaction is:

(Plagioclase)
$$Na_{0.35}Ca_{0.67}Al_{1.63}Si_{2.35}O_8 + 0.83Ca^{2+} + 0.24Fe^{3+} + 0.33Al^{3+} + 0.5H_2O + 2.86e^-$$

(Clinozoisite)
$$\rightarrow 0.76Na_{0.05}Ca_{1.97}(Fe_{0.32}Al_{2.58})Si_{3.01}O_{11}(OH) + 0.31Na^+ + 0.05Si^{4+} + 0.31O_2$$
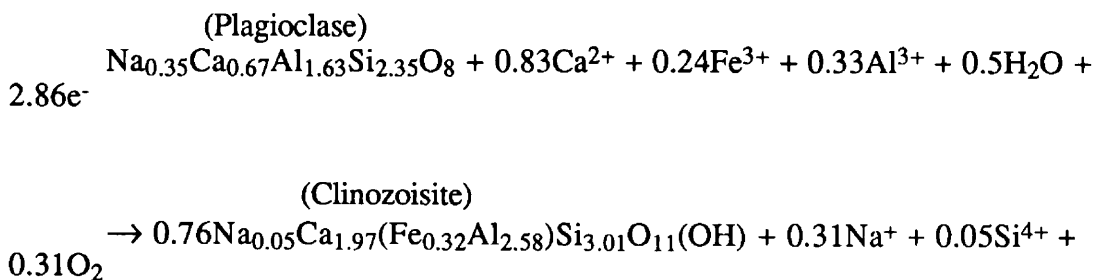
Thus it appears that the production of later-formed hornblende and epidote both require consumption of aluminum and iron. Since aluminum is not very mobile in the

fluid medium during low-grade metamorphism, this mass imbalance of aluminum is not easily resolved. Additional digestion of plagioclase, beyond that necessary for isovolumetric production of epidote, may have taken place in order to provide aluminum for the later-formed hornblende. Any further alteration of epidote or plagioclase to white mica must necessarily involve the addition of potassium. Since white mica is not at all abundant, this addition of potassium is considered insignificant.

Summary

It appears that production of the two most abundant metamorphic minerals, later-formed hornblende and epidote, are consistent with epidote-amphibolite facies retrograde metamorphism of the diabase. Reactions were apparently enhanced by the abundance of locally available water, as indicated by the presence of quartz-epidote veinlets with pervasively metamorphosed selvages. It is difficult to ascertain with certainty whether or not constituents were added or substracted from the bulk rock composition during metamorphism without better data on mineral compositions and better controls on molar quantities of products and reactants.

The extent to which retrograde reactions proceeded seems controlled in part by proximity to the still hot granophyre and in part by thickness of the diabase. Considering the absence of actinolite and the near absence of chlorite, reactions are interpreted to have stalled out before falling to the greenschist metamorphism characteristic of many mid-ocean ridge basalts (Humphris and Thompson 1978a). This may have resulted from rapid cooling in the absence of a suitable external heat source to further drive reactions.
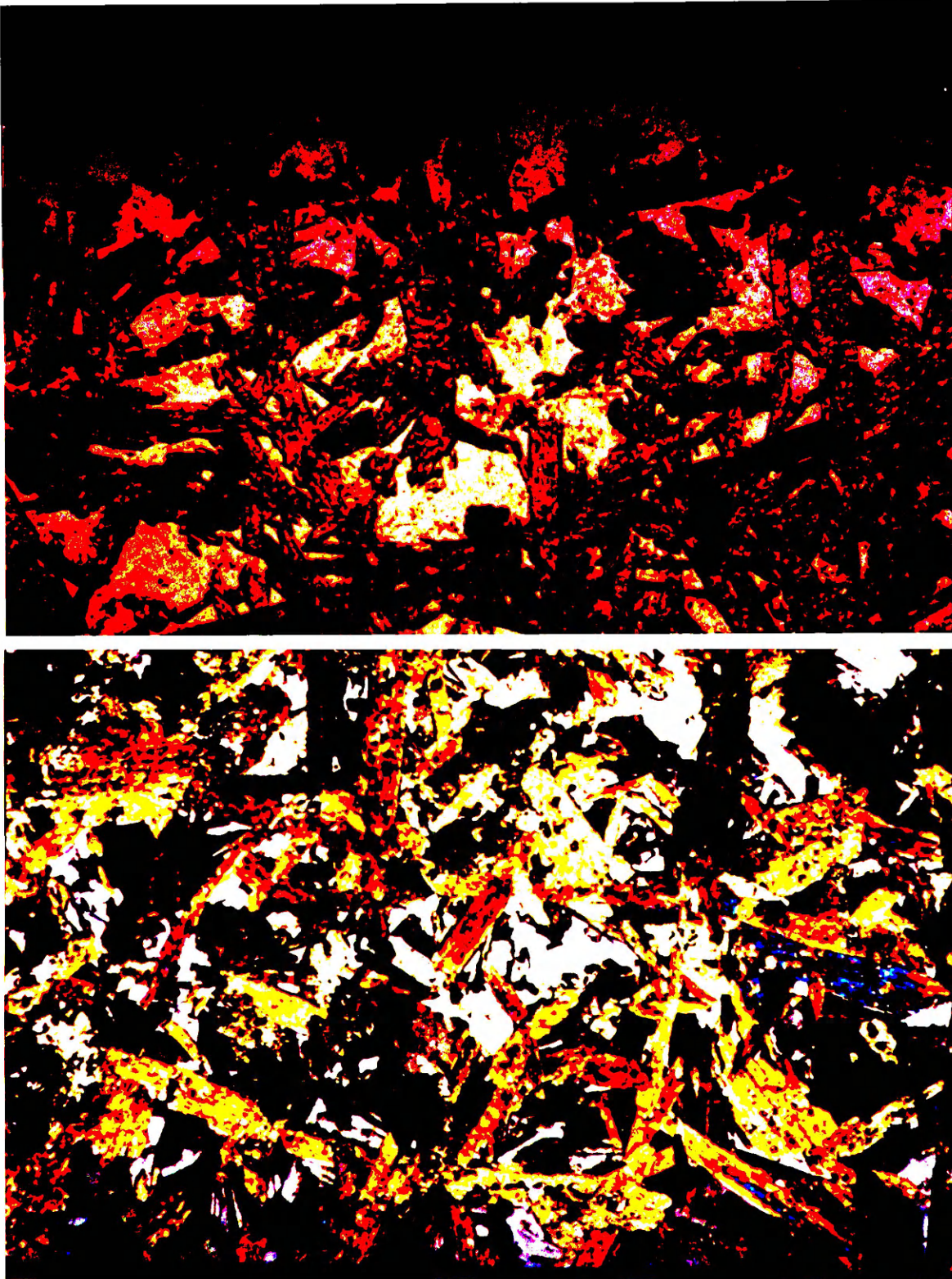
Figure 17. Less altered chill margin of the Plains Sill. 3.5mm FOV. Top: plane light, Bottom: crossed polars.

Figure 18. Highly altered diabase of the Plains Sill (3.5mm FOV).

Figure 19. Quartz-epidote veinlet with local extreme alteration (3.5mm FOV).
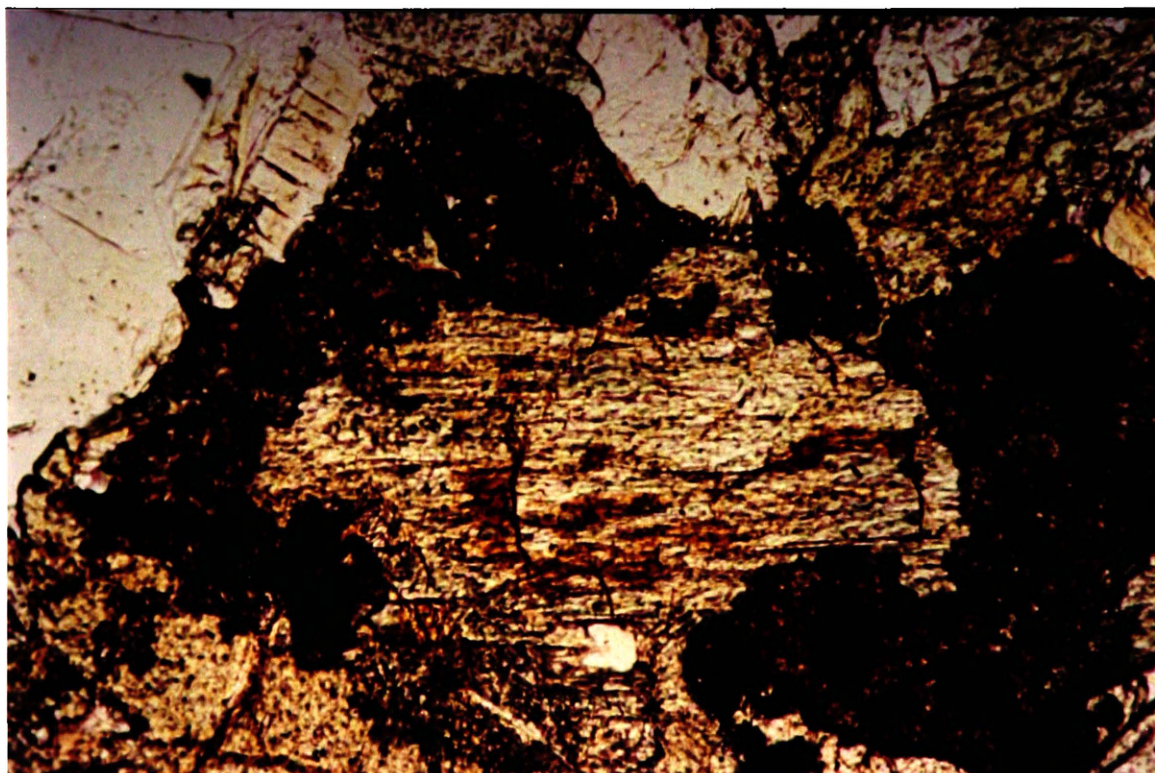
Figure 20. Ilmenite surrounded by sphene (1mm FOV).

Figure 21. Overgrowths of blue-green hornblende on green hornblende (3.5mm FOV).
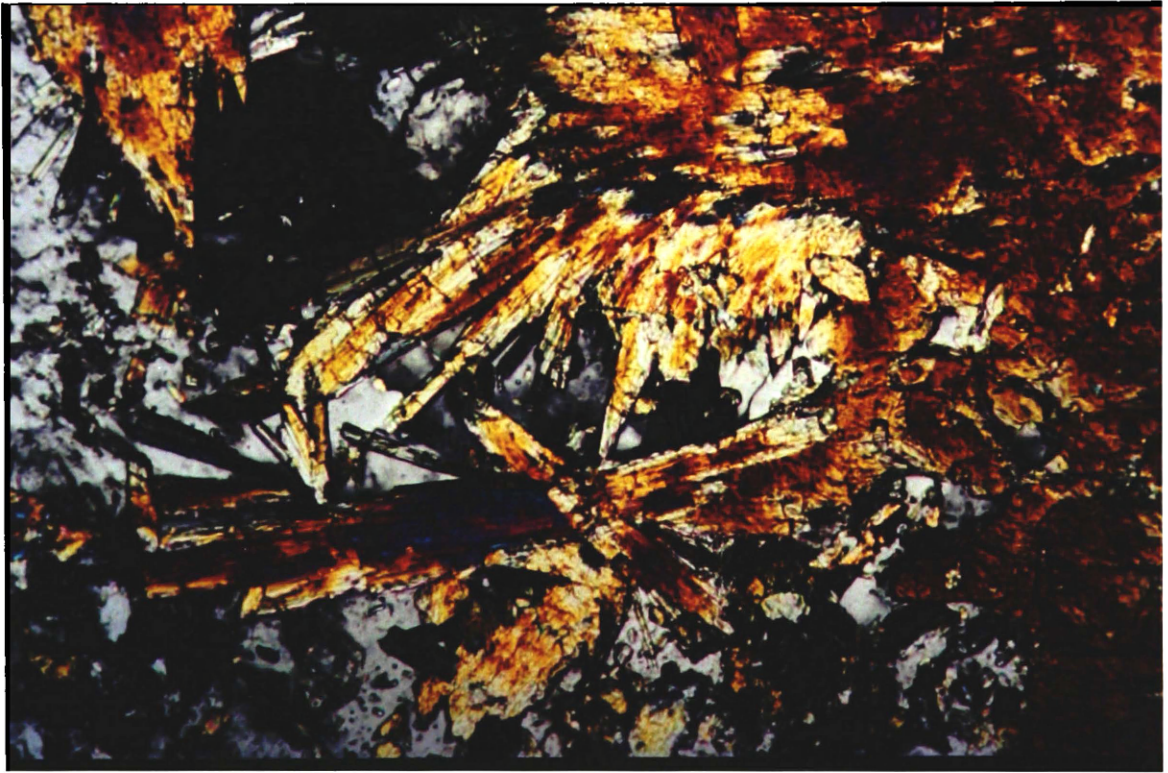
Figure 22. Later-formed hornblende nucleating on larger earlier-formed hornblende crystals (1mm FOV).

Figure 23. Biotite alteration of hornblende (1mm FOV).
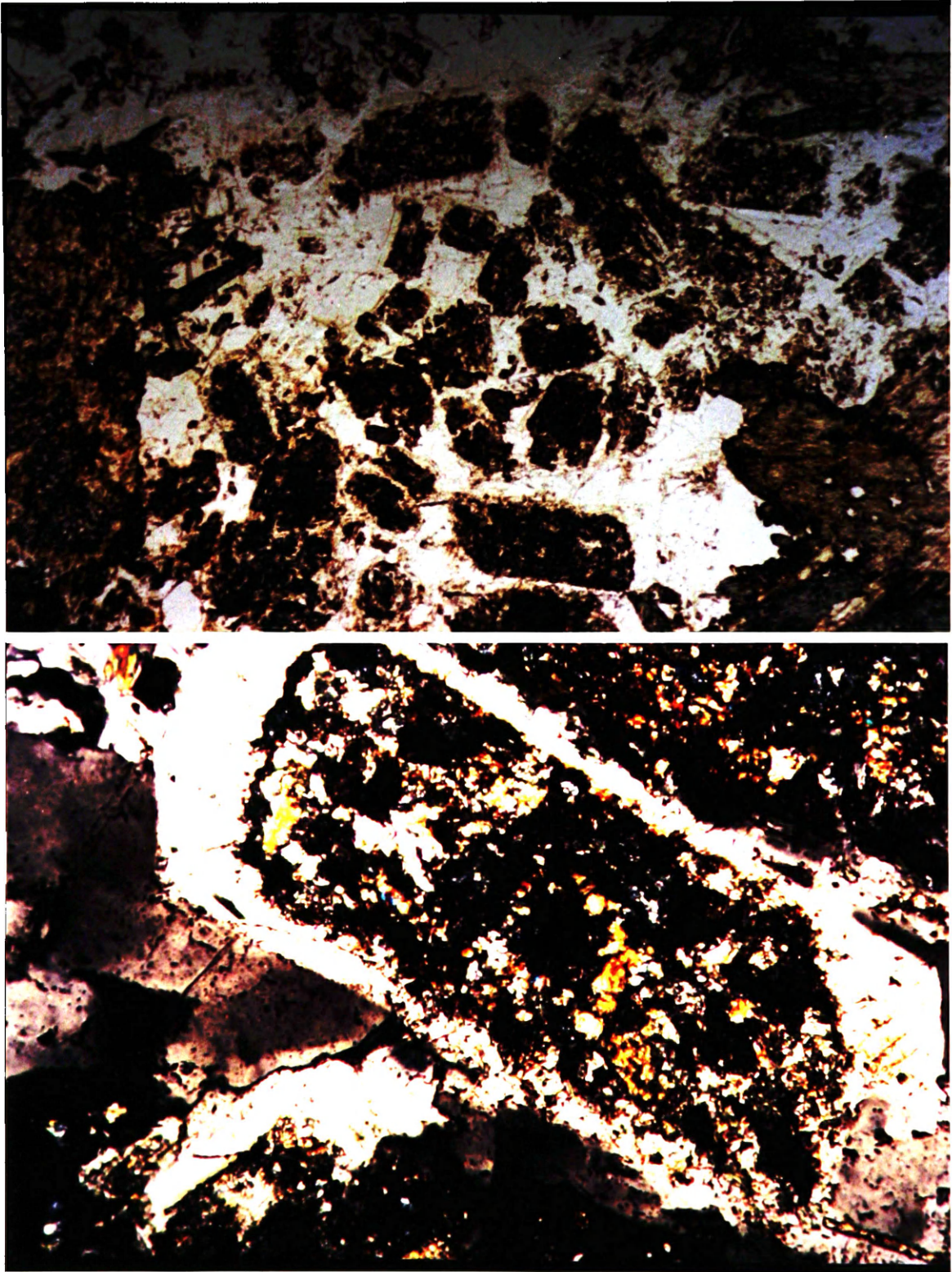
Figure 24. Epidote alteration in plagioclase cores. Top: 3.5mm FOV, plane light; Bottom: 1mm FOV, crossed polars.

Hydration of the Plains Sill Magma: An Unresolved Question

The general absence of either primary or relict pyroxene and the ubiquitous presence of hornblende in the Plains Sill raises the question, "Did pyroxene ever crystallize from the initial melt?" Though it is probably impossible to answer this question with certainty, an assessment of the likelihood that hornblende was the dominant primary mafic phase is certainly warranted. A discussion of experimental and petrographic data follows.

Experimental Data

Wones and Gilbert (1982) assert "If H_2O content were to be maintained at a level appropriate to amphibole stoichiometry (about 2 wt %) in liquids of basaltic composition, then the resulting rock would consist of more than 50 percent amphibole...Accordingly, the common lack of amphibole, particularly in gabbro but also in basalts, is due to extreme water undersaturation." Clearly, if a basaltic magma cannot dissolve enough water to satisfy hornblende stoichiometry, hornblende will not form in the early stages of crystallization. Microprobe data show that hornblendes from the Plains Sill contain approximately 3.8 wt % (OH), requiring roughly 1.9 wt % dissolved H_2O to satisfy their stoichiometry. Thus, assessment of the likelihood that hornblende crystallized as the dominant mafic phase requires assessment of the likelihood that the Plains Sill magma was able to dissolve at least 1.9% H_2O.

A number of experimental studies (Burnham and Jahns 1962; Hamilton et al. 1964; Burnham 1975) have been carried out to determine the solubility of water in various silicate melts at a variety of pressures and oxygen fugacities. The pressure required to dissolve 1.9% water into a Columbia River Basalt (50.5 wt % SiO_2) is approximately 0.55 kilobars and the pressure required to dissolve 1.9% water into a

Mount Hood andesite (58.4 wt % SiO_2) is approximately 0.25 kilobars (Hamilton et al. 1964). The typical Plains Sill diabase contains about 53.1 wt % SiO_2 and would, on the basis of composition, likely require emplacement pressures somewhere in between. Straight interpolation suggests a requisite pressure of about 0.45 kilobars.

Since dissolved water content is largely dependent on pressure, discussion of the depth of emplacement of the Plains Sill should precede estimates of dissolved water content. It is of critical importance in this case because the H_2O solubility vs. pressure curves cited in the above studies tend to flatten out as they approach zero pressure, so a small change in pressure translates into a large change in water solubility. Buckley and Sears (1993) and Höy (1989) attribute the granosediment layer and the accompanying ovoid structures to fluidization of the enclosing wet sediments, as did Krynauw et al. (1988) for similar features proximal to the Grunehogna Sill in Antarctica. A calculated critical pressure of saline seawater of 312 bars is taken by Kokelaar (1982) to be the maximum pressure at which fluidization can take place. The premises are 1) that fluidization as described by Kokelaar (1982) cannot occur above the critical pressure of seawater and 2) fluidization must occur for granosediments and ovoids to form.

I do not believe that fluidization, as described, need be invoked to create these features. Relatively rapid dewatering of high porosity sediments could likely destroy all signs of bedding on the scale of meters above the sill and ovoids could form from the more lithified fragments. Thicker sequences of granosediments may have been disturbed, at least in part, by exsolution of a supercritical fluid from the granophyric magma, a process not subject to the same pressure constraints as simple boiling of pore water (Jahns and Burnham 1969). However, if simple boiling of pore water were to have taken place, the critical pressure of seawater is probably not sufficiently high to cause dissolution of the requisite amount of water into the mafic magma.

Note also that fluid overpressures within fine-grained sediments can exist to depths of several kilometers and can persist for tens or even hundreds of millions of years (Hunt 1979). Thus, it is possible that the Plains Sill intruded at pressures greater than 312 bars and that the soft-sediment deformation features caused by sill emplacement, may not require presumed near surface conditions. In this case, pressures may be high enough to dissolve considerably more water into the basaltic magma, facilitating the crystallization of primary amphibole.

Mudge (1968) reviewed field data from the western United States, and showed that emplacement depths of concordant intrusions were generally restricted to between 3000 and 7500 feet (approximately 900-2275 meters). A priori knowledge of rock densities and the presence or absence of an overlying ocean of given depth is required to translate this data into a range of emplacement pressures. In any case, the emplacement pressure is likely to be significantly less than one kilobar. In terms of assessing the likelihood of hornblende crystallizing as the primary mafic phase, this is clearly an inadequate estimate, as the range of possible pressures yields possible dissolved water contents spanning the desired 1.9 wt % threshold. There are no surficial features of comparable age within the overlying Belt stratigraphy with which to adequately constrain emplacement depth. Further refinement of this estimate would require conjecture beyond that with which I am comfortable.

Another way of looking at the problem is to consider at what pressure-temperature conditions hornblende can exist in equilibrium with a basaltic melt under water-saturated conditions. Clearly if the hornblende stability field in pressure-temperature space does not overlap with melt conditions, then hornblende cannot crystallize as a primary phase. A review of hornblende stability experiments by Helz (1982) shows no low-pressure experimental data at condition $P_{H_2O}=P_{total}$ for tholeiitic basalts. Stability fields are extrapolated from higher temperatures (Figure 25). The

size of the stability field is also dependent on oxygen fugacity and the degree of silica-saturation in the magma. Silica-saturated magmas, such as the Plains Sill, have smaller hornblende stability fields. This has the effect of increasing the pressure below which hornblende cannot exist in equilibrium with melt. Though a definitive answer does not emerge from existing experimental data, present data for silica and water-saturated basaltic magmas suggest that hornblende cannot exist in equilibrium with a tholeiitic, silica-saturated melt at pressures much below 1 kilobar (Figure 25). Even if hornblende could exist stably with the melt, the convergence of the hornblende stability line and the low-pressure solidus line severely restricts the temperature range over which it could actually crystallize.

With regard to experimental data, note that it is not clear that the requisite 1.9% water must actually be dissolved in the melt for hornblende to crystallize. For example, water saturation lowers viscosity and consequently enhances diffusion rates. Since hornblende would be the only hydrous phase crystallizing in significant quantities, and it comprises roughly 60% of the rock, perhaps only 60% of the presumed 1.9% of the water need be dissolved. And if excess water were present, but not necessarily dissolved, could the dissolved water, taken up by hornblende, be replenished only to facilitate further crystallization of hornblende? To the best of my knowledge, these scenarios are not adequately addressed in the experimental literature and may offer alternative perspectives on the situation.

Though one might construe a very specific set of conditions under which hornblende could crystallize as the dominant mafic phase at low pressures, based on existing experimental data, it would be pleading a special case to presume that it actually did. Examination of cuttings from the thirteen mafic sills encountered in the Arco 1 Paul Gibbs borehole in northwestern Montana shows that all but one contain no pyroxene. The Paradise and Whiskey Gulch Sills also contain no pyroxene or relict

pyroxene and descriptions of the Crossport Sills (Bishop 1974) and the Moyie Sills (Höy 1989) report none either. Relict pyroxene is supposedly found toward the center of one of the thicker Moyie Sills in the Kimberly area of southeastern British Columbia (R. J. W. Turner, personal communication 1994). Thus, special conditions invoked for the Plains Sill would have to be extended to almost all occurrences of mafic igneous rocks in the lower Belt, a tenuous scenario at best.

Petrographic Data

Examination of the finer-grained chill zones from the top and bottom of the Clear Creek sections and the bottom of the Three Lakes Peak Trail section show relatively unaltered-looking hornblende and plagioclase with few blue-green hornblende overgrowths or clusters of finer-grained needle-shaped hornblende crystals, and almost no epidote. It seems unlikely that, if pyroxene had been the primary mafic phase, chilling of the marginal zone of the sill would allow retrograde metamorphic reactions to uniformly proceed just to the point of complete recrystallization of clinopyroxene to hornblende and no further. A more plausible scenario is that the chill margins have experienced relatively little metamorphism in the course of cooling, and that the hornblende present is in fact primary hornblende.

Whereas experimental data restrict the probability that hornblende crystallized as the primary mafic phase, petrographic information and the mineralogy of the sill suggest that it may well have. However, the argument that any conclusion drawn for the Plains Sill must be extended to most other mafic igneous bodies in the lower Belt, applies here as well. It seems equally unlikely that primary pyroxene is so consistently altered to hornblende as it is that emplacement conditions were uniformly such that primary hornblende could crystallize from the melt.

Thus the question of hydration of the Plains Sill magma and dominant crystallization of primary hornblende is not easily resolved as neither enough experimental data at low pressures is available, nor are the conditions of emplacement of the Plains Sill well enough established. Both scenarios seem equally plausible or implausible depending on how one chooses to view the situation.
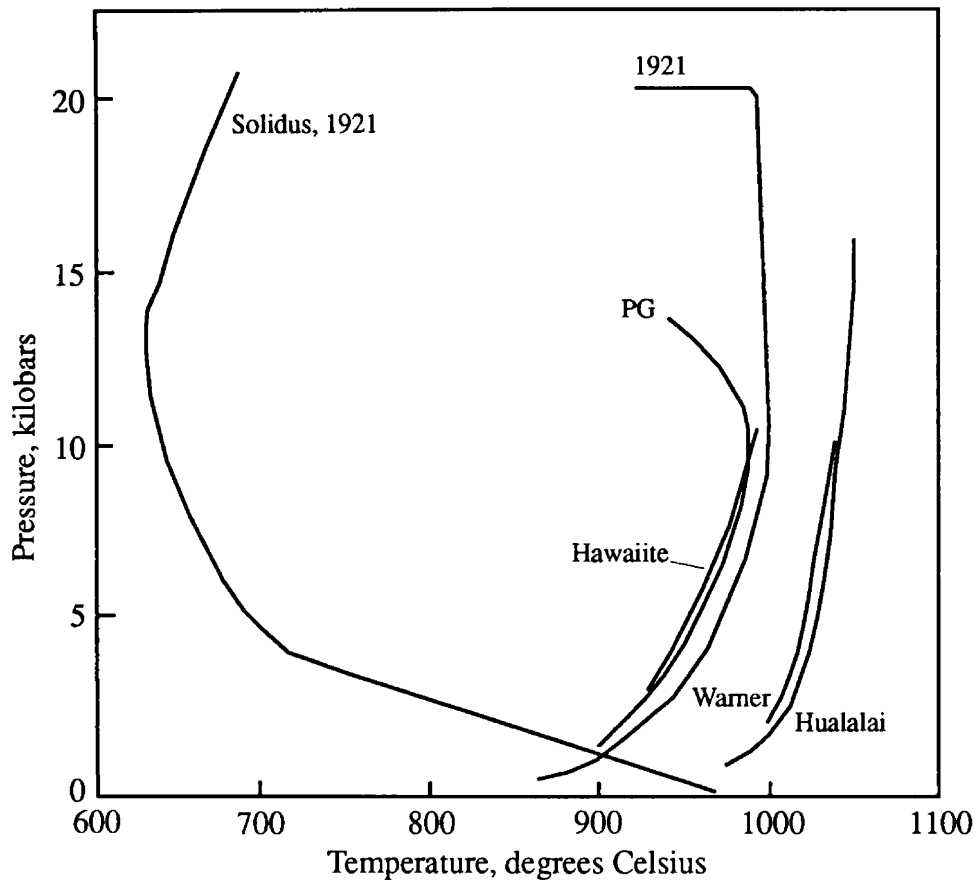
Figure 25. Amphibole-in curves for various basalts at $P_{H2O}=P_{total}$
(from Helz 1982). Redox condition is controlled by the HM buffer.
Solidus 1921 refers to the 1921 Kilauea olivine tholeiite eruption.
PG=Picture Gorge tholeiite, 1921=1921 Kilauea tholeiite, Hawaiite=
oxidized hawaiite, Warner=Warner high-alumina basalt, Hualalai=
Hualalai alkali basalt.

Origin of the Granophyre

Origin of granophyre and its relationship to gabbroic intrusions is, historically, a much debated question in petrology. There are numerous occurrences where gabbro-granophyre proportions are reasonable for igneous differentiation processes such as crystal fractionation, filter-pressing, liquid immiscibility or a combination of these (i.e. Hotz 1953; Walker 1958; McBirney and Nakamura 1974; McBirney 1975). However, in many gabbro-granophyre bodies, there is a disproportionately large volume of granophyre, requiring explanation by other processes. A brief and certainly incomplete survey of the literature shows a number of reported possibilities including partial melting of the country rock adjacent to the intrusion contact (Walraven 1985), pervasive contact metasomatism of country rock (Augustithis 1982a), localized collection of a late-stage magmatic differentiate (Ernst 1960), assimilation of country rock into a late-stage magma fraction (Blackadar 1956), and simple fusion of country rocks (Smith and Silver 1975; Hawkes 1929).

In assessing the origin of the granophyre, it is of primary importance to determine whether the granophyric rocks are derived from the country-rock sediments or from the diabase magma and of secondary importance to assess which processes likely dominated during formation. A number of techniques have been used to this end with the majority of studies using field evidence and geochemical analyses. Other researchers have used a variety of isotopes including sulfur (Sasaki and Smith 1979) and rubidium-strontium (Walraven 1985) and other techniques including zircon distribution and morphology (Poldervaart 1956) and phenocryst analysis (Bruiyn 1975). Geologists from the Geological Survey of Canada (T. Höy; R. J. W. Turner, personal communication 1994) believe that the granophyre accompanying the sill

underlying the Sullivan Deposit, is of metasedimentary origin. I assess field,

geochemical and rubidium-strontium data in addressing this question.

Strontium Isotopes

Two samples each from the diabase, granophyre, granosediments and

sediments at the Three Lakes Peak Trail section were analyzed for strontium isotopes

(Table 2) in an attempt to show an isotopic affinity of the granophyre for either the

diabase or the overlying granosediments and sediments. In the case where the

granophyre represents a differentiated fraction from the basaltic magma, it should retain

the same initial $^{87}Sr/^{86}Sr$ ratio as the diabase and should lie on the same isochron. In

the case where the granophyre is sediment-derived, it should retain the same initial

$^{87}Sr/^{86}Sr$ ratio as the sediments and granosediments and lie on a different isochron

from the diabase. Figure 26 shows a whole-rock isochron diagram for all samples. As

all eight samples lie on the same isochron and since it is unlikely that the sediment and

granosediment are derived from the diabase magma, it appears that all samples

equilibrated with respect to initial $^{87}Sr/^{86}Sr$ ratios during emplacement or subsequent

hydrothermal activity.

The initial $^{87}Sr/^{86}Sr$ ratio of 0.707024 appears somewhat higher than typical

basalt values and somewhat lower than values for common sedimentary rocks, though

it is not out of the acceptable ranges for either (Faure 1986, p. 117-140). One of two

mechanisms for homogenization of initial strontium ratios seems likely. Contamination

of the diabase magma by enclosing sediments is one possibility. This would lower the

abundance of strontium in the diabase magma as the sediment and granosediment range

from 23-69 ppm strontium and the diabase averages about 100 ppm strontium. Indeed,

compiled strontium abundances (Hyndman 1985, p. 205) from various basalts types

are all far greater than the approximately 100 ppm in the Plains Sill diabase (Tables 5,

7). However, abundances of major oxides suggest that, if the diabase magma was contaminated with sediment, it probably was not contaminated with much, otherwise the bulk composition of the diabase would stray more significantly from that of normal basalt.

The other possibility is that initial ratios between diabase, granophyre and sediment were equilibrated through post-crystallization hydrothermal action and exchange of strontium between rock types. Circulation of hydrothermal fluids would not necessarily equilibrate strontium abundances amongst rock types but may result in sufficient exchange to homogenize $^{87}Sr/^{86}Sr$ ratios. In the process, an uncertain amount of strontium may have been lost from the diabase, producing the unusually low Sr values as compared with typical basalts. Thus basalt discrimination diagrams using strontium as an "immobile" trace-element might be viewed with suspicion (Figure 31).

Though the $^{87}Sr/^{86}Sr$ data do not provide evidence as to whether the granophyre is magma or sediment derived, the data are not without implications. They show that thick basaltic sills may generate hydrothermal systems capable of homogenizing strontium ratios on the scale of hundreds of meters. Numerous studies have been done using strontium isotopes to assess the genesis of various igneous rocks, and several have used initial ratios to assess the origin of granophyre associated with basaltic rocks (i.e. Walraven 1985; Kalsbeek and Jepsen 1983). To the best of my knowledge, none shows such a clear example of initial-ratio equilibration with the country rocks during sill emplacement into wet sediments.

The whole-rock isochron age (1200±94 Ma) for the strontium data is interesting as well. It does not correspond with published U-Pb (zircon) dates of about 1445 Ma (Höy 1989) from Moyie Sills in southeastern British Columbia, a U-Pb (zircon) age of 1433 Ma from granophyre in the Crossport C Sill (Zartman et al. 1982), or other similar U-Pb dates on zircon from the lower Belt igneous rocks (reviewed in Burwash

1993). This suggests that $^{87}Sr/^{86}Sr$ values were either fully reset back to initial values at approximately 1200 Ma, or partially reset at some unspecified time thereafter. It is possible that $^{87}Sr/^{86}Sr$ ratios were reset during a later magmatic event within the Belt at 1120-1130 Ma (Wooden et al. 1978). With radiogenic ^{87}Sr residing preferentially in the potassium/rubidium-bearing minerals, in this case principally biotite and muscovite, respective closure temperatures of ~320°C and ~500°C (Ghent et al. 1988) put an upper temperature constraint on any post-1200 Ma thermal/metamorphic events. No attempt is made here to further quantify this observation.

Sediment-Derived Possibilities for Origin of the Granophyre

In the case of the Plains Sill, most sediment-derived possibilities for the origin of the granophyre can be eliminated by field relations, geochemical evidence or thermal considerations. Pervasive contact metasomatism of Prichard sediments is unlikely as there is little compositional change and no textural change in the granophyre with distance from the diabase. In addition, there is no correlation between the thickness of the diabase (and hence, the amount of available heat) and the thickness of the granophyre. Simple fusion of pelitic composition Prichard sediments can be eliminated on the same grounds, as well as by the fact that there are no relict sedimentary features in the granophyre.

Assimilation of sediments into a late-stage magmatic differentiate is equally unlikely because of the sharp textural and composition contacts between diabase and granophyre and between granophyre and granosediments. In addition, the heat required to raise the contaminating sediment to melt temperatures, as well as the heat of fusion required to actually melt them, would likely cool and crystallize the late-stage magma fraction before substantial assimilation could take place.

The argument can be made that perhaps the granophyre is simply an advanced, coarser-grained version of the thick overlying granosediment. This is unlikely for several reasons. First, the distinct (albeit minor) chemical differences between the two, coupled with the fact that each is close to internally homogeneous, suggests different source material. Second, the sharp textural (grain size) contact between granophyre and granosediment, coupled with the internal consistency of grain size, suggests that they formed form different processes. One might counter-argue that the coarser grain-size of the granophyre reflects its proximity to the sill, though this should produce a gradation of decreasing grain size away from the hot diabase and a gradational textural contact with the granosediment. Third, the pervasive alteration of the granosediment matrix to white mica suggests loose consolidation and pervasive exposure to altering hydrothermal fluids, while the relative lack of such in the granophyre is consistent with crystallization as a relatively impenetrable rock and thus less exposure to altering fluids.

Melting or partial melting of country rock is unlikely as contact metamorphic assemblages do not indicate sufficiently high temperatures, nor is there any evidence of partial melting remnants in the sediments. The mineralogy of the granophyre does not indicate a ternary minimum partial melt from Prichard metasedimentary rocks as alkali feldspars are not present. This could be an artifact of metamorphism though if original alkali feldspars were strongly albitized during post-crystallization metamorphism. Chemically, the granophyre does fall within acceptable range of ternary minimum melts. It is not clear on what scale the composition of Prichard sediments varies, nor is it clear exactly if or how the few analyzed sediment samples proximal to the sill (71501, 71502, 72019, 72020, B.S. I, B.S. II, 72755, 72756) have been compositionally altered. In no case, however, does the composition of the granophyre match the composition of the enclosing sediments, indicating that the granophyre likely did not

result from wholesale melting of sediment and migration of resulting magma to form a sharp interface with the granosediments.

In addition, simplified heat flow modeling in the vicinity of cooling intrusive sheets (Jaeger 1968) shows that under dry conditions, where conductive heat flow between sill and country rock dominates, the highest contact temperature is approximately half the temperature of the heat source. In the case of intrusion of a 1200°C diabase magma into wet sediments, where sediment-pore water is likely to convect heat quickly away from the sill-sediment contact, it is unlikely that contact temperatures would reach ternary minimum temperatures of just under 700°C in the quartz-albite-orthoclase system at 2 kilobars P_{H_2O} (Hyndman 1985, p. 309). Compounding this is the fact that the minimum melt temperature for granite under water saturated conditions, increases sharply at pressures below two kilobars, so that contact temperatures may have to reach upwards of 800-900°C to induce melting (Hyndman 1985, p. 311). A scan through the literature shows no cases where basaltic sills are reported to induce wholesale melting of country rock. Even the thicker gabbroic layered intrusions emplaced at relatively shallow levels rarely induce significant melting of the country rock.

Diabase Magma Derived Possibilities for the Origin of the Granophyre

Though there is strong circumstantial evidence that the granophyre is not of sedimentary origin, this does not mean that one can immediately default to the alternative hypothesis, which is that the granophyre is of magmatic origin and ultimately derived from the diabase magma. However, abundance of miarolitic cavities, the presence of well developed granophyric intergrowths and the granophyre inclusions in the overlying granosediments is taken as strong evidence that the granophyre was, at one time, molten. Its location, without exception, is either at the

top of the diabase or sandwiched between the lower diabase and a relatively thin upper diabase, suggestive of a genetic relationship. Inherent in addressing the diabase-derived options for the origin of the granophyre, is discussion of the differentiation of the diabase. The question then becomes, what magmatic process was dominantly responsible for its formation? Various models for magmatic differentiation have been proposed through the history of petrologic research, including liquid immiscibility, crystal fractionation, filter-pressing, and volatile transfer.

Liquid Immiscibility. Field and geochemical evidence including the relatively homogeneous diabase magma, the typically sharp, concordant compositional boundary between diabase and granophyre and the existence of felsic segregations and veinlets within the diabase, is immediately suggestive of liquid immiscibility, followed by accumulation of the separated liquid. Under certain conditions, magmas will separate into two immiscible phases and indeed varying quantities of immiscible interstitial glass are present in many basalts (Roedder 1979). Philpotts (1979) reports that immiscible silica-rich liquids comprise at least 32% of a single tholeiitic basalt sample from Southbury, Connecticut.

Experimental work by Philpotts (1976, 1979, 1982) shows the presence of significant immiscibility fields on the SiO_2 - $(Na_2O+K_2O+Al_2O_3)$ - $(TiO_2+FeO*+MnO+MgO+CaO+P_2O_5)$, SiO_2 - $(Na_2O+K_2O+Al_2O_3+MgO)$ - $(TiO_2+FeO*+MnO+CaO+P_2O_5)$ and the standard FMA ternary diagrams at temperatures appropriate to basalt crystallization. The point in the crystallization history at which immiscible separation occurs depends largely upon oxygen fugacity and the point at which magnetite crystallizes out of the melt. Based on the shape of the immiscibility field, iron-enrichment, typical in differentiation of tholeiitic magmas, enables the residual magma to intersect the immiscibility field earlier during

crystallization (Philpotts 1990, p. 252), thus increasing the likelihood of significant immiscible separation. Calc-alkaline basalts, which typically do not undergo iron-enrichment, are less likely to separate because a greater proportion of the original magma will have crystallized by the time the residual magma reaches the immiscibility field.

Iron-enrichment trends are thought to reflect the low oxygen fugacity caused by generally low water contents in tholeiitic basalts. In the case of the Plains Sill, where water contents were probably at saturation level, producing higher oxygen fugacity, magnetite is likely to have crystallized early, thus minimizing iron-enrichment and reducing the likelihood of encountering the immiscibility field with any significant volume of remaining magma. Under dry conditions, tholeiitic basalts can split after approximately 70% crystallization (Philpotts 1990, p. 253), already enough to inhibit physical separation of the two immiscible fractions. With only minor iron-enrichment brought on by higher oxygen fugacity (from increased dissolved water content), significantly more of the parent magma would have to crystallize before reaching the immiscibility field, both reducing the volume of immiscibly separated granitic magma and compounding its inability to physically separate.

In addition, experimental data show that certain elements are strongly partitioned into either the felsic liquid or the iron-rich liquid. For example, TiO_2, Al_2O_3 and P_2O_5 show very strong partitioning into the iron-rich phase (Philpotts 1982). Comparing relative abundances between the Plains Sill diabase and granophyre, TiO_2 is about equally partitioned between diabase and granophyre, Al_2O_3 is slightly higher in the diabase and P_2O_5 is strongly partitioned into the granophyre. These distributions are not immediately suggestive of liquid immiscibility. There is also no evidence of the existence of the iron-rich liquid.

So, whereas field evidence suggests that liquid immiscibility may have played an important role in the formation of the granophyre by separating a granitic liquid from the basaltic magma, this conclusion is not entirely compatible with present experimental data. It should be noted though, that the available experimental data was at different conditions than those for the emplacement of the Plains Sill. Factors not adequately addressed in the literature are the effects of high water contents on the shape and size of the immiscibility field and the degree to which water saturation might enhance the ability of the silica-rich liquid to physically separate by lowering magma viscosity. If water saturation increased the size of the immiscibility field such that the original magma composition was close to its boundary, perhaps early immiscible separation could have produced the relatively uniform diabase composition as well as a significant amount of granophyric magma. In this case, the immiscibility field would have to be sufficiently altered in shape so as to have the diabase and the granophyre representing the two immiscible compositions. It is not clear what effect water-saturation would have on the partitioning of TiO_2, Al_2O_3 and P_2O_5 between the silica and iron-rich phases.

Fractionation by Crystal Settling. The Plains Sill diabase at the Three Lakes Peak Trail section shows weak upward differentiation trends of increasing SiO_2, TiO_2, FeO, Na_2O and P_2O_5 and decreasing MgO and CaO. These major-oxide trends, although rather subdued, are typical of those attributed to crystal fractionation of tholeiitic magmas. Chromium and nickel have a known affinity for mafic phases and show pronounced upward decreasing trends. Both the major-oxide and trace-element trends are similar to the more strongly differentiated underlying Paradise Sill. It is not clear whether the difference in degree of differentiation between the Plains and Paradise Sills reflects different magmatic processes or different conditions of emplacement.

Whereas it appears that crystal settling may have taken place to some degree in the Plains Sill, the weak chemical trends and sharp compositional boundary suggest that it probably did not produce significant quantities of granophyric magma. Were all the early formed mafic phases and plagioclase crystals to have settled to the bottom of the sill, the next generation of crystals would have to form in equilibrium with a new composition of melt. Given the composition of hornblendes and plagioclase at the bottom of the diabase relative to the overall composition of the sill, and assuming no subsequent compositional alteration, the residual magma would have enriched rapidly in silica and more pronounced fractionation trends would likely result, as in the Paradise Sill. Though trends of most major-oxides and trace-elements are compatible with the formation of granophyre by fractional crystallization, iron and silica are not. Iron, which is seen increasing upward in both the Plains and Paradise Sills, is noticeably depleted in the granophyre relative to the diabase. Silica, which increases by only 1 wt. % from the bottom to the top of the sill, is markedly higher in the granophyre. Thus it is not likely that fractionation by crystal settling alone generated significant quantities of granophyric magma.

Filter Pressing. Bishop (1974) invokes filter pressing to explain an anomalously thick granophyre layer at the top of one of the stratigraphically equivalent Crossport Sills. In situ crystallization and the simultaneous development of a silica-rich mesostasis would overcome the difficulty of forming significant granophyric magma while displaying only weak differentiation trends within the diabase. Complete filter pressing or simply a density driven rise of this residual magma might produce the sharp diabase-granophyre compositional contact at the Three Lakes Peak Trail and Seepay Ridge Sections and partial separation could produce the gradational contact seen at the Clear Creek section. Blebs of granophyric magma within the diabase could form from

coalescence of interstitial droplets prior to crystallization. Veinlets of granophyric magma could form if the crystallized surrounding rock was rigid enough to channel migrating granophyric magma. What filter-pressing can't immediately account for are the strong nickel and chromium trends, though perhaps an initial phase of crystal settling followed by largely in situ crystallization could produce both these trends and the other weaker differentiation trends.

Volatile Transfer. Transfer of constituents by upward moving volatiles (pneumatolitic action) is another process probably acting upon the Plains Sill. Coarse-grained vein-like structures (Figure 7) are present within the diabase and suggest transport of constituents in a volatile medium. Though the granophyric veinlets within the diabase do not necessarily require transfer of constituents in a water-dominated fluid medium, they can certainly arise from such a process. The problem then becomes constructing a scenario whereby granitic components are dissolved in a fluid medium and transported to the top of the diabase magma to form granophyre.

The volatile transfer process necessarily involves dissolution of granitic constituents into a water-dominated supercritical fluid. The primary constituents in the granophyre are SiO_2, Al_2O_3, FeO, Na_2O and K_2O - essentially the primary constituents in granites and pegmatites. Quantitative modeling of this volatile transfer process is not within the scope of this paper despite an abundance of literature concerning dissolved constituents in supercritical fluids (i.e. Wasserburg 1958; Anderson and Burnham 1965; Currie 1968; Woodland and Walther 1987; Walther and Woodland 1993). There are too many poorly constrained variables both in the experimental data and in the specific case of the Plains Sill to make a quantitative determination. In some capacity, we already know that supercritical fluids can dissolve sufficient constituents to crystallize significant quantities of granitic rock. Indeed this is the very essence of

pegmatite genesis. Using supercritical pegmatitic fluids as a conceptual model, two scenarios involving transfer of granitic constituents in a water-rich fluid medium may pertain to the Plains Sill.

If initial crystallization of the silica-saturated diabase magma produced a more granitic residual melt, heated pore-waters passing upwards through the sill may dissolve enough of these granitic constituents to separate significant quantities of granophyre material from the diabase. The resulting fluid would be very much like pegmatitic fluid exsolving out of water-saturated granitic melts in that the primary component of the fluid is water and there are enough dissolved constituents to produce a significant amount of granitic rock upon cooling or pressure release. Alternatively, if the original magma itself was water-saturated beyond the stoichiometric requirements of primary mineral phases (be they clinopyroxene or hornblende), water build-up in the late stage, more felsic magma fraction may result in exsolution of a pegmatite-like supercritical fluid.

The former scenario does not require dissolution of significant water into the diabase magma, whereas the latter scenario does not require significant post-crystallization interaction with heated pore-waters. A combination of these two alternatives is possible. It is unlikley that heated pore-water dissolved much in the way of granitic constituents from the sediments as temperatures distal from the sill were probably not high enough. In both cases, the pegmatite-like fluid, once separated from the diabase, is free to migrate up-dip and accumulate as long as it stays fluid.

Migration and accumulation would no doubt be enhanced by the fluid's relatively low viscosity. Figure 27 shows a conceptual model whereby either pore water from the initially wet Prichard sediments dissolves granitic constituents as it passes upwards through the sill and is heated, or a water-saturated diabase magma exsolves a water-rich fluid high in dissolved granitic constituents. This fluid then

migrates up-dip where the sill cuts up-section from the Prichard D to the the Prichard E and accumulates to form the anomalous thicknesses of granophyre higher in the section. Volatile transfer of constituents, as described, probably took place in some capacity during emplacement of the sill and interaction with sediment pore-water. However, it remains unclear the extent to which volatile transfer actually contributed to the formation of the granophyre.

All the major-oxide trends and most of the trace-element trends in the Plains Sill are not problematic to the volatile transfer model. Indeed, removal of granitic constituents may serve to subdue geochemical trends within the Plains Sill as opposed to the Paradise sill. Amongst the trace-elements, chromium and nickel trends are the strongest and warrant discussion. Chromium, which is used in some basalt discrimination diagrams (i.e. Garcia 1978), is found to be immobile at least during low-grade metamorphism of oceanic basalts (Humphris and Thompson 1978b) though other studies have shown it to be mobile under certain conditions (Augustithus 1982b). It is not clear how chromium behaves at higher temperatures. Empirical data from oceanic basalts (Humphris and Thompson 1978b) and experimental data at 200°C and 500 bars (Bischoff and Dickson 1975) both show that minor but significant amounts of nickel mobilize into circulating water-rich fluids under low-grade metamorphic conditions. Nickel is also found to be mobile in saline supercritical fluids between 550°C and 750°C (Fahlquist and Popp 1987). Thus the possibility that the chromium and nickel trends result from high-temperature volatile transfer processes is not ruled out.

Summary. Field and geochemical evidence suggest that the bulk of the granophyre is not derived directly from the enclosing Prichard sediments, though some contamination by sediments may be reasonably expected. Rather, it appears that the

granophyre resulted primarily from magmatic processes and is derived from the original Plains Sill magma.

A model for differentiation of the diabase to produce granophyre magma cannot be established with certainty as it is not clear the degree to which crystal settling, liquid-immiscibility, filter-pressing or volatile transfer enabled separation of a granitic magma or fluid. Crystal settling and liquid immiscibility seem the least likely to have contributed much to the formation of the granophyre. Filter-pressing may have contributed significantly though in the case where a water-rich granitic interstitial fluid forms in the latest stages of crystallization and is subsequently separated from the diabase, it is not clear at what point filter-pressing and volatile transfer merge into the same process. Transfer of granitic constituents by dissolution into upward migrating fluids heated by the sill could explain separation of diabase and granophyre as well as the subdued geochemical trends in the diabase. Though this process is probably the hardest to quantify and the least understood of the magmatic processes, it may be able to explain the most. In any case, separated granophyric magma likely migrated up-section along the top of the sill where the sill climbed up-section from the Prichard D to the top of the Prichard E. Accumulation in the Prichard E produced anomalously thick granophyre layers whereas migration from the Prichard D left little or no granophyre.

Sample	Rock Type	87Sr/86Sr	2 Sigma	Sr ppm	87Rb/86Sr	Rb ppm
72705	Diabase	0.71602	0.000127	98.2	0.561	19
72718	Diabase	0.718652	0.000036	113	0.763	29.9
72730	Granophyre	0.772491	0.000029	82.5	3.84	109
72737	Granophyre	0.775578	0.000015	77.4	3.93	105
72746	Granosediment	0.831605	0.000014	56.9	7.43	144
72752	Granosediment	0.906153	0.000016	40.5	11.7	160
72755	Sediment	0.882732	0.000021	27.8	9.43	89
72756	Sediment	0.900389	0.000019	24	11.7	95.5

Table 2. Strontium data for samples from the Three Lakes Peak Trail section. All analyses performed by Dr. Kurtis Kyser of the University of Saskatchewan.
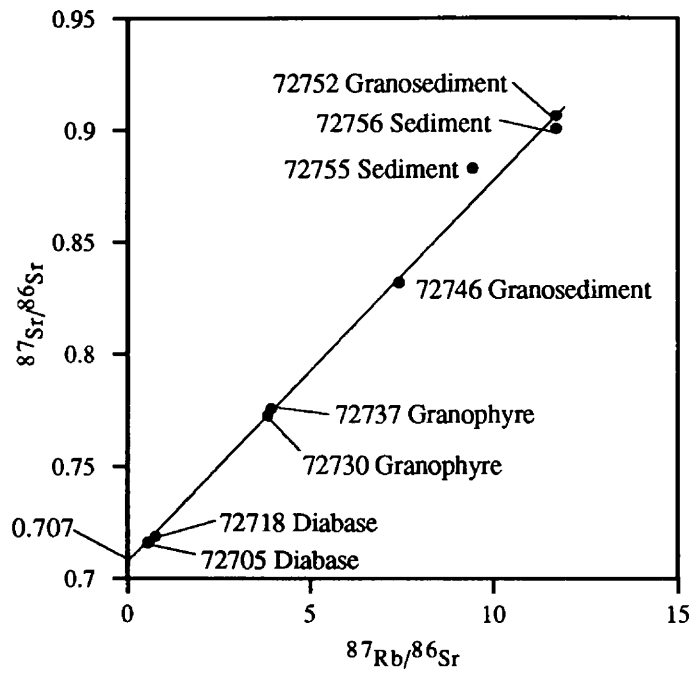
Figure 26. Rubidium-strontium whole-rock isochron diagram for diabase, granophyre, granosediment and sediment samples from the Three Lakes Peak Trail section. Initial strontium ratios were homogenized during hydrothermal activity following sill emplacement. The isochron age is 1200+/-94 Ma.
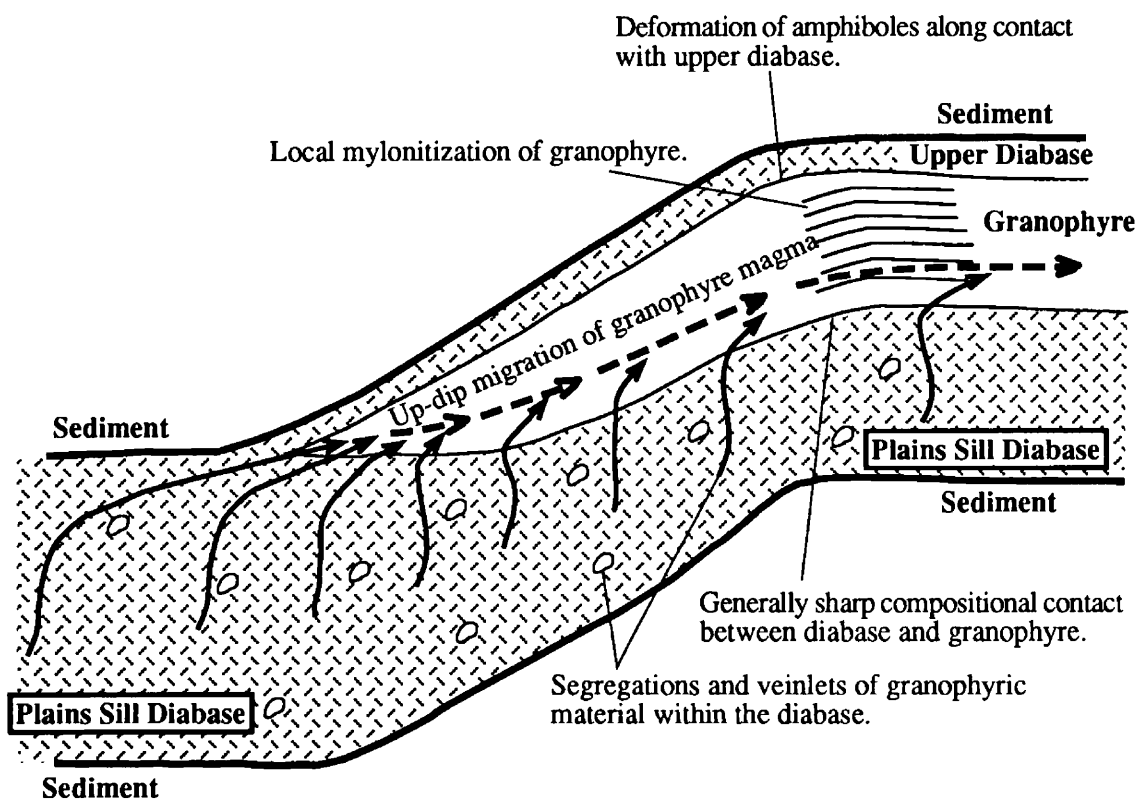
Figure 27. Conceptual model for the formation of the granophyre.

Basalt Chemistry and Tectonic Implications

Basalt Chemistry

X-ray fluorescence major-oxide and trace element analyses for the Clear Creek

East and Three Lakes Peak Trail sections are presented Tables 4-7. ICP major-oxide

and trace-element analyses for the Seepay Ridge section and a single section through

the Paradise Sill are presented in Tables 8-11. Four additional samples toward the

bottom of the Paradise Sill were taken for XRF analysis in order to obtain certain trace-

element data used in discrimination diagrams (Table 12). In addition, the data are

plotted with respect to position in the sills in Figures 38-45.

Though the Plains and Paradise sills are both altered to varying degrees, it is not

clear that there has been significant chemical exchange with the altering fluids or host

Prichard sediments. At the Three Lakes Peak Trail section, the diabase shows a general

upward increase in the degree of metamorphism (see Metamorphism of the Plains Sill),

accompanied by various weak geochemical trends. Less mobile trace-elements,

especially those used in basalt discrimination diagrams, show little variation with

degree of alteration, suggesting minimal loss during crystallization and metamorphism.

Though isotope analyses indicate that initial $^{87}Sr/^{86}Sr$ ratios were homogenized on the

scale of hundreds of meters from the sill, it is not clear how much strontium was lost

from the diabase rocks. Thus, the Ti-Zr-Sr discrimination diagram (Figure 31) should

be viewed with caution.

Of crucial importance is titanium, which is used in many of the discrimination

diagrams. Garcia (1978) compiled studies on the effect of ocean-floor metamorphism

on titanium abundances and found that in some cases titanium appears immobile, while

in others, titanium is gained or lost in varying degrees. In the case of the Plains Sill,

common alteration of ilmenite to sphene, indicates that titanium was mobile at least on

the submillimeter scale. The weak upward trend of increasing titanium in the diabase (Figure 38), accompanied by a general increase in metamorphism from the bottom to the top of the sill, suggests that wholesale titanium loss probably did not occur. In this regard, I will operate under the assumption that significant amounts of titanium were neither gained nor lost during the course of cooling and metamorphism.

Figures 28-34 show a number of trace-element and major-oxide discrimination diagrams used to characterize basalt composition rocks. All diabase samples from the weakly differentiated Plains Sill are included. Only samples from the relatively undifferentiated lower part of the Paradise Sill are included as silica contents up to 65 weight percent in the more differentiated upper portion preclude use in basalt diagrams.

There is little discrimination between different sections through the Plains Sill. The Paradise Sill only discriminates itself from the Plains Sill in the TiO_2-K_2O-P_2O_5 and the SiO_2-K_2O diagrams. Figure 28 shows both the Plains and Paradise sills to be tholeiitic, whereas Figure 29 places them more specifically in the high-iron tholeiite field. Figures 30 and 31 show strong ocean-floor basalt affinities, though strontium loss may have moved data points in Figure 31 away from the calc-alkaline field. Though Figure 32 has both sills showing a calc-alkaline affinity, the positive slope of their distribution, likely indicative of increasing titanium with differentiation, is typical of oceanic basalts (Garcia 1978). The Plains Sill shows a mixed affinity with oceanic and continental basalts in Figures 33 and 34. On both the TiO_2-K_2O-P_2O_5 and the SiO_2-K_2O diagrams, samples from the Three Lakes Peak Trail section, Clear Creek East section and the Paradise Sill plot more toward the continental basalt field while samples from the Seepay Ridge section plot more toward the oceanic basalt field. In both cases the Paradise Sill shows a strong geochemical affinity toward continental basalts. A high flux of water through the sills may have altered the abundance of more mobile K_2O, thus resulting in inaccurate affinities in Figures 33 and 34.

Tectonic Implications and the Sill-Sediment Complex Model

Höy (1989) presented geochemical data for the Moyie Sills in southeastern

British Columbia. Some are sub-alkaline, high-iron tholeiites geochemically similar to

the Plains and Paradise Sills, whereas others are alkaline basalts. The distinction

between tholeiitic and alkalic basalts is not indicative of differing tectonic environments

(Pearce and Cann 1973), and thus the two suites are not mutually incompatible. Both

suites of sills show mixed geochemical and tectonic affinities with trace-element

characteristics of both ocean-floor and within-plate basalts. There is also geochemical

similarity with a suite of equivalent-age mafic dikes intruding continental crustal rocks

of the Tobacco Root Mountains (Wooden et al. 1978). Höy argues that both the mixed

geochemical signature of the Moyie Sills and the geochemical and age similarity to the

extensional dikes is supportive of an incipient or young continental rift setting for early

Belt deposition as proposed by Sears (1978) and Winston (1984).

Nothing inherent in the geochemistry of the Plains and Paradise Sills detracts

from this argument and it may be that the mixed ocean-floor vs. continental affinities

are indicative of a transitional tectonic setting from a continental rift to an oceanic rift

environment. Indeed, a number of continental flood basalts whose extrusion preceded

transition to an oceanic rift environment, show strong oceanic affinities on the TiO_2-

K_2O-P_2O_5 diagram (Pearce et al. 1975). Examples include the Deccan Traps preceding

development of the Carlsberg Ridge, the Tertiary basalts of the Scoresby Sund area in

East Greenland, preceding the opening of the Atlantic Ocean and the basalts of Baffin

Island and West Greenland whose extrusion may have preceded the opening of the

Labrador Sea (Pearce et al. 1975).

The Arco 1 Paul Gibbs borehole in northwest Montana drilled into the lowest

Prichard Formation. It encountered thirteen mafic sills ranging in thickness from less

than ten meters to nearly 500 meters (Figure 35). These sills comprise approximately 21% of the sill-sediment package encountered in the borehole. Other aspects of the Gibbs borehole are reviewed in Boberg (1985) and Harrison et al. (1985). That the lower Belt Supergroup contains such a high proportion of mafic sills, suggests a similarity with Einsele's (1985) extensional sill-sediment complex model as applied to the presently spreading Guaymas Basin in the Gulf of California. In this model, rapid sedimentation during rifting inhibits extrusion of basalts and instead favors emplacement as sills. Successively younger sills are thought to intrude above older sills in the sill-sediment column, controlled by the lower lithostatic loads and reduced resistance to lateral intrusion imposed by less lithified, nearer surface sediments (Figure 36).

Sedimentation rates during early Belt deposition are not well constrained owing to poor geochronological control and the fact that the base of the section is nowhere exposed. Assuming constant sedimentation throughout Belt time yields a very low overall rate of less than 3cm/1000 years (Obradovich and Peterman 1968). They suggest, however, that deposition of the Belt occurred episodically in three distinct periods with hiatuses of at 200 million years between them, allowing for substantially higher sedimentation rates within depositional periods. Accurate evaluation of early Belt sedimentation rates will require more definitive geochronology, including better control on the initiation of rifting and sedimentation.

All but one of the sills from the borehole, show similar hydration effects as the Plains Sill, with no evidence of primary pyroxene. It is impossible from the bore cuttings to ascertain sill-sediment relationships, though judging from the paucity of anhydrous mafic phases and pervasive hydration of the sills, not just in the borehole but in the Belt Basin as a whole, it seems likely that most were emplaced under hydrous conditions. This would be in accord with the sill-sediment complex model, however,

without precision geochronology on all sills in the lower Belt, it will be impossible to

ascertain if in fact younger sills intrude above older sills.
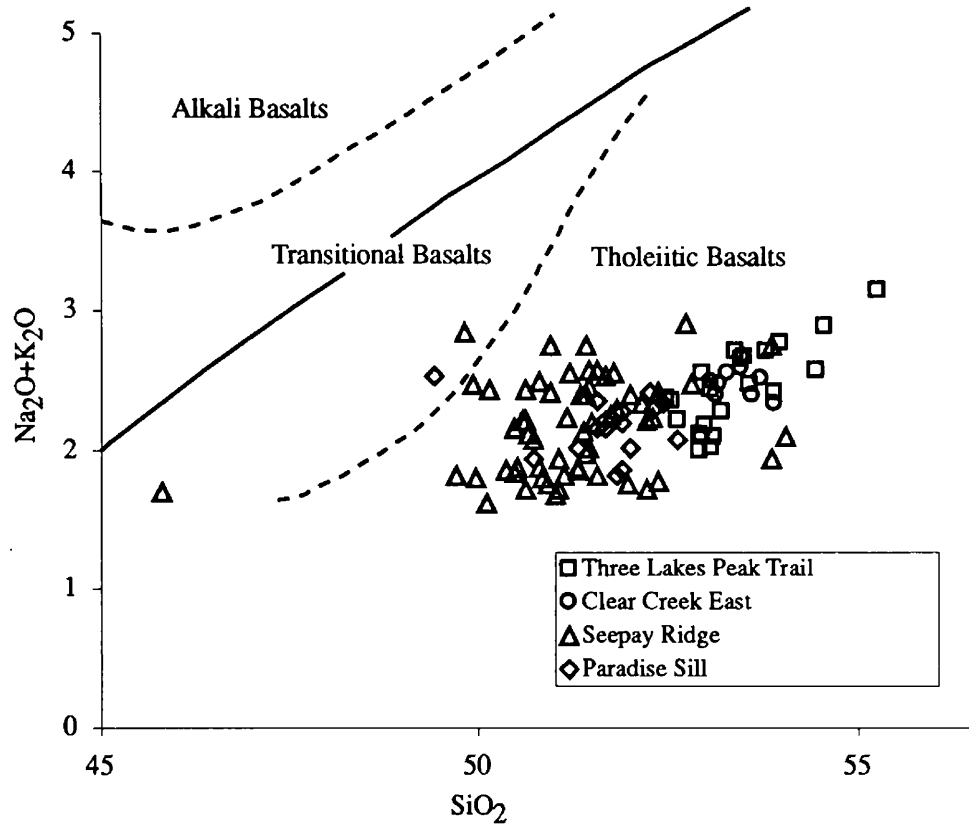
Figure 28. Alkali-silica diagram showing the dominantly tholeiitic character of the Plains and Paradise Sills. Plot after Hyndman (1985).
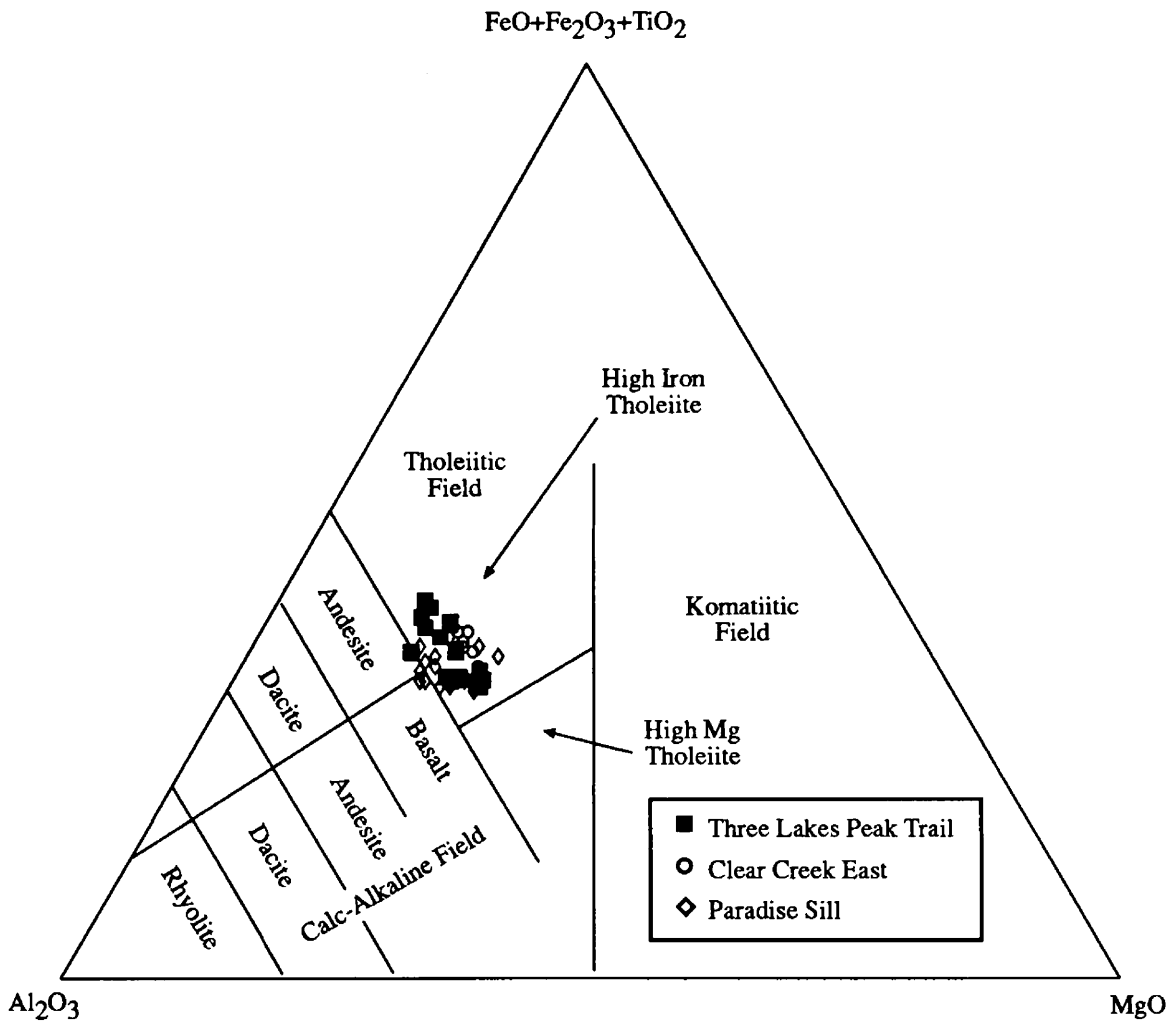
Figure 29. Discrimination diagram showing the dominantly high-iron signature of the Plains and Paradise Sills. Plot after Jensen (1976).
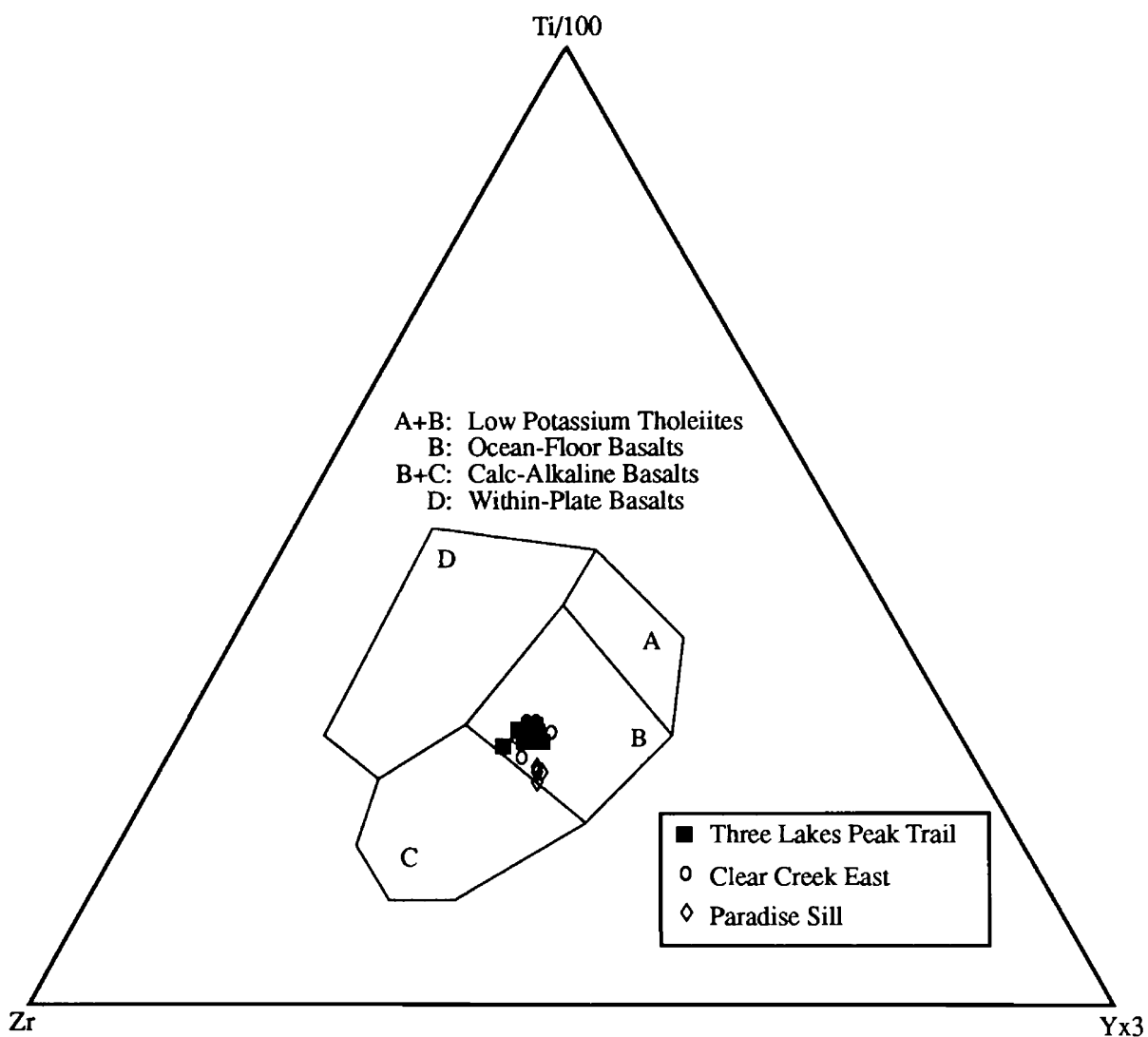
Figure 30. Ti/100-Zr-Yx3 discrimination diagram of samples from the Three Lakes Peak Trail and Clear Creek East sections of the Plains Sill amd four samples of the Paradise Sill. Plains Sill samples show an ocean-floor affinity but also plots within the low-potassium tholeiite and calc-alkaline basalt fields. The Paradise sill shows chemical similarity to both ocean-floor and calc-alkaline basalts. Plot after Pearce and Cann (1973).

Ti/100

A: Low Potassium Tholeiites
B: Calc-Alkaline Basalts
C: Ocean-Floor Basalts

■ Three Lakes Peak Trail

o Clear Creek East

◇ Paradise Sill

C

A

B

Zr

Sr/2
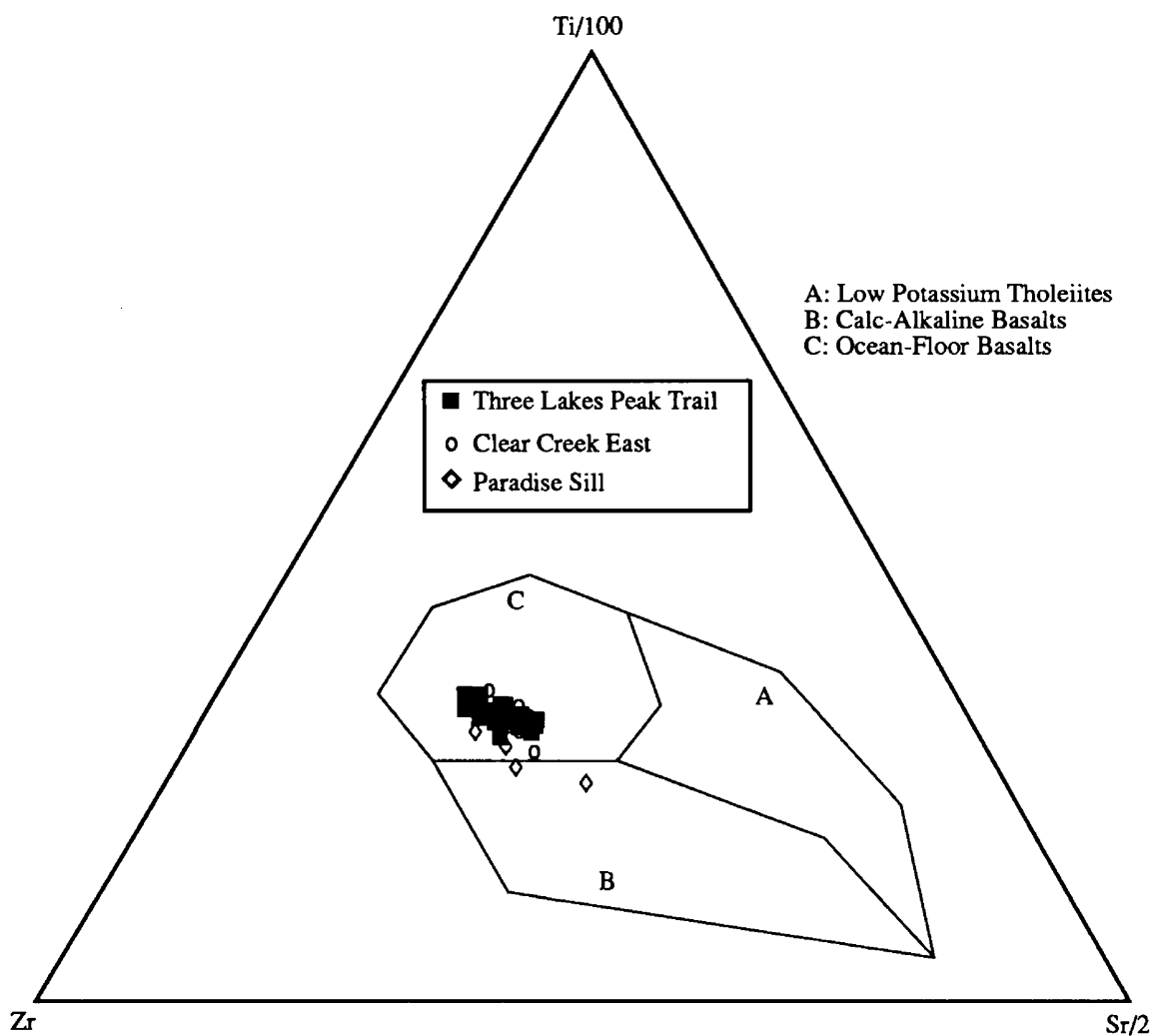
Figure 31. Ti/100-Zr-Sr/2 discrimination diagram for Plains Sill samples from the Three Lakes Peak Trail and Clear Creek East sections, as well as four samples from the Paradise Sill. The diagram shows a strong ocean-floor affinity though the possibility of strontium and/or titanium loss during cooling and metamorphism exists. Plot after Pearce and Cann (1973).
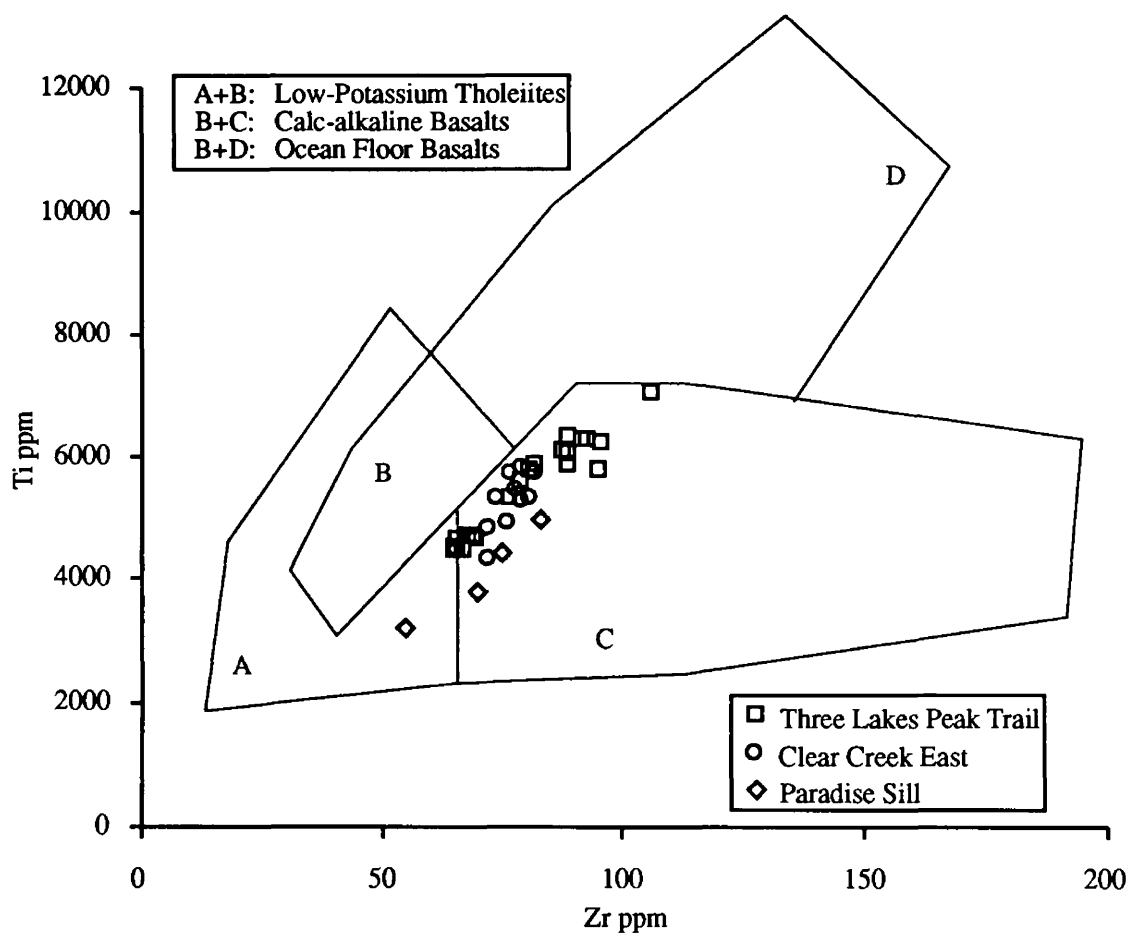
Figure 32. Ti-Zr discrimination diagram (after Pearce and Cann, 1973) of Plains Sill samples from the Three Lakes Peak Trail and Clear Creek East sections as well as four samples from the Paradise Sill. Though most samples plot in the calc-alkaline field, the positive slope of their distribution is typical of ocean-floor basalts (Garcia, 1978).
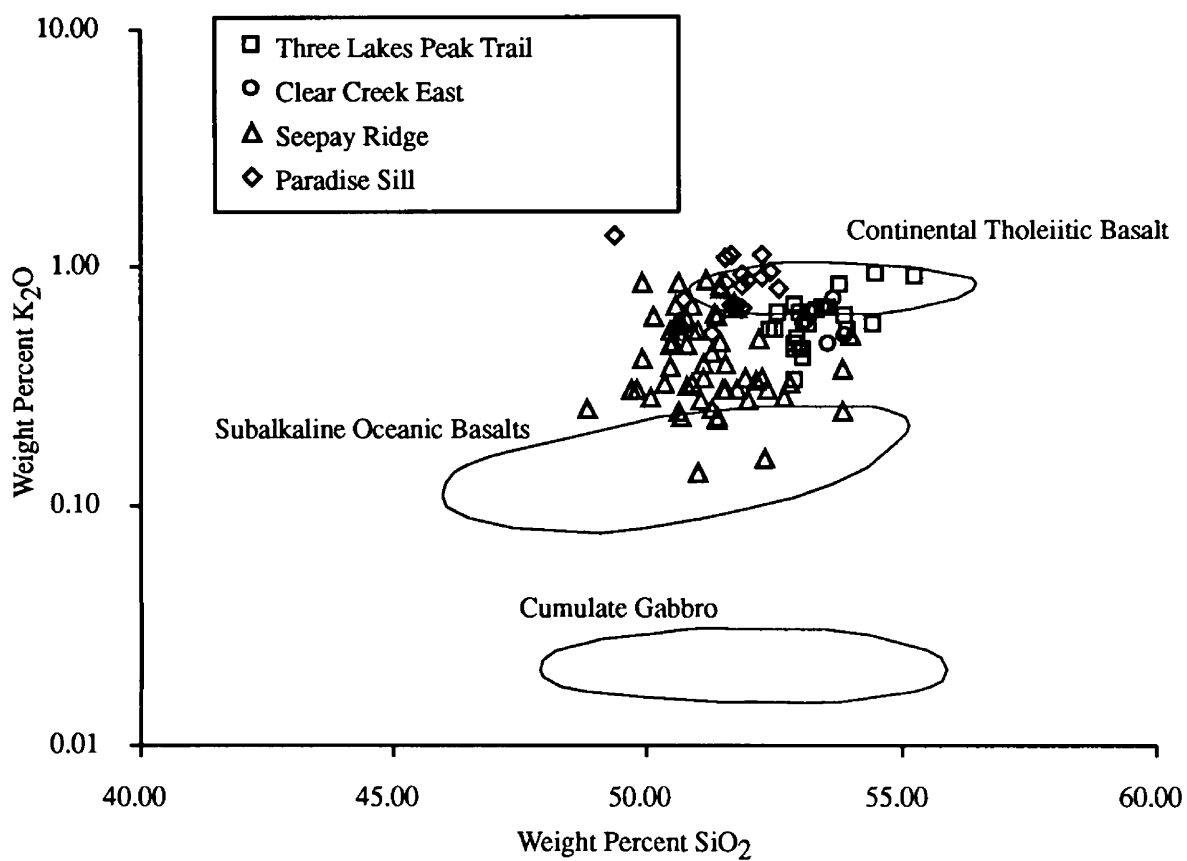
Figure 33. Semi-log plot of K_2O vs. SiO_2 showing a dominantly continental affinity for the Paradise Sill and samples of the Plains Sill from the Three Lakes Peak Trail and Clear Creek East sections. Plains Sill samples from the Seepay Ridge section show mixed continental and oceanic affinities. Plot adapted from Coleman and Donato (1979).
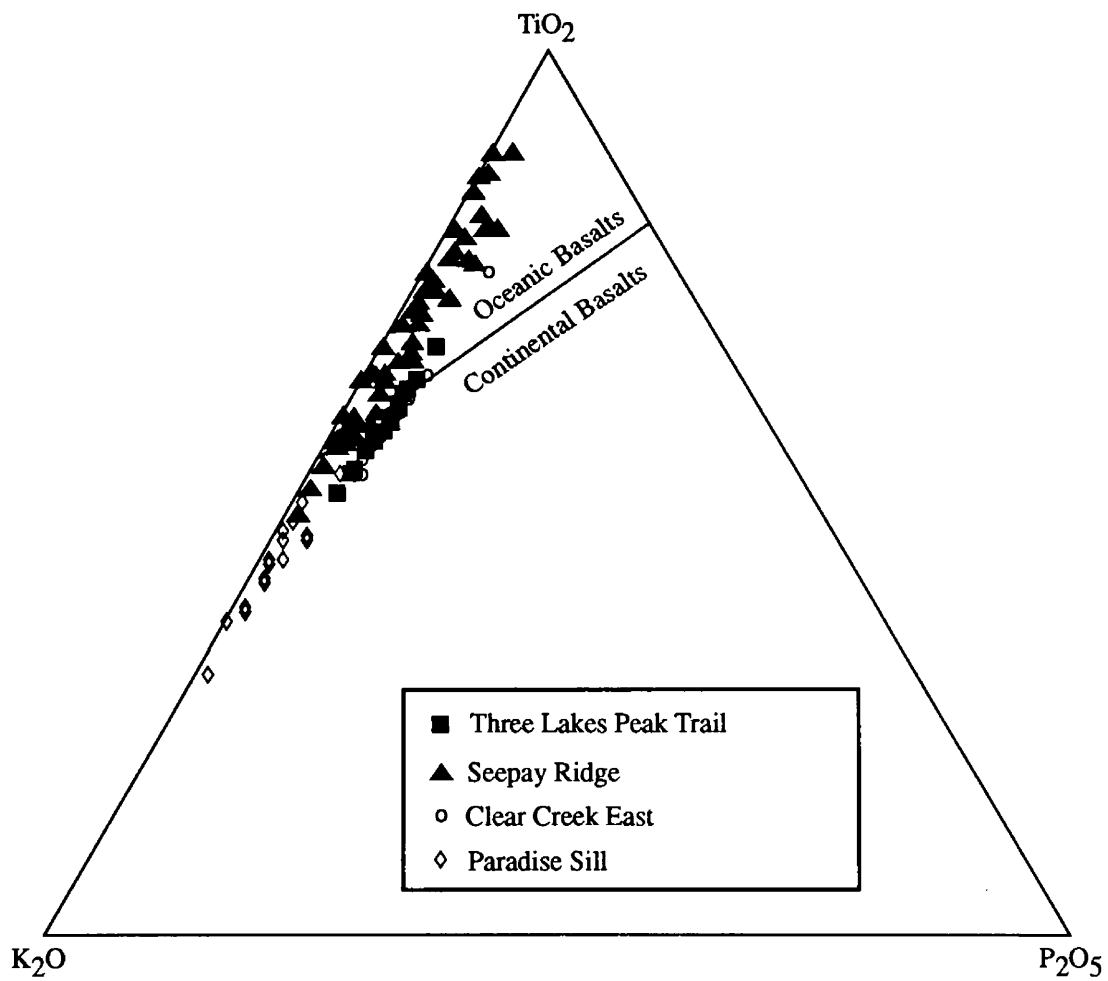
Figure 34. TiO_2-K_2O-P_2O_5 discrimination diagram indicating a mixed continental-oceanic affinity for sections of the Plains Sill and a dominantly continental affinity for the Paradise Sill. Plot after Pearce et al. (1975).
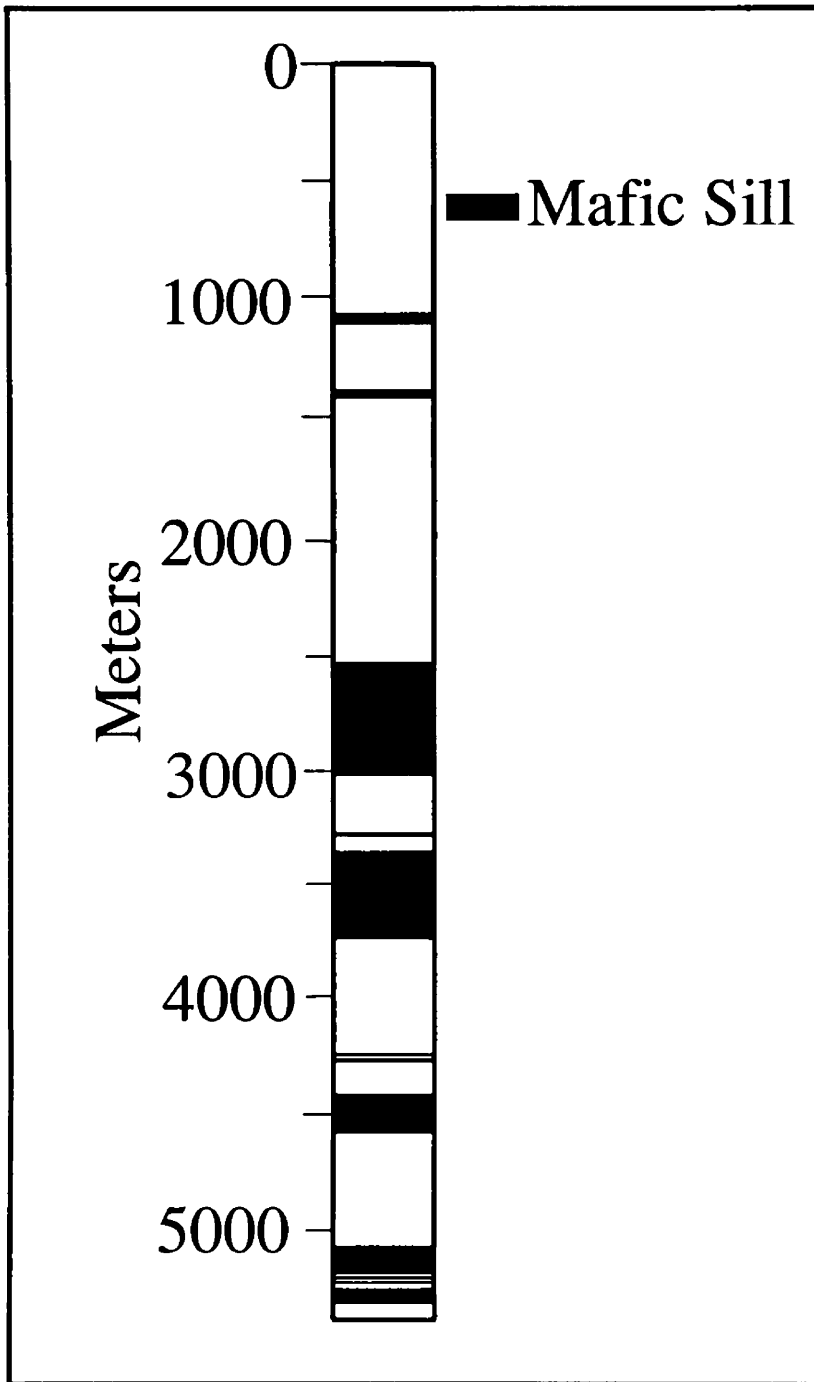
Figure 35. Simplified log of the Arco 1 Paul Gibbs borehole in northwest Montana. The hole was drilled in the lowest Prichard Formation and was abandoned before reaching basement. It encountered thirteen mafic sills comprising over 20% of the section.
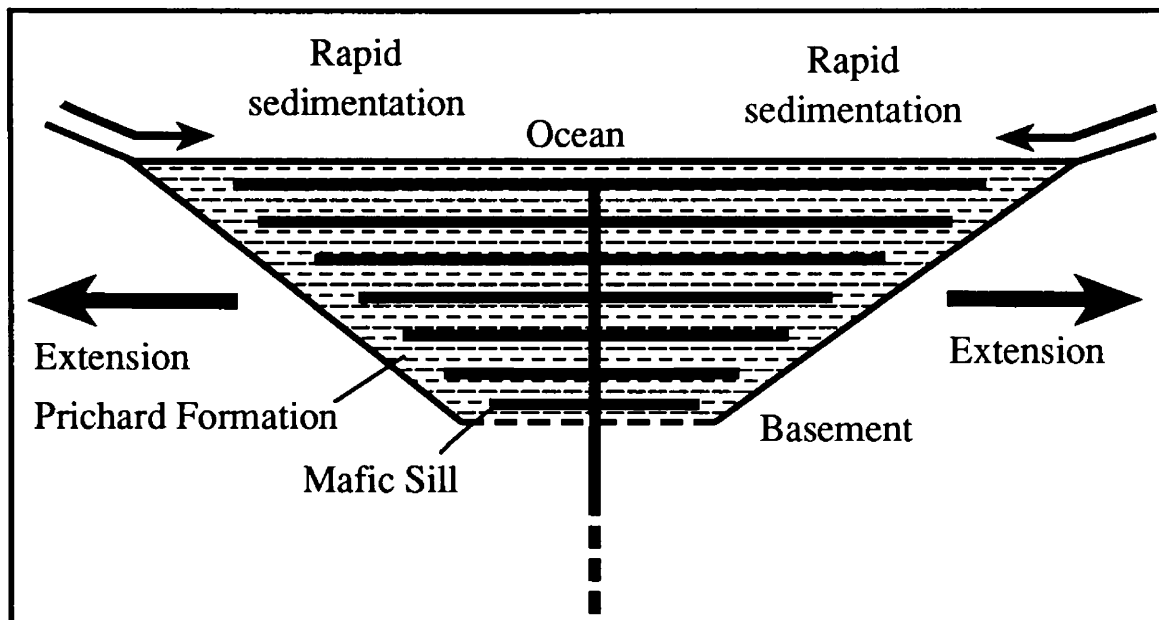
Figure 36. Schematic sill-sediment complex model for early Belt deposition and intrusion of mafic sills. The model assumes an extensional environment but makes no attempt to characterize basement response to extension.

Emplacement of the Plains Sill into Wet Sediments

The above field, laboratory, and geochemical observations and analysis culminate in the following emplacement model into wet sediments for Plains Sill (Figure 37). Basaltic magma, presumably derived from pressure-relief partial melting during the course of continental rifting, was emplaced into the still-wet sediments of the Prichard Formation.

During crystallization of the original magma, a fluid rich in granitic constituents separated from the diabase to ultimately form the granophyre. The mechanism for differentiation is unknown but likely involved filter-pressing and/or transfer of constituents by dissolution into a high-temperature water-rich fluid compositionally similar to pegmatitic fluid. This fluid migrated along the roof of the sill driven by the density difference between it and the diabase magma below. Mylonitic textures in the granophyre and the deformation textures in amphiboles of the already crystallized upper-diabase in the Clear Creek Section suggest the sedimentary pile was subsiding, likely due to dewatering of sediments, as the granophyre was cooling and still behaving plastically. The general absence of granophyre in sections where the Plains Sill intrudes the Prichard D suggests that the granophyre may have migrated up-dip as the sill climbed up-section from the Prichard D to E. It accumulated in the Prichard E to form the anomalously thick granophyre zones. Indeed, the very fact that the Plains Sill ever cut up section likely resulted in the thick granophyre layer. In the case of a perfectly horizontal sill, there is no driving force to cause a separated magma fraction to migrate anywhere except to the top of the sill, in which case it would not occur in disproportionate quantities.

Where the granophyre is absent (Quinns Hot Springs, SW Flank of Seepay Creek Anticline, and Boyer Creek sections) or is capped by the upper diabase (Clear

Creek and Seepay Ridge sections), sill-sediment interaction appears to be minimal.
Disturbance of the sediments occurs on the scale of meters from the upper contact of the
sill, if that. Where the upper diabase is absent (Clear Creek Knob, McGlaughlin
Creek, and Three Lakes Peak Trail sections), sediments overlying the granophyre are
disturbed to the point of compositional and textural homogeneity on the scale of
hundreds of meters. Perhaps the upper diabase, having crystallized early, served to
stifle sill-sediment interaction by virtually sealing off the granophyre from the overlying
sediments.

If it is true that volatile transfer played a significant role in the formation of the
granophyre, the separated fluid would have to exsolve substantial quantities of water
during crystallization. Exsolution of this excess water may ultimately have resulted in
the thicker granosediment layers where the upper diabase is absent. Evidence that
disruption of the sediments was contemporaneous with crystallization of the
granophyre comes from the rounded granophyre inclusions within the granosediments.
The soupy overlying sediments were unable to hold the exsolved fluid in a typical vein-
like form, and thus the fluid either rose as bubbles or was convected upwards during
reconstitution, thereby assuming a generally rounded form and crystallizing into the
granophyric inclusions.

At the top of the granosediment layer, massive reconstituted sediments grade
into complexly folded sediments with primary bedding preserved. At this interface,
ovoids developed as partially lithified fragments remained intact to form the cores, and
likely reacted with surrounding circulating fluids to form the concentric rinds.
Hydrothermal circulation driven by heat from the sill caused pervasive greenschist
facies metamorphism of the granosediments and overlying sediments.
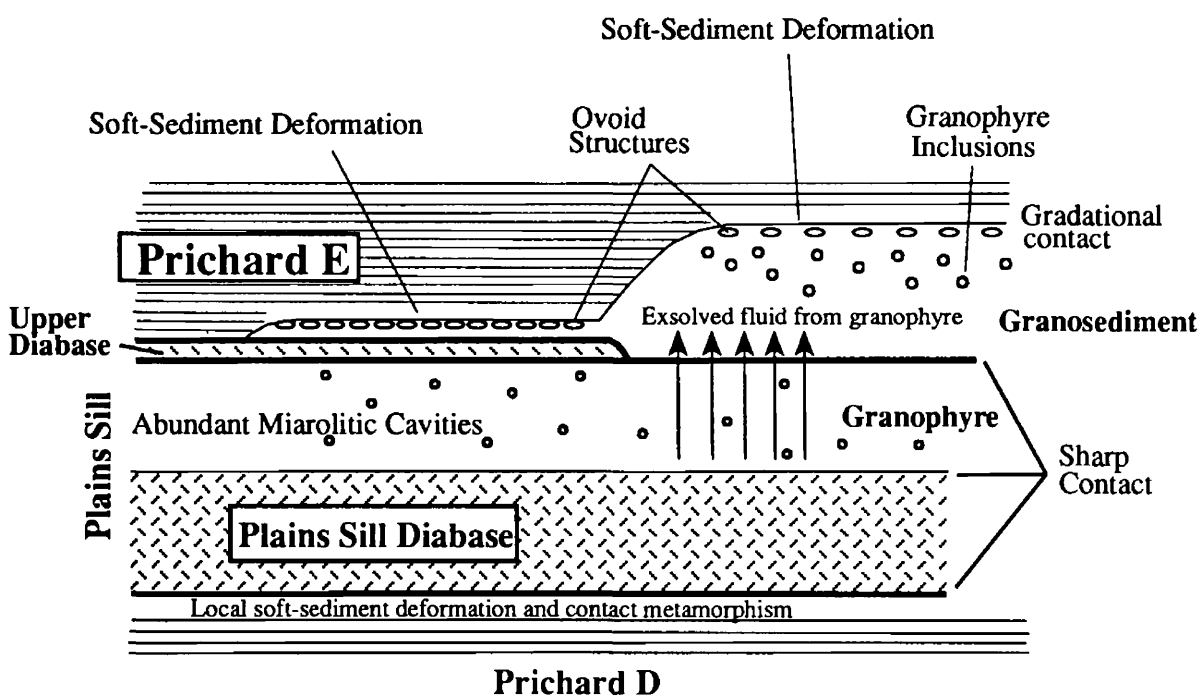
Figure 37. Conceptual model for the emplacement of the Plains Sill into wet sediments.

Summary and Conclusions

1) The Middle Proterozoic Plains Sill is a thick diabase-granophyre body (>250 meters) exposed near Plains and Perma in western Montana. It was emplaced into the wet sediments of the Prichard Formation, resulting in soft-sediment deformation, ovoid structures and thick sequences of reconstituted granosediment.

2) Variably thick granophyre directly overlies the Plains Sill diabase. It is generally absent where the sill intrudes the Prichard D lower in the section, and often anomalously thick where the sill intrudes the Prichard E. A late-stage felsic magma fraction developed as the diabase crystallized. Subsequent filter-pressing or dissolution of this magma fraction into heated sediment-derived water resulted in separation of the granophyre fluid from the diabase. Where the Plains Sill cut up-section from the Prichard D to the Prichard E, the granophyre fluid migrated up-dip and accumulated to form the thicker granophyre zones.

3) Retrograde metamorphism of the diabase is consistent with the epidote-amphibolite facies, with hornblende and plagioclase variably altered to lower-temperature blue-green hornblende and epidote. Later-formed hornblende shows a consistent compositional shift to higher Al_2O_3 and FeO* and lower SiO_2 and MgO. Degree of metamorphism generally increases upward through the sill, perhaps due to the insulating effects of the overlying, still hot granophyre.

4) There is no evidence of primary or relict pyroxene within the sill indicating that the magma may have incorporated sufficient water during emplacement into wet sediments to crystallize primary hornblende as the dominant mafic phase. Current

pressure constraints on emplacement of the sill suggest that it is unlikely that the magma was capable of dissolving enough water to satisfy the stoichiometry of hornblende. Petrographically, it appears that the chilled margins, presumably the portion of the sill cooling fastest, shows relatively little alteration of plagioclase and hornblende, suggesting that perhaps hornblende is the primary mafic phase. Thus, it is impossible to ascertain with certainty whether the magma was sufficiently hydrated during emplacement under hydrous conditions to crystallize as an amphibole gabbro, or whether all pyroxene was altered to hornblende shortly after crystallization.

5) Geochemical discrimination diagrams show the Plains Sill diabase to be a high-iron tholeiite with mixed oceanic and continental affinities, consistent with other rift-related basalts, in particular, continental flood basalts whose extrusion precedes extension into an oceanic basin.

6) The Plains Sill is one in a suite of mafic sills intruded into the lower Belt Supergroup. Mafic sills can comprise over 30% of the lower Belt sill-sediment section. The sills appear to reflect basin-wide magmatic events often accompanying rift environments. Rapid initial sedimentation during early Belt time may have inhibited extrusion of mafic magma as ocean-floor basalts.

#	Sample	SiO$_2$	TiO$_2$	Al$_2$O$_3$	FeO*	MnO	MgO	CaO	Na$_2$O	K$_2$O	Total	Si	Ti	Al	Fe	Mn	Mg	Ca	Na	K	Sum	Description
Plagioclase		Weight % Oxide										Number of cations based on 8 oxygens										
1	72701	48.55	0.02	31.31	0.15	0.03	0.07	15.08	2.38	0.18	97.77	2.27	0.00	1.72	0.01	0.00	0.01	0.75	0.22	0.00	4.98	Core of zoned plag (2)
2	72701	48.57	0.00	32.00	0.36	0.02	0.06	15.49	2.76	0.07	99.33	2.24	0.00	1.74	0.01	0.00	0.00	0.77	0.25	0.01	5.01	Rim of zoned plag (1)
3	72701	51.26	0.02	30.17	0.18	0.00	0.04	13.57	3.90	0.09	99.22	2.35	0.00	1.63	0.01	0.00	0.00	0.67	0.35	0.01	5.01	Core of zoned plag (4,74)
4	72701	54.15	0.03	27.82	0.72	0.03	0.05	10.88	5.33	0.16	99.17	2.47	0.00	1.50	0.03	0.00	0.00	0.53	0.47	0.01	5.02	Rim of zoned plag (3)
5	72706	53.08	0.10	28.62	0.67	0.00	0.11	11.67	4.74	0.20	99.19	2.43	0.00	1.54	0.03	0.00	0.01	0.57	0.42	0.01	5.01	Core of zoned plag encased in qtz (6)
6	72706	52.77	0.07	29.15	0.26	0.02	0.11	12.14	4.34	0.32	99.18	2.41	0.00	1.57	0.01	0.00	0.01	0.59	0.38	0.02	5.00	Rim of zoned plag encased in qtz (5)
7	72711	52.52	0.06	28.99	0.86	0.01	0.12	12.35	4.43	0.07	99.41	2.40	0.00	1.56	0.03	0.00	0.01	0.61	0.39	0.00	5.01	Core of zoned plag (8)
8	72711	56.12	0.00	27.43	0.22	0.01	0.03	10.10	6.02	0.08	100.00	2.53	0.00	1.46	0.01	0.00	0.00	0.49	0.53	0.00	5.01	Rim of zoned plag (7)
9	72715	56.89	0.00	24.38	0.09	0.00	0.03	6.98	7.11	0.04	95.51	2.66	0.00	1.34	0.00	0.00	0.00	0.35	0.64	0.00	5.00	Core of zoned plag (10, 77)
10	72715	56.84	0.03	27.30	0.01	0.06	0.00	9.77	6.08	0.03	100.11	2.55	0.00	1.44	0.00	0.00	0.00	0.47	0.53	0.00	4.99	Rim zoned plag (9)
11	72718	53.38	0.10	29.32	0.23	0.00	0.06	11.84	4.69	0.12	99.75	2.42	0.00	1.57	0.01	0.00	0.00	0.58	0.41	0.01	5.00	Plag crystal
12	72724	68.17	0.00	19.54	0.02	0.02	0.00	0.47	11.21	0.03	99.46	2.99	0.00	1.01	0.00	0.00	0.00	0.02	0.95	0.00	4.98	Stand alone plag crystal
13	72724	67.24	0.00	20.25	0.02	0.02	0.04	1.41	10.87	0.14	99.99	2.95	0.00	1.05	0.00	0.00	0.00	0.07	0.92	0.01	5.00	Plag from qtz-plag intergrowth
14	72724	67.57	0.00	19.71	0.13	0.00	0.05	0.68	11.03	0.10	99.28	2.98	0.00	1.02	0.00	0.00	0.00	0.03	0.94	0.01	4.99	Stand alone plag crystal
15	72724	68.91	0.02	19.80	0.00	0.02	0.01	0.60	11.31	0.05	100.73	2.99	0.00	1.01	0.00	0.00	0.00	0.03	0.95	0.00	4.98	Plag from qtz-plag intergrowth
16	72737	69.04	0.00	19.45	0.00	0.00	0.01	0.49	11.33	0.09	100.41	3.00	0.00	1.00	0.00	0.00	0.00	0.02	0.95	0.01	4.98	Stand alone plag crystal
17	72737	66.54	0.03	21.05	0.00	0.02	0.00	2.32	10.39	0.04	100.39	2.91	0.00	1.08	0.00	0.00	0.00	0.11	0.88	0.00	4.99	Plag from qtz-plag intergrowth
18	72743	69.55	0.02	19.28	0.02	0.00	0.04	0.07	11.60	0.06	100.64	3.01	0.00	0.98	0.00	0.00	0.00	0.00	0.97	0.00	4.98	Stand alone plag crystal
19	72743	69.54	0.00	19.66	0.00	0.00	0.00	0.41	11.73	0.06	101.40	3.00	0.00	1.00	0.00	0.00	0.00	0.02	0.98	0.00	5.00	Coarse untwinned feldspar crystal
20	72743	68.29	0.00	19.58	0.08	0.00	0.00	0.91	11.18	0.09	100.13	2.98	0.00	1.01	0.00	0.00	0.00	0.04	0.95	0.01	4.99	Stand alone plag crystal
21	BLEB II	69.28	0.00	19.59	0.01	0.03	0.03	0.24	11.63	0.06	100.87	3.00	0.00	1.00	0.00	0.00	0.00	0.01	0.98	0.00	4.99	Plag from qtz-plag intergrowth
22	BLEB II	69.13	0.02	19.25	0.00	0.02	0.02	0.14	11.39	0.05	100.02	3.01	0.00	0.99	0.00	0.00	0.00	0.01	0.96	0.00	4.98	Plag from qtz-plag intergrowth
23	BLEB II	69.85	0.02	19.33	0.08	0.01	0.04	0.07	11.61	0.04	101.04	3.01	0.00	0.98	0.00	0.00	0.00	0.00	0.97	0.00	4.98	Stand alone plag crystal - twinned
24	BLEB II	68.74	0.00	19.32	0.04	0.03	0.01	0.46	11.31	0.07	99.97	3.00	0.00	0.99	0.00	0.00	0.00	0.02	0.96	0.00	4.98	Stand alone plag crystal - twinned
25	BLEB III	61.49	0.00	24.37	0.02	0.00	0.00	6.19	8.35	0.06	100.48	2.72	0.00	1.27	0.00	0.00	0.00	0.29	0.72	0.00	5.00	Stand alone plag crystal
26	BLEB III	63.03	0.00	23.53	0.00	0.01	0.03	5.34	8.91	0.04	100.89	2.77	0.00	1.22	0.00	0.00	0.00	0.25	0.76	0.00	5.00	Stand alone plag crystal
27	BLEB III	61.17	0.01	24.52	0.03	0.00	0.03	6.46	7.85	0.05	100.12	2.71	0.00	1.28	0.00	0.00	0.00	0.31	0.68	0.00	4.98	Stand alone plag crystal
28	BLEB III	62.22	0.00	23.94	0.00	0.00	0.01	6.00	8.37	0.04	100.59	2.74	0.00	1.24	0.00	0.00	0.00	0.28	0.72	0.00	4.99	Plag from qtz-plag intergrowth
Hornblende		Weight % Oxide										Number of cations based on 22 oxygens and 2 (OH); all Fe as Fe(II)										
29	72701	44.11	0.36	13.04	16.32	0.29	9.61	12.13	1.20	0.33	97.39	6.57	0.04	2.29	2.03	0.04	2.13	1.94	0.35	0.06	15.45	Average looking hornblende
30	72701	45.70	0.29	11.73	15.66	0.24	10.24	12.21	1.06	0.31	97.44	6.76	0.03	2.05	1.94	0.03	2.26	1.94	0.30	0.06	15.36	Average looking hornblende
31	72701	44.59	0.32	12.93	15.55	0.29	9.64	11.99	1.07	0.30	96.67	6.65	0.04	2.27	1.94	0.04	2.14	1.92	0.31	0.06	15.36	Average looking hornblende
32	72701	47.87	0.38	9.41	14.37	0.31	11.93	12.24	0.79	0.17	97.48	7.01	0.04	1.63	1.76	0.04	2.61	1.92	0.22	0.03	15.26	Elongate, finer-grained crystal
33	72706	44.58	0.38	12.69	15.64	0.20	9.79	11.90	1.08	0.32	96.59	6.66	0.04	2.23	1.95	0.03	2.18	1.90	0.31	0.06	15.37	Coarse hornblende, internal xls (34)
34	72706	44.27	0.33	13.00	16.19	0.30	9.85	11.88	1.16	0.33	97.31	6.59	0.04	2.28	2.02	0.04	2.18	1.89	0.33	0.06	15.43	Internal xls to #33
35	72706	51.39	0.12	5.58	12.64	0.26	14.39	12.27	0.59	0.09	97.33	7.44	0.01	0.95	1.53	0.03	3.11	1.90	0.17	0.02	15.16	Coarse hornblende, internal xls (36)
36	72706	51.41	0.17	5.28	12.71	0.22	14.52	12.54	0.51	0.08	97.42	7.44	0.02	0.90	1.54	0.03	3.13	1.95	0.14	0.02	15.17	Internal xls to #35
37	72711	41.93	0.35	14.36	18.87	0.25	7.39	11.90	1.39	0.61	97.05	6.38	0.04	2.57	2.40	0.03	1.68	1.94	0.41	0.12	15.56	Altered feathery Hb, w/biotite (57)
38	72711	46.37	0.24	9.80	17.09	0.27	10.42	11.92	1.01	0.29	97.41	6.91	0.03	1.72	2.13	0.03	2.31	1.90	0.29	0.06	15.38	Core coarse hornblende (39)
39	72711	41.65	0.16	14.63	19.06	0.27	7.47	11.74	1.33	0.45	96.96	6.34	0.02	2.63	2.43	0.04	1.69	1.95	0.39	0.09	15.57	Deep blue-green rim of #38
40	72711	49.19	0.18	6.99	15.58	0.32	12.04	12.25	0.77	0.13	97.44	7.24	0.02	1.21	1.92	0.04	2.64	1.93	0.22	0.03	15.25	Core coarse hornblende (41)
41	72711	40.66	0.22	16.22	18.61	0.30	6.74	11.98	1.36	0.73	96.83	6.20	0.03	2.92	2.37	0.04	1.53	1.96	0.40	0.14	15.59	Deep blue-green rim of #40
42	72711	46.88	0.20	9.00	16.68	0.28	10.90	12.11	0.80	0.31	97.14	6.99	0.02	1.58	2.08	0.03	2.42	1.93	0.23	0.06	15.35	Intergrown with biotite (59)
43	72715	50.53	0.20	6.31	15.58	0.25	12.31	12.18	0.46	0.16	97.97	7.37	0.02	1.08	1.90	0.03	2.68	1.90	0.13	0.03	15.15	Core coarse Hb xl (44,45)
44	72715	41.19	0.30	14.75	19.40	0.29	6.77	11.78	1.37	0.53	96.38	6.33	0.03	2.67	2.49	0.04	1.55	1.94	0.41	0.10	15.56	Needly alt product of #43
45	72715	42.53	0.31	14.37	19.05	0.27	7.25	11.74	1.40	0.58	97.51	6.43	0.04	2.56	2.41	0.04	1.63	1.90	0.41	0.11	15.52	Needly alt product of #43
46	72715	44.64	0.26	11.37	17.91	0.31	9.01	11.74	1.05	0.41	96.70	6.74	0.03	2.02	2.26	0.04	2.03	1.90	0.31	0.08	15.41	Coarse xl w/ altered appearance
47	72715	41.43	0.24	14.58	19.39	0.33	6.90	11.91	1.26	0.63	96.67	6.34	0.03	2.63	2.48	0.04	1.57	1.95	0.37	0.12	15.56	Coarse xl w/ altered appearance
48	72715	50.98	0.18	5.68	15.00	0.32	12.66	12.34	0.64	0.13	97.93	7.43	0.02	0.98	1.83	0.04	2.75	1.93	0.18	0.02	15.17	Coarse hornblende xl (49)
49	72715	43.08	0.28	13.52	18.83	0.27	7.82	11.56	1.29	0.49	97.13	6.52	0.03	2.41	2.38	0.03	1.76	1.87	0.38	0.09	15.48	Growing off #48 into adjacent qtz

Table 3. Microprobe data for samples from the Three Lakes Peak Trail section.

#	Sample	SiO2	TiO2	Al2O3	FeO*	MnO	MgO	CaO	Na2O	K2O	Total	Si	Ti	Al	Fe	Mn	Mg	Ca	Na	K	Sum	Description
Hornblende (continued)																						
50	72718	45.50	0.28	11.04	16.89	0.29	9.94	12.20	1.14	0.36	97.62	6.77	0.03	1.94	2.10	0.04	2.21	1.95	0.33	0.07	15.43	Coarse hornblende xl (51)
51	72718	42.14	0.22	15.59	18.31	0.27	7.14	11.90	1.30	0.54	97.40	6.35	0.03	2.77	2.31	0.03	1.60	1.92	0.38	0.10	15.49	Long needly xl growing off #50
52	72718	43.72	0.31	13.09	17.59	0.28	8.78	12.00	1.26	0.44	97.48	6.55	0.03	2.31	2.21	0.04	1.96	1.93	0.37	0.08	15.48	Coarse hornblende xl (53)
53	72718	42.70	0.32	14.35	17.88	0.26	7.94	11.96	1.19	0.49	97.10	6.44	0.04	2.55	2.25	0.03	1.78	1.93	0.35	0.09	15.47	Long needly xl growing off #52
54	72718	41.84	0.33	15.71	18.12	0.31	6.99	11.86	1.46	0.53	97.13	6.32	0.04	2.80	2.29	0.04	1.57	1.92	0.43	0.10	15.51	Elongate Hb xl, likely alt product
55	72718	43.67	0.30	14.70	17.23	0.26	7.50	11.70	1.37	0.50	97.22	6.53	0.03	2.59	2.16	0.03	1.67	1.88	0.40	0.10	15.38	Coarse hornblende xl (56)
56	72718	41.87	0.31	15.38	18.26	0.23	7.35	11.82	1.31	0.53	97.05	6.33	0.03	2.74	2.31	0.03	1.66	1.92	0.38	0.10	15.51	Needly growth from #55
Biotite		Weight % Oxide										Number of cations based on 20 oxygens and 4 (OH); all Fe as Fe(II)										
57	72711	35.78	1.83	16.92	20.43	0.10	10.30	0.02	0.07	8.88	94.34	5.52	0.21	3.08	2.64	0.01	2.37	0.00	0.02	1.75	15.61	Intergrown with hornblende (37)
58	72711	35.52	1.61	17.59	19.61	0.14	9.83	0.16	0.12	7.88	92.47	5.54	0.19	3.23	2.56	0.02	2.29	0.03	0.04	1.57	15.46	Fine-grained biotite - alt product?
59	72711	40.70	1.04	12.73	17.93	0.23	11.60	4.78	0.25	5.11	94.37	5.81	0.11	2.14	2.14	0.03	2.47	0.73	0.07	0.93	14.44	Intergrown with needly amph (42)
60	72715	36.05	1.68	17.19	19.72	0.14	10.66	0.02	0.10	9.32	94.88	5.52	0.19	3.10	2.53	0.02	2.44	0.00	0.03	1.82	15.66	Fine-grained biotite - alt product?
61	72724	34.28	2.80	17.12	27.18	0.29	4.23	0.00	0.05	9.46	95.41	5.03	0.31	2.96	3.34	0.04	0.93	0.00	0.01	1.77	14.40	Abundant fine-grained clusters
62	72737	34.66	2.48	16.90	27.14	0.21	5.04	0.02	0.08	9.27	95.81	5.47	0.30	3.15	3.58	0.03	1.19	0.00	0.02	1.87	15.61	Abundant fine-grained clusters
63	72743	35.36	2.34	16.73	23.48	0.25	7.61	0.01	0.08	9.36	95.21	5.51	0.27	3.08	3.06	0.03	1.77	0.00	0.02	1.86	15.62	Abundant fine-grained clusters
64	72743	34.69	2.32	17.08	23.11	0.23	7.31	0.04	0.05	9.44	94.28	5.47	0.27	3.17	3.05	0.03	1.72	0.01	0.02	1.90	15.63	Abundant fine-grained clusters
65	BLEB II	34.70	1.75	17.61	23.33	0.15	7.32	0.02	0.13	9.07	94.08	5.47	0.21	3.27	3.07	0.02	1.72	0.00	0.04	1.82	15.62	Fine-grained clusters
Muscovite		Weight % Oxide										Number of cations based on 20 oxygens and 4 (OH)										
66	72724	46.01	0.33	32.99	2.83	0.00	0.72	0.00	0.20	10.71	93.78	6.28	0.03	5.30	0.32	0.00	0.15	0.00	0.05	1.86	14.00	Alteration of plag within intergrowth
67	72724	46.49	0.63	32.73	2.72	0.05	0.87	0.00	0.32	11.04	94.85	6.28	0.06	5.22	0.31	0.01	0.18	0.00	0.08	1.90	14.04	Coarse musc intergrown w/ biotite
68	72724	46.28	0.21	32.58	2.89	0.04	0.94	0.01	0.29	11.00	94.25	6.30	0.02	5.23	0.33	0.00	0.19	0.00	0.08	1.91	14.06	Alteration of plag within intergrowth
69	72737	45.67	0.70	33.36	2.37	0.02	0.75	0.00	0.42	10.86	94.14	6.21	0.07	5.35	0.27	0.00	0.15	0.00	0.11	1.88	14.04	Coarse musc intergrown w/ biotite
70	72737	45.65	0.21	32.90	2.61	0.05	0.85	0.03	0.44	10.85	93.58	6.25	0.02	5.31	0.30	0.01	0.17	0.00	0.12	1.90	14.08	Alteration of plag within intergrowth
71	72743	46.01	0.45	33.30	2.11	0.00	1.03	0.01	0.36	10.83	94.11	6.24	0.05	5.33	0.24	0.00	0.21	0.00	0.09	1.87	14.03	Abundant fine-grained musc
72	72743	47.45	0.39	32.29	2.12	0.00	0.95	0.01	0.32	10.82	94.34	6.40	0.04	5.14	0.24	0.00	0.19	0.00	0.08	1.86	13.96	Abundant fine-grained musc
73	BLEB II	46.33	0.32	33.16	1.82	0.04	1.12	0.00	0.52	10.53	93.85	6.28	0.03	5.30	0.21	0.00	0.23	0.00	0.14	1.82	14.01	Within enclosing granosediment
Epidote		Weight % Oxide										Number of cations based on 12 oxygens and 1 (OH)										
74	72701	39.39	0.02	28.83	4.64	0.07	0.03	24.03	0.05	0.04	97.09	3.07	0.00	2.58	0.32	0.01	0.00	1.97	0.05	0.00	8.00	Altering in core of #3
75	72701	39.72	0.04	28.35	4.89	0.10	0.03	23.78	0.30	0.02	97.23	3.10	0.00	2.63	0.26	0.01	0.00	1.90	0.09	0.00	8.00	Fine-grained, not alt from plag?
76	72706	40.21	0.03	28.88	4.02	0.18	0.04	23.04	0.57	0.04	97.02	3.24	0.00	2.56	0.21	0.01	0.00	1.72	0.23	0.00	7.98	Coarse-grained, not alt from plag?
77	72715	38.77	0.01	27.50	6.90	0.17	0.08	24.16	0.08	0.00	97.67	3.01	0.00	2.52	0.45	0.01	0.01	2.01	0.01	0.00	8.01	Epidote in core of #9
78	72718	39.98	0.00	32.72	0.60	0.04	0.06	24.70	0.01	0.01	98.13	3.03	0.00	2.92	0.04	0.00	0.01	2.00	0.00	0.00	8.00	Epidote in core of trashed plag
Chlorite		Weight % Oxide										Number of cations based on 20 oxygens and 16 (OH)										
79	72701	25.12	0.10	21.06	22.35	0.26	17.45	0.03	0.02	0.02	86.40	5.30	0.02	5.24	3.95	0.05	5.49	0.01	0.01	0.01	20.07	Feathery looking alteration product
80	BLEB II	24.40	0.12	20.79	29.73	0.32	11.59	0.00	0.06	0.07	87.07	5.33	0.02	5.35	5.43	0.06	3.77	0.00	0.02	0.02	20.00	Abundant within bleb
Ilmenite		Weight % Oxide										Number of cations based on 3 oxygens										
81	72701	0.04	53.36	0.08	43.08	2.77	0.22	0.12	0.00	0.00	99.66	0.00	1.01	0.00	0.91	0.06	0.01	0.00	0.00	0.00	1.99	Enclosed in sphene (87)
82	72706	0.01	53.78	0.09	42.42	3.20	0.22	0.24	0.00	0.00	99.96	0.00	1.01	0.00	0.89	0.07	0.01	0.01	0.00	0.00	1.99	Enclosed in sphene (88)
83	72711	0.00	53.96	0.10	43.15	3.05	0.19	0.04	0.00	0.00	100.50	0.00	1.01	0.00	0.90	0.06	0.01	0.00	0.00	0.00	1.99	Fine-grained disseminations
84	72715	1.89	53.45	0.10	41.16	2.42	0.20	1.59	0.00	0.00	100.82	0.05	0.98	0.00	0.84	0.05	0.01	0.04	0.00	0.00	1.97	Fine-grained disseminations
85	72718	0.01	53.15	0.06	43.85	2.77	0.17	0.07	0.00	0.00	100.08	0.00	1.00	0.00	0.92	0.06	0.01	0.00	0.00	0.00	1.99	Fine-grained disseminations
86	72724	0.05	53.50	0.05	42.53	3.87	0.08	0.02	0.00	0.02	100.12	0.00	1.01	0.00	0.89	0.08	0.00	0.00	0.00	0.00	1.99	Fine-grained disseminations
Sphene		Weight % Oxide										Number of cations based on 5 oxygens										
87	72701	30.42	38.67	1.33	0.45	0.05	0.08	28.73	0.03	0.04	99.81	1.00	0.95	0.05	0.01	0.00	0.00	1.01	0.00	0.00	3.03	Enlcosing ilmenite (81)
88	72706	28.39	43.41	0.44	1.95	1.32	0.02	25.90	0.04	0.02	101.50	0.93	1.06	0.02	0.05	0.04	0.00	0.90	0.00	0.00	3.00	Enclosing ilmenite (82)
Rutile		Weight % Oxide										Number of cations based on 2 oxygens										
89	72706	0.00	100.60	0.14	0.19	0.00	0.00	0.22	0.06	0.01	101.23	0.00	1.00	0.00	0.00	0.00	0.00	0.00	0.00	0.00	1.00	Very rare!

Table 3 continued.
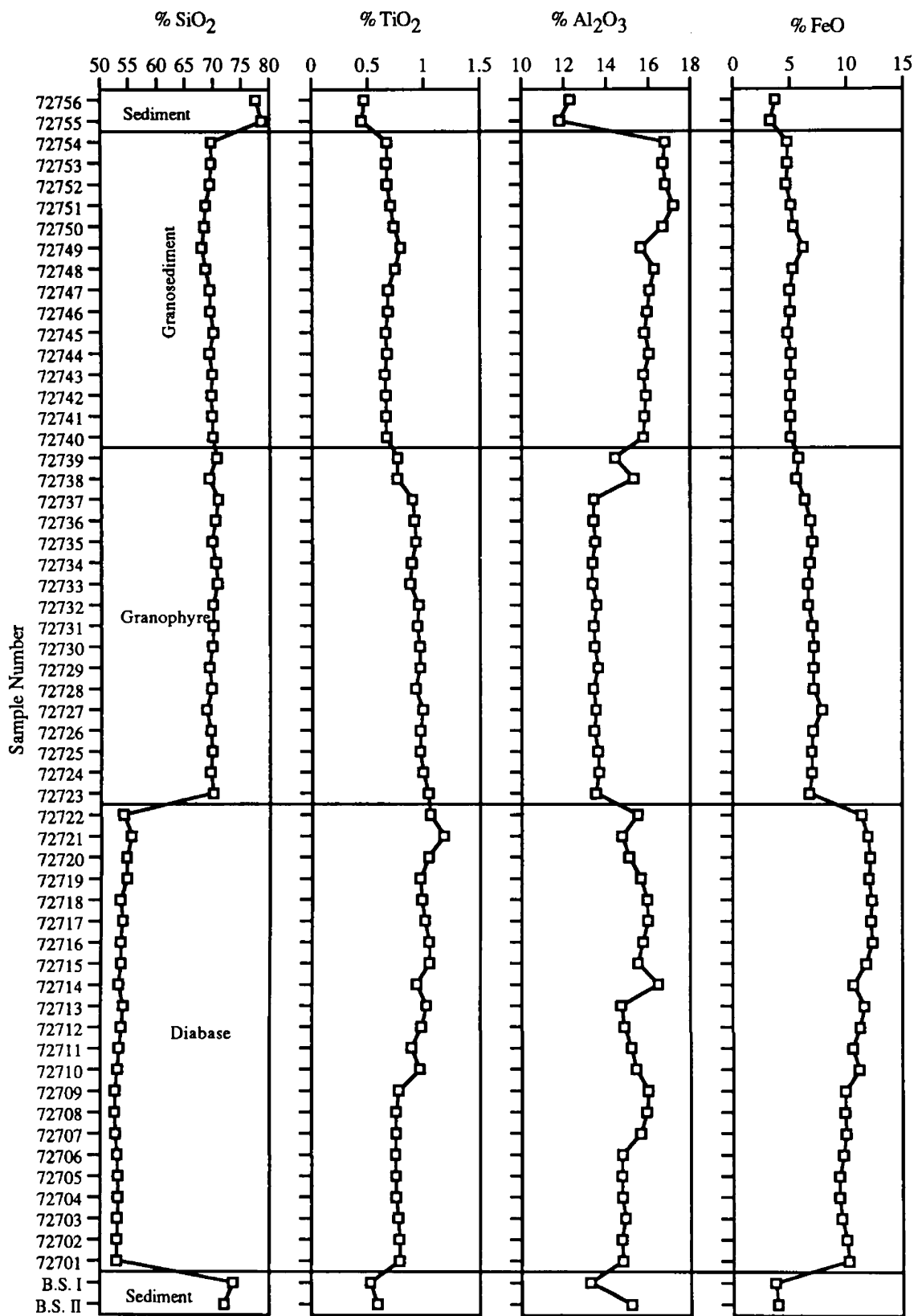
Figure 38. Major-oxide profiles upward through the Plains Sill at the Three Lakes Peak Trail Section. Continuous samples taken over 7 meter intervals.

% MnO   % MgO   % CaO   % K₂O

% MnO axis: 0   0.1   0.2
% MgO axis: 0   2   4   6   8   10
% CaO axis: 0   5   10   15
% K₂O axis: 0   1   2   3   4   5

Sample Number

72756
72755
Sediment

72754
72753
72752
72751
72750
72749
72748
72747
72746
72745
72744
72743
72742
72741
72740

Granosediment

72739
72738
72737
72736
72735
72734
72733
72732
72731
72730
72729
72728
72727
72726
72725
72724
72723

Granophyre

72722
72721
72720
72719
72718
72717
72716
72715
72714
72713
72712
72711
72710
72709
72708
72707
72706
72705
72704
72703
72702
72701

Diabase

B.S. I
B.S. II
Sediment
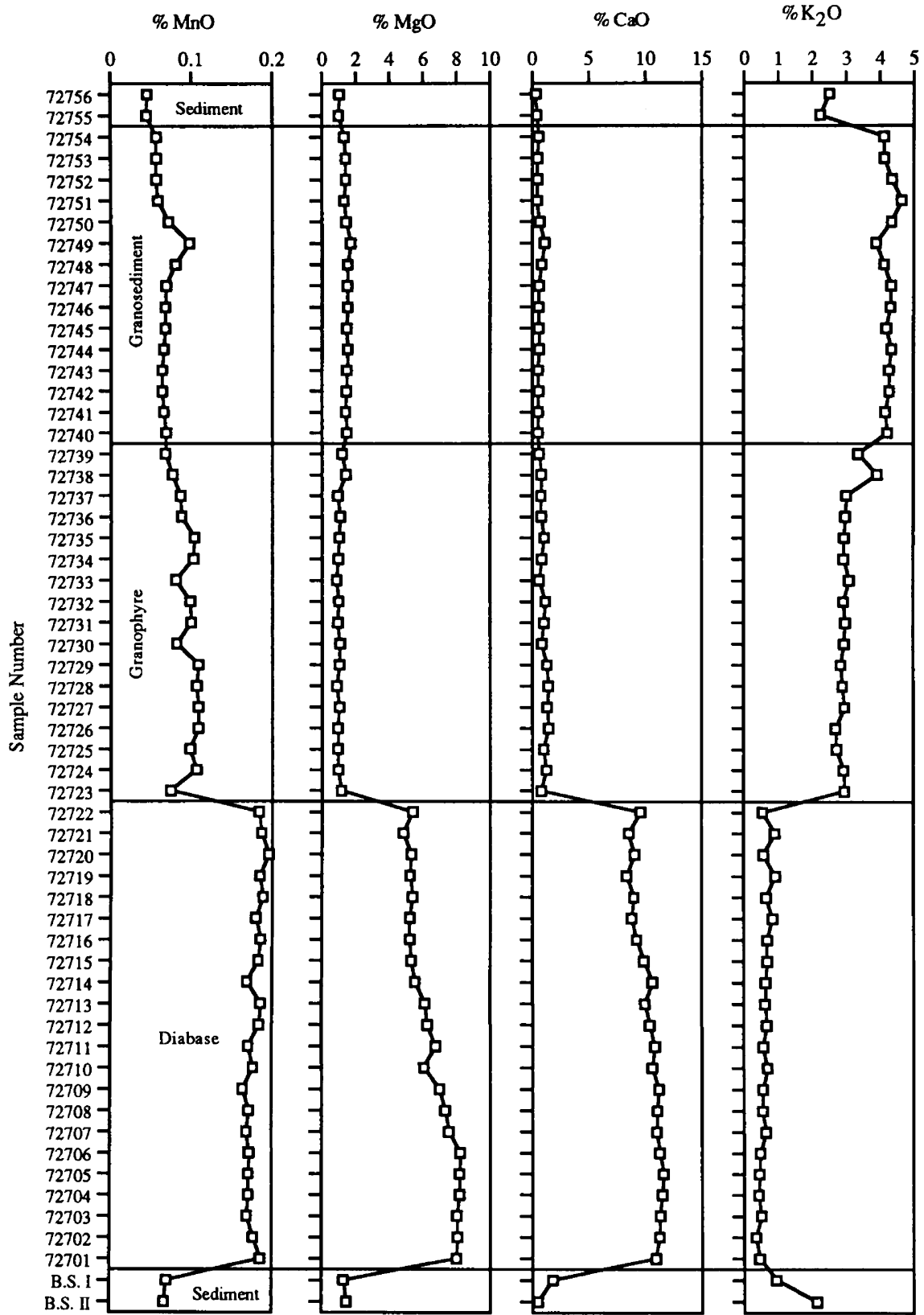
Figure 38 continued.
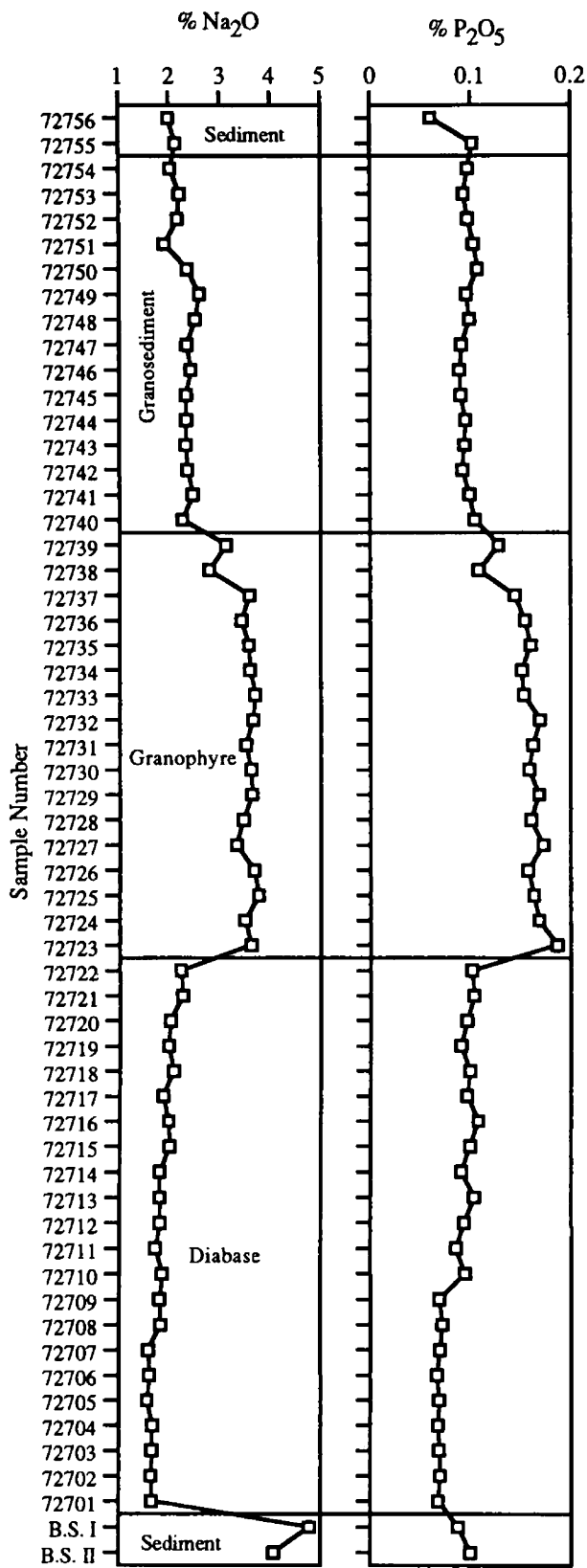
Figure 38 continued.
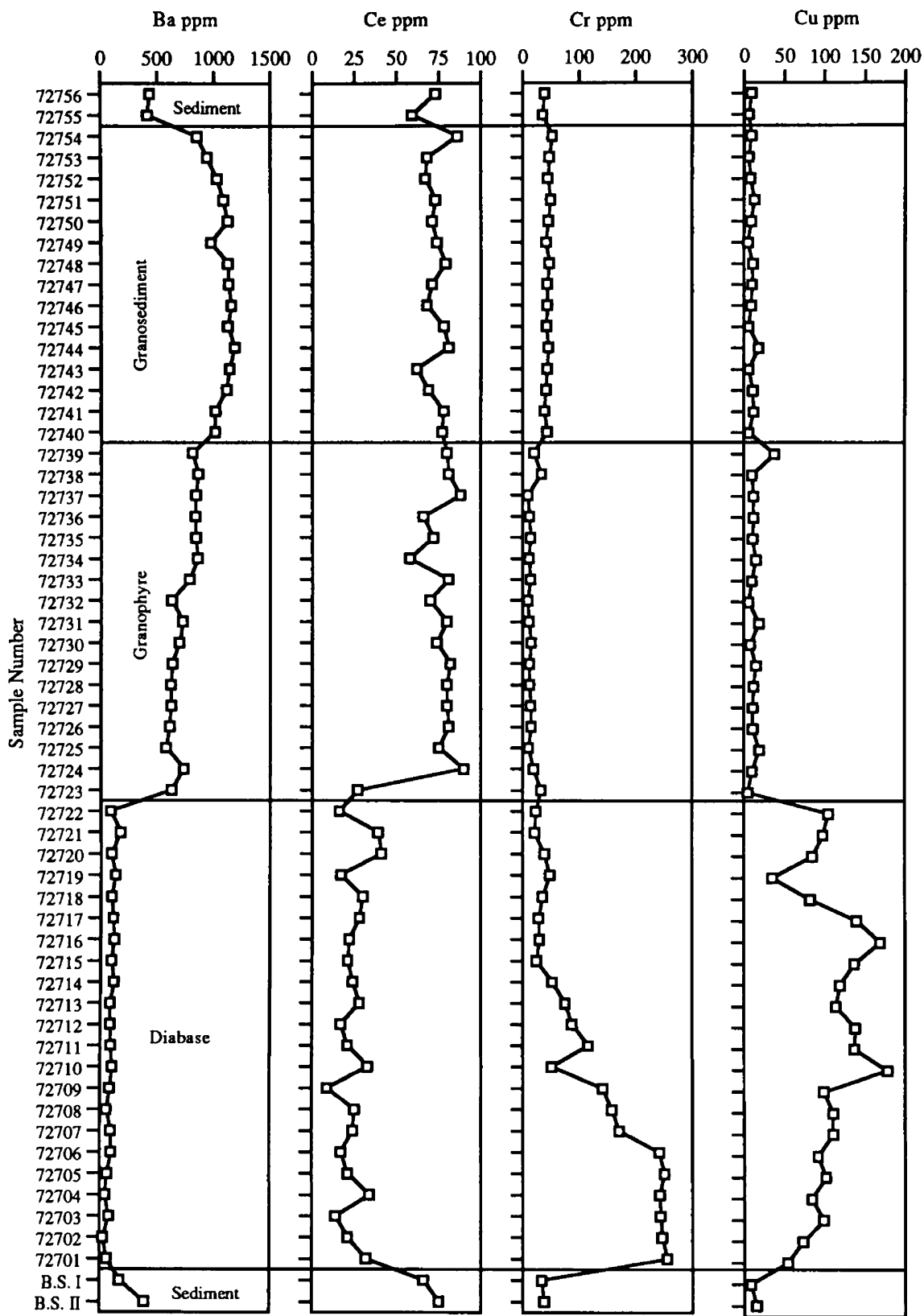
Figure 39. Trace-element profiles through the Plains Sill at the Three Lakes Peak Trail Section. Continuous samples taken over 7 meter intervals.
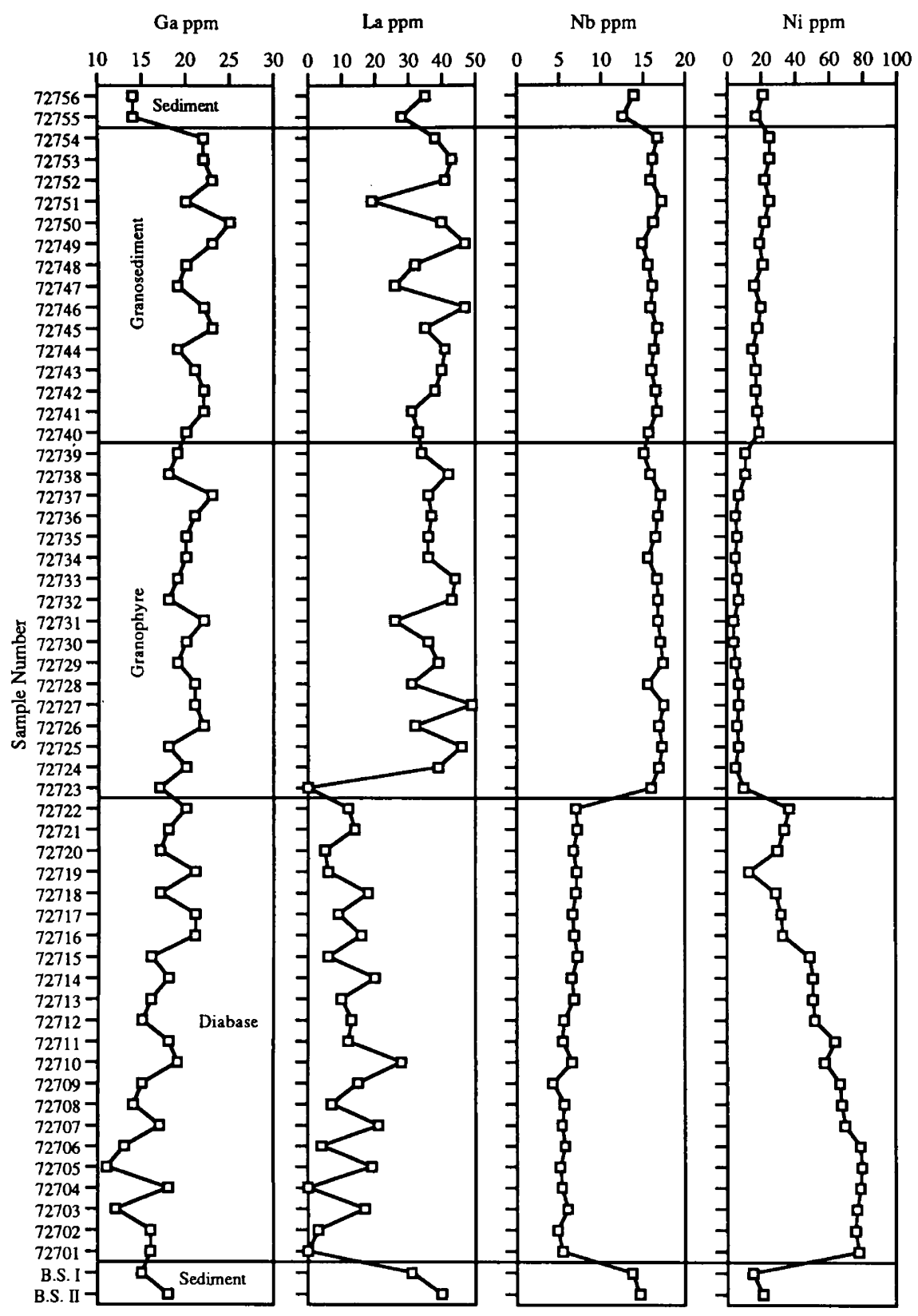
Figure 39 continued.
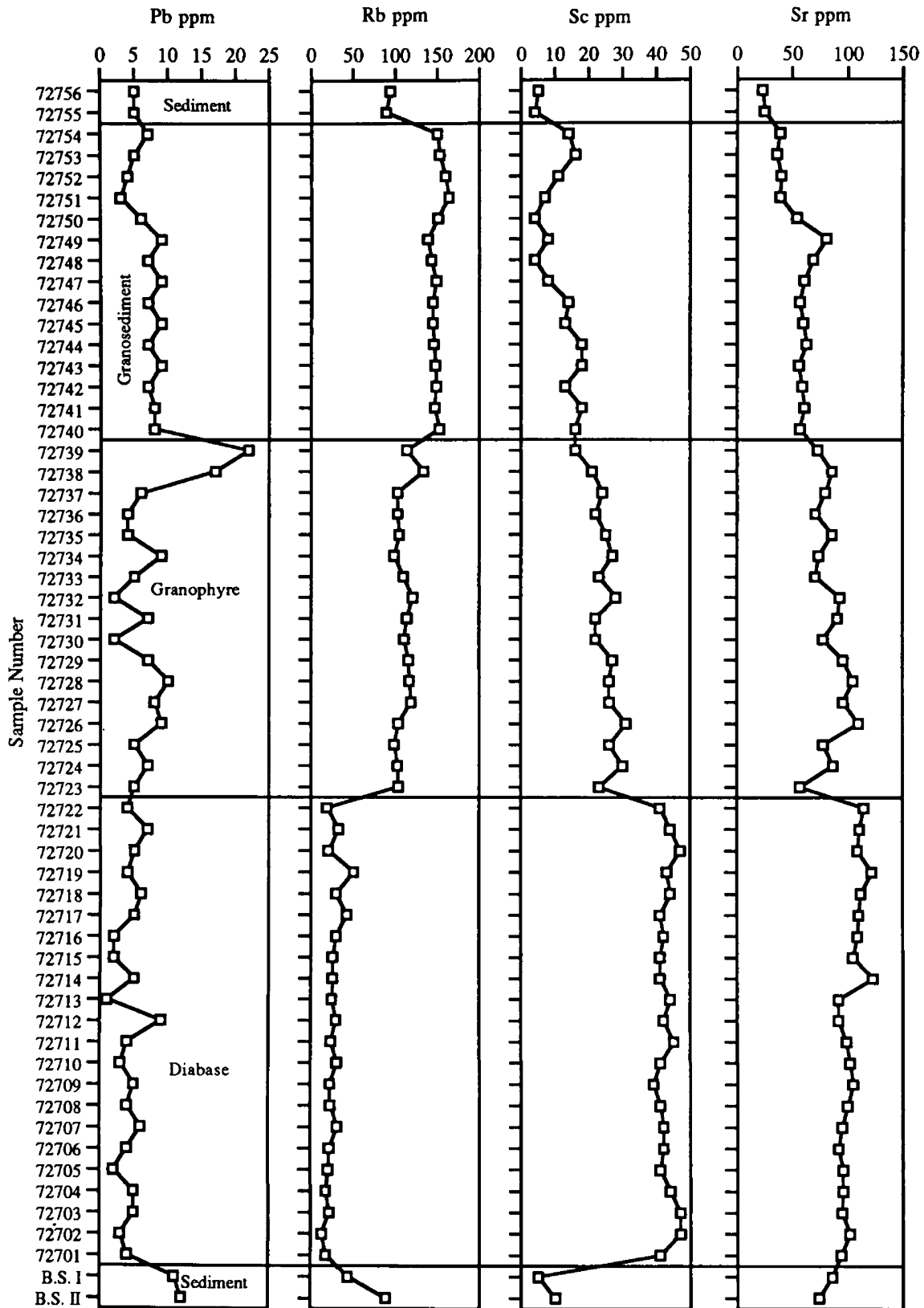
Figure 39 continued.
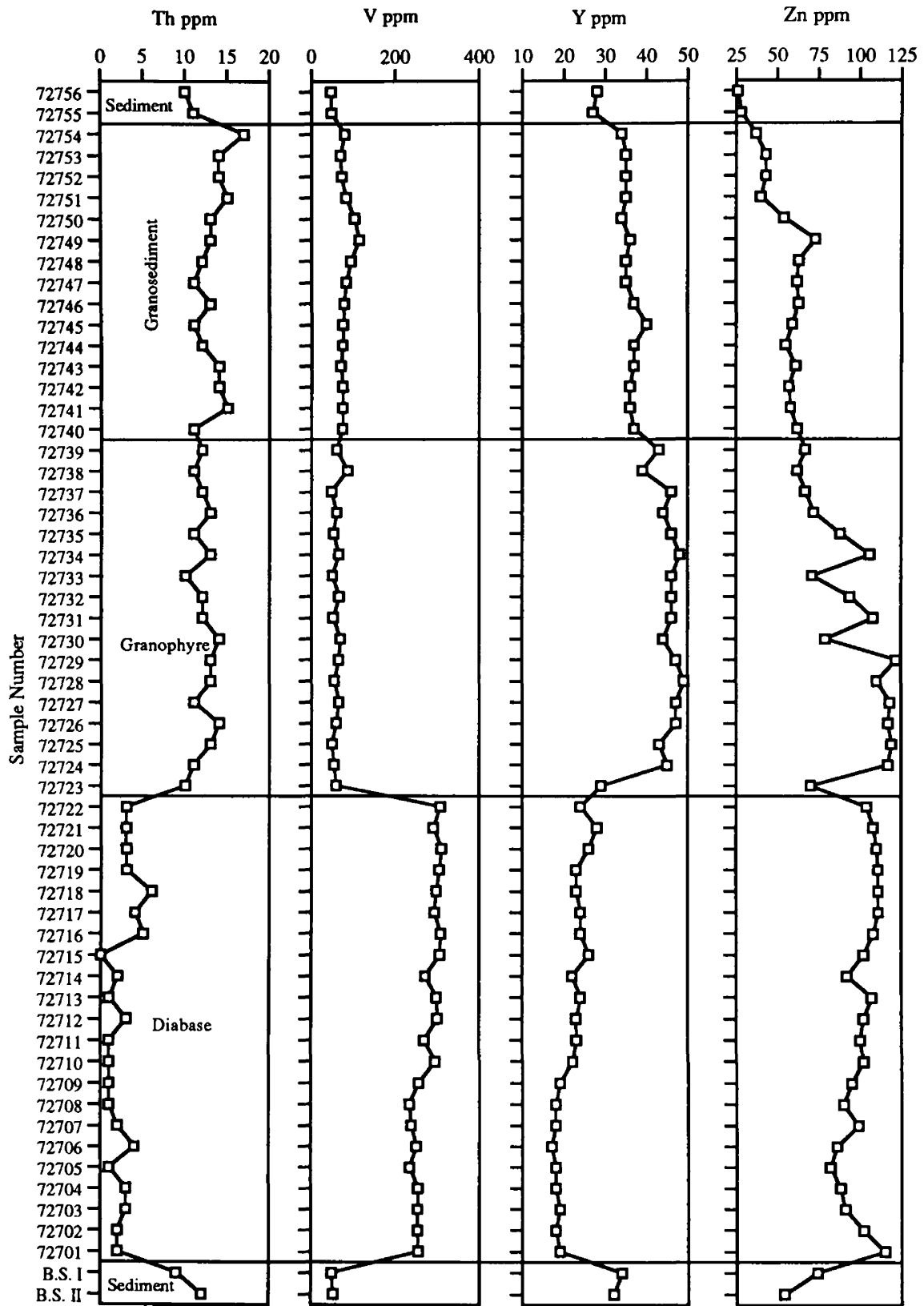
Figure 39 continued
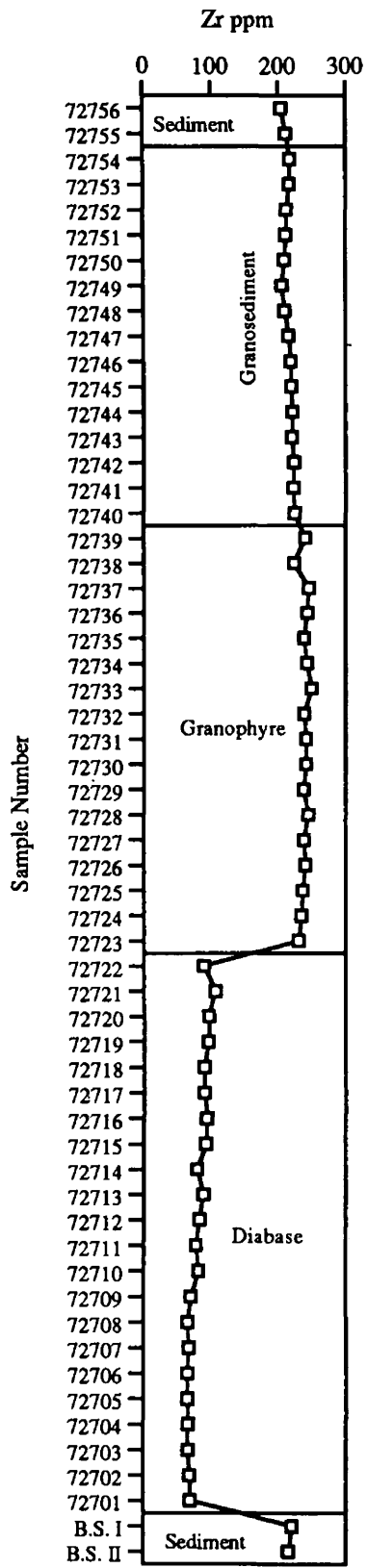
Figure 39 continued.
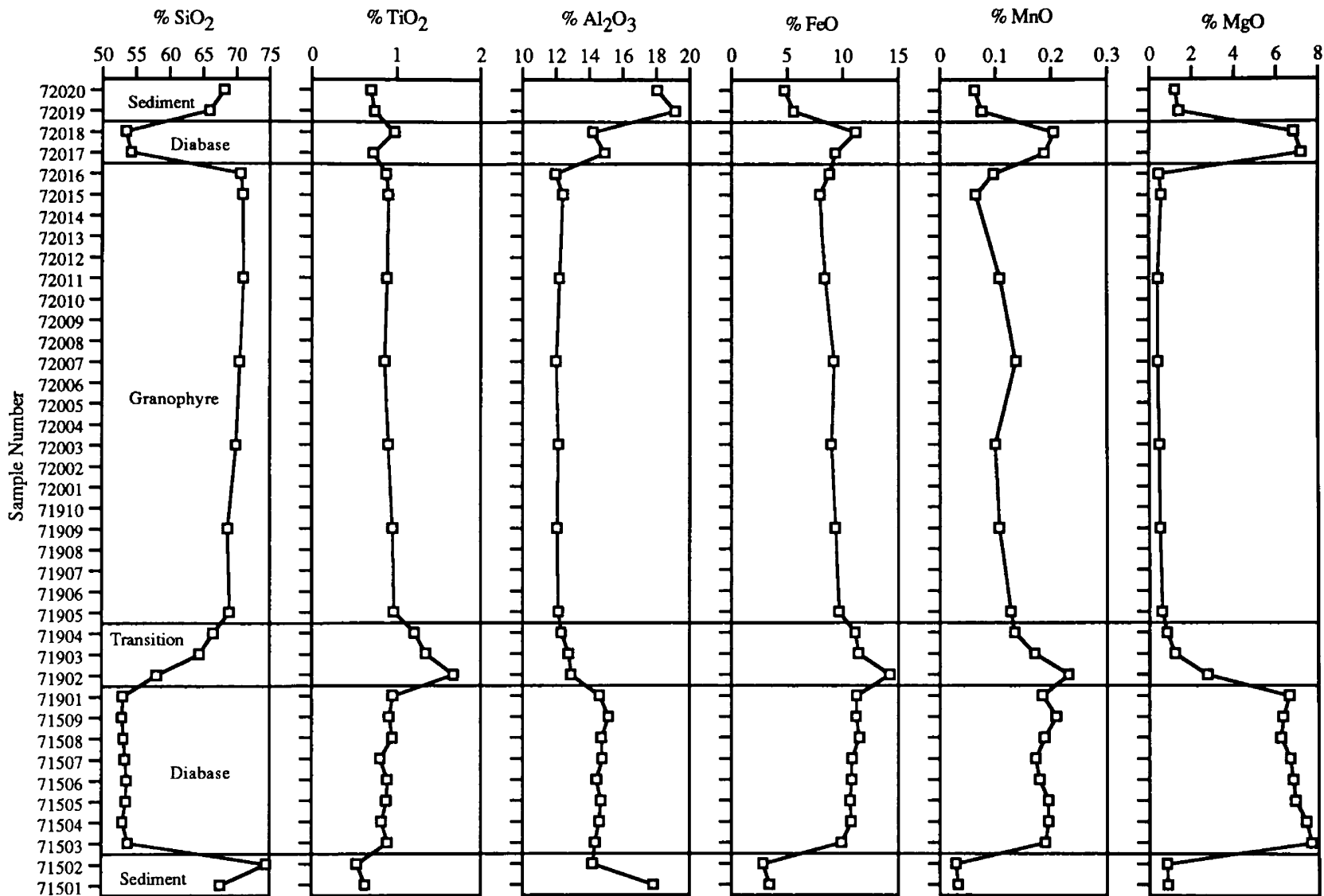
Figure 40. Major-oxide profiles upward through the Plains Sill at the Clear Creek Section. Continuous samples taken over 6 meter intervals. Only every fourth sample through the granophyre was analyzed.
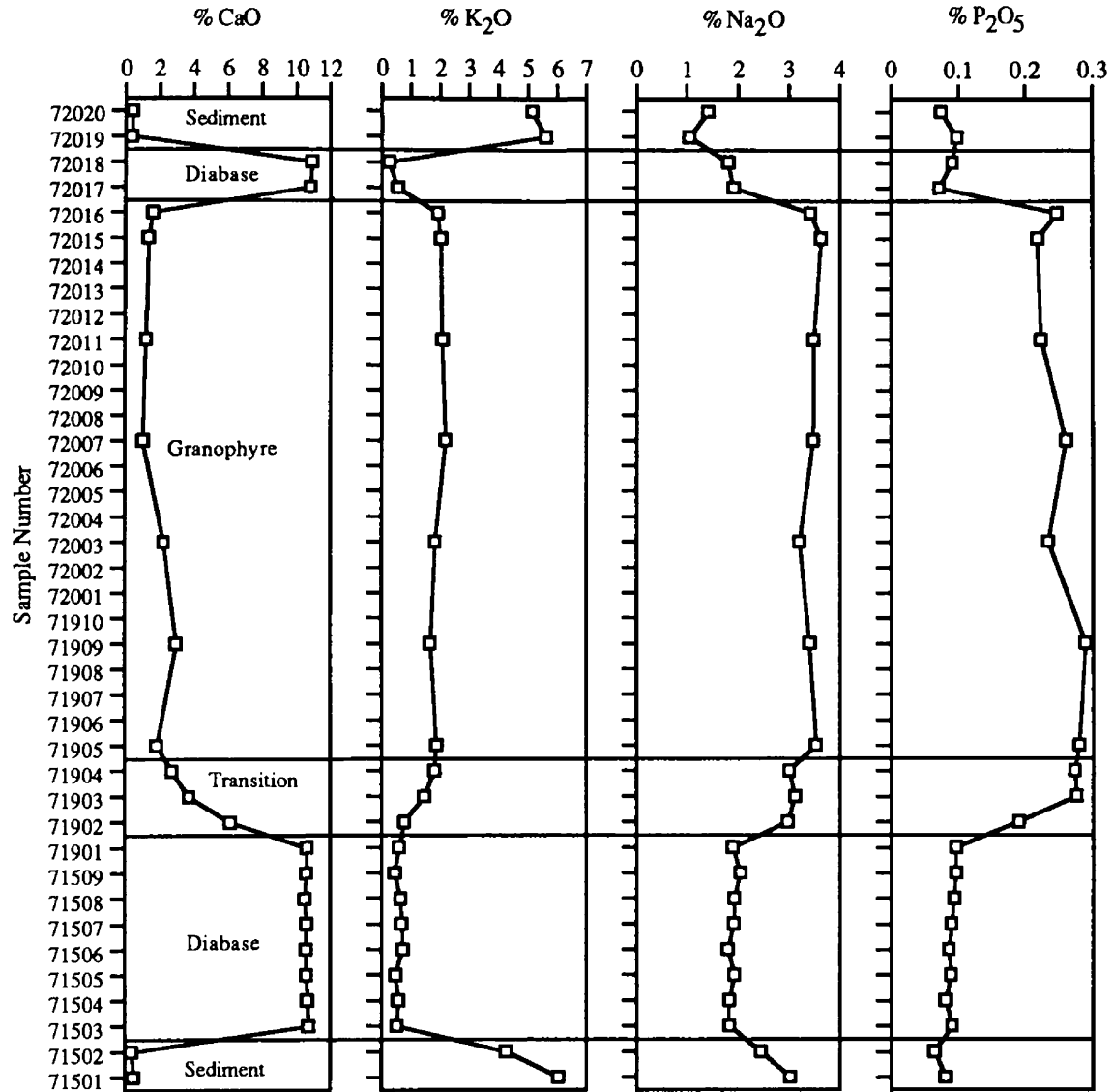
Figure 40 continued.
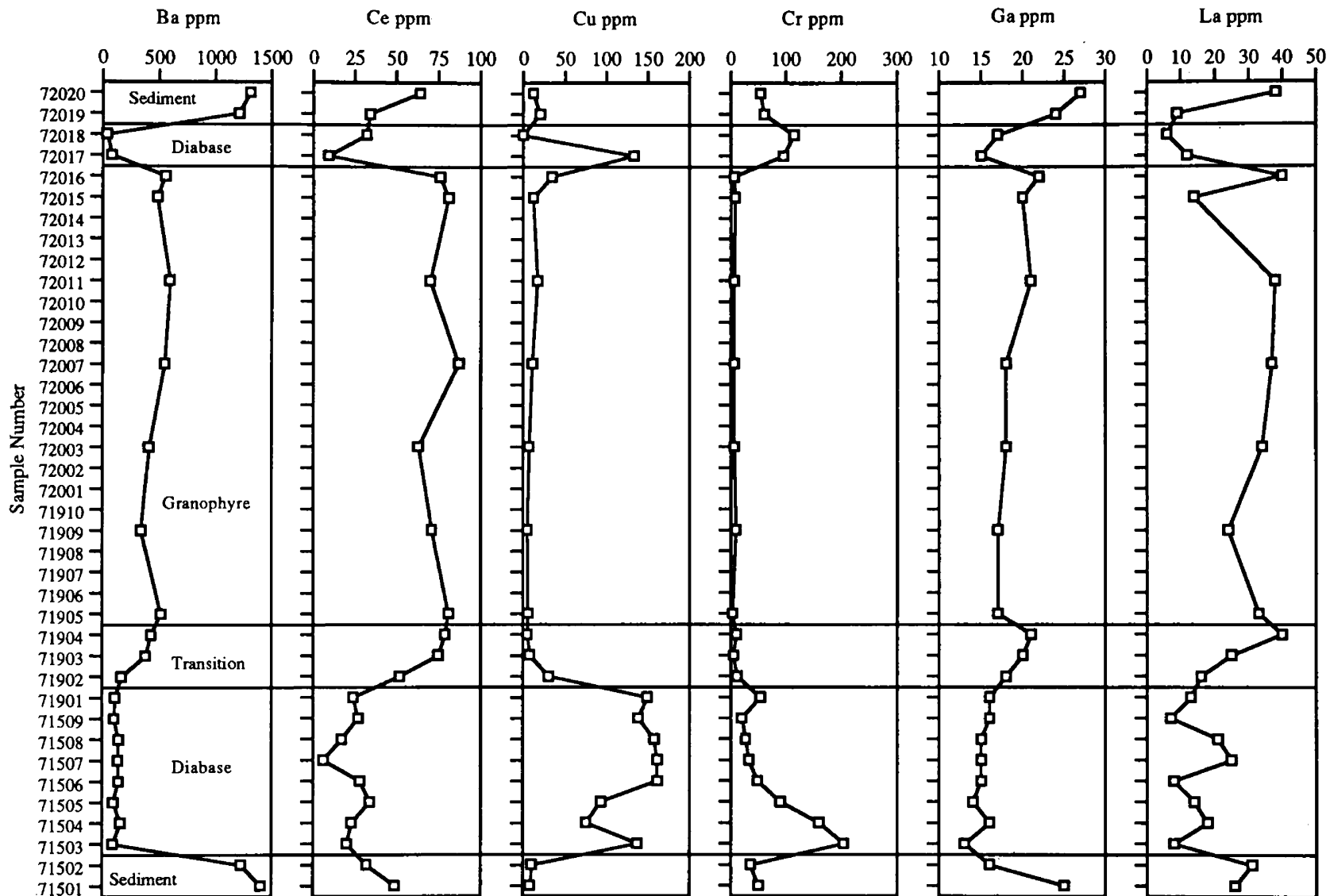
Figure 41. Trace-element profiles upward through the Plains Sill at the Clear Creek Section. Continuous samples taken over 6 meter intervals.
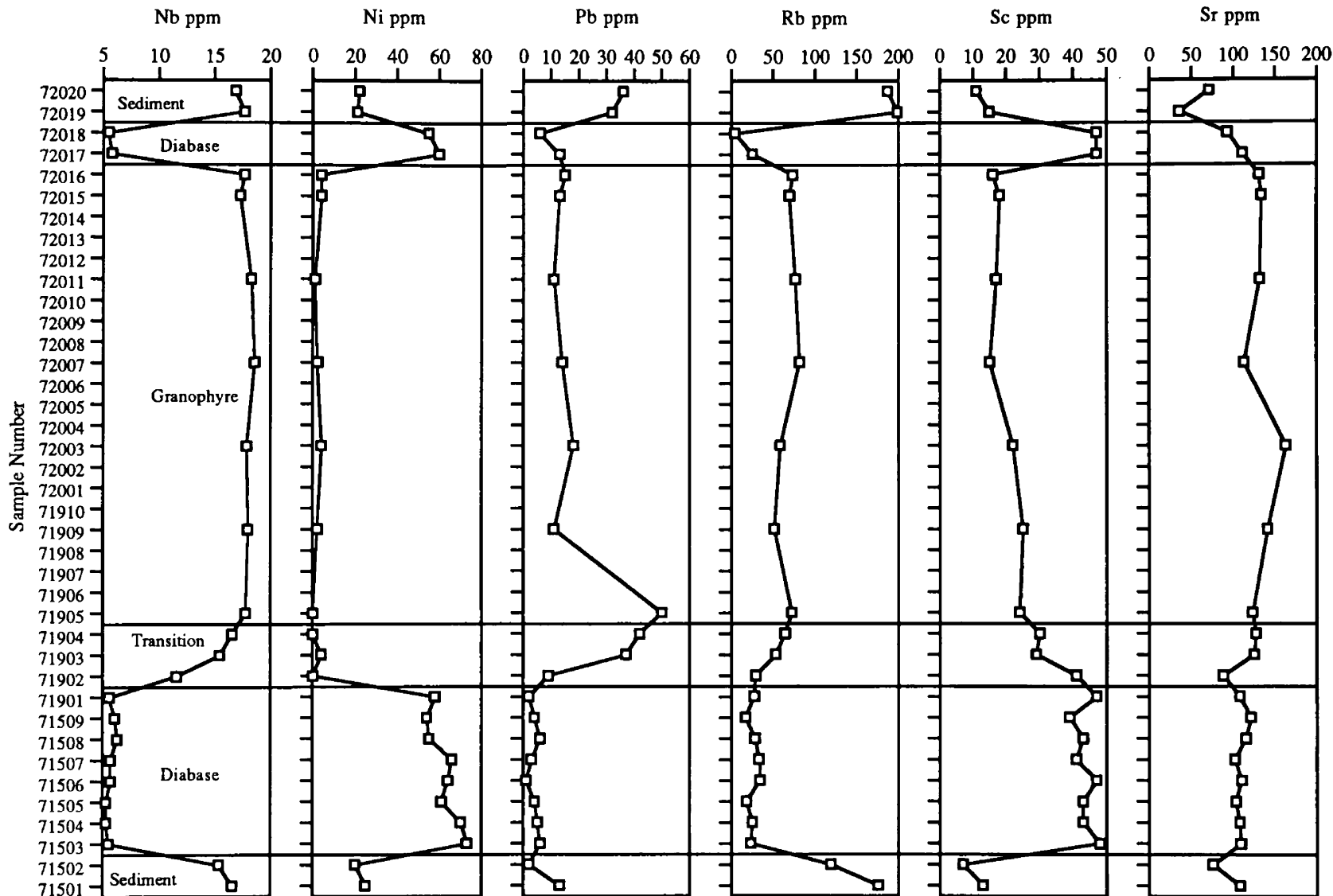
Figure 41 continued.
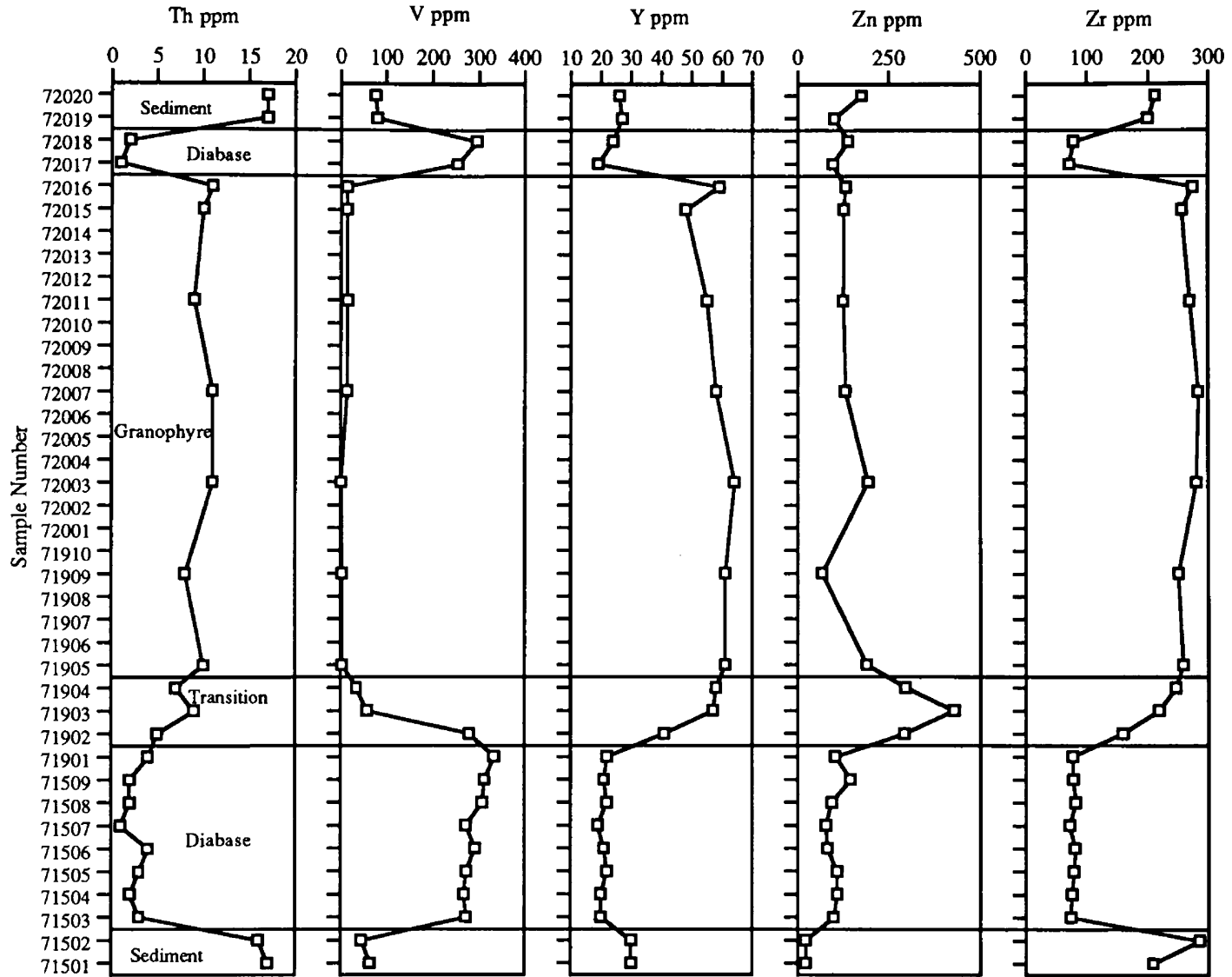
Figure 41 continued.
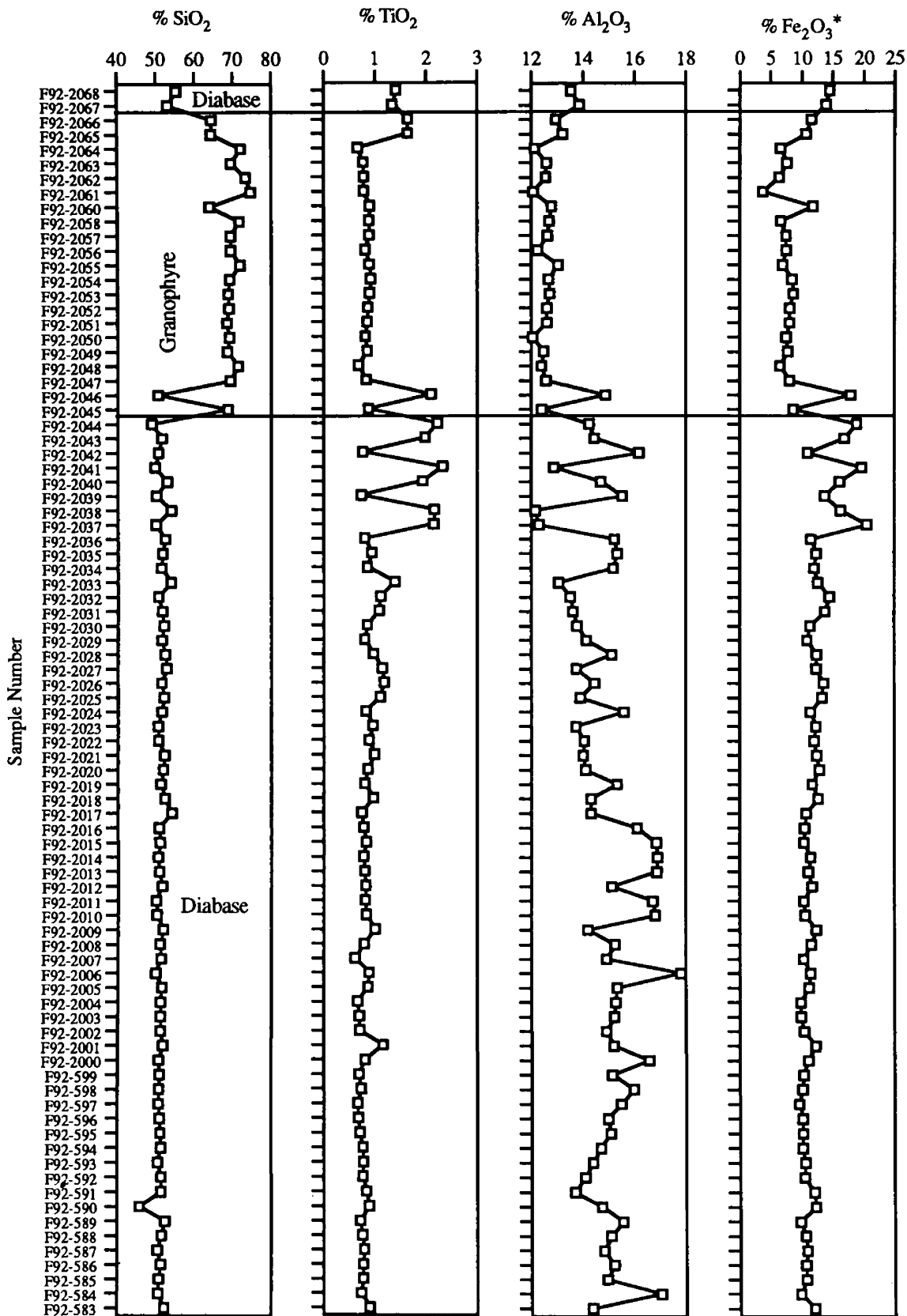
Figure 42. Major-oxide profiles through the Plains Sill at the Seepay
Ridge Section. Continuous samples taken over ~4 meter intervals.
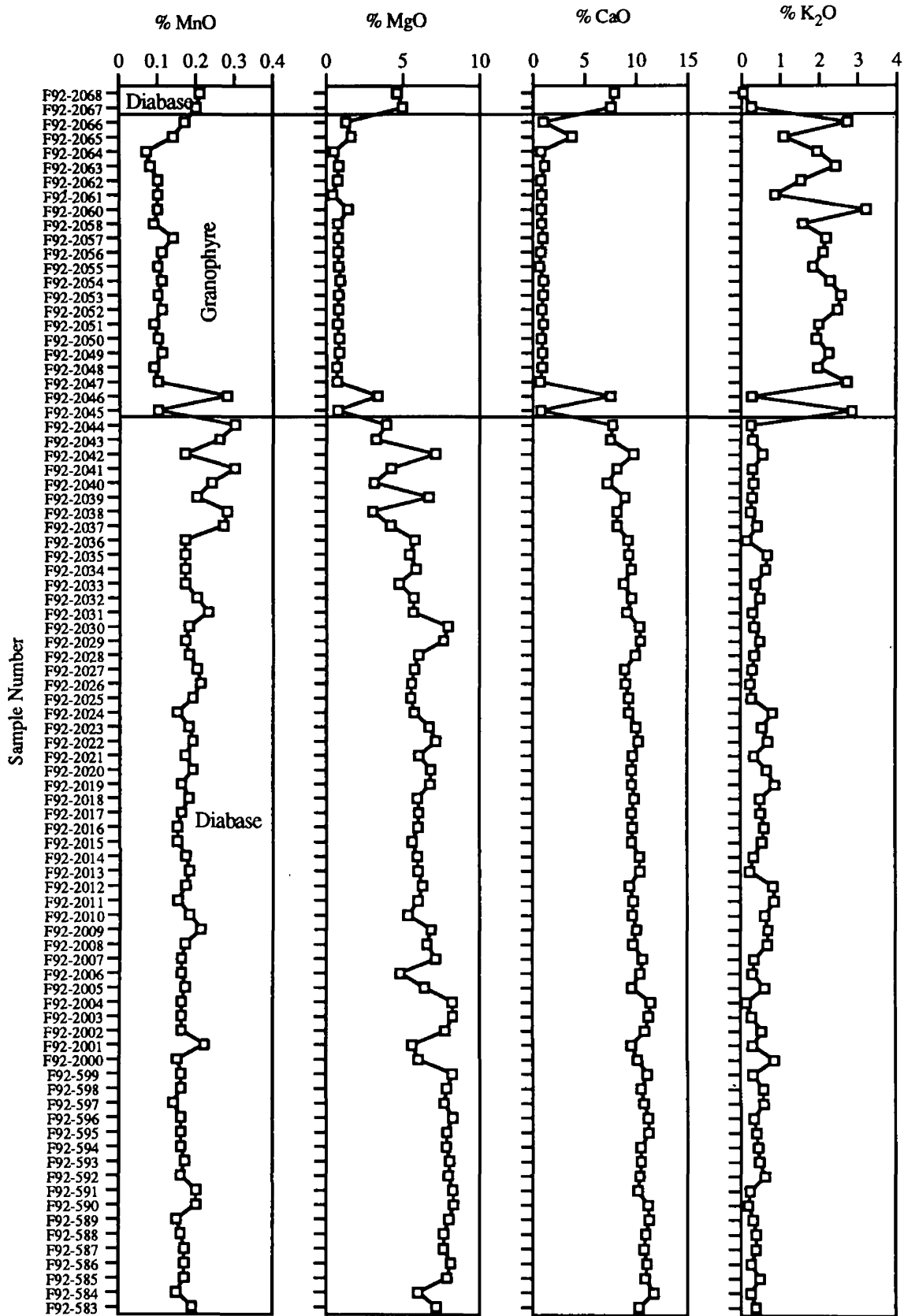
Figure 42 continued.
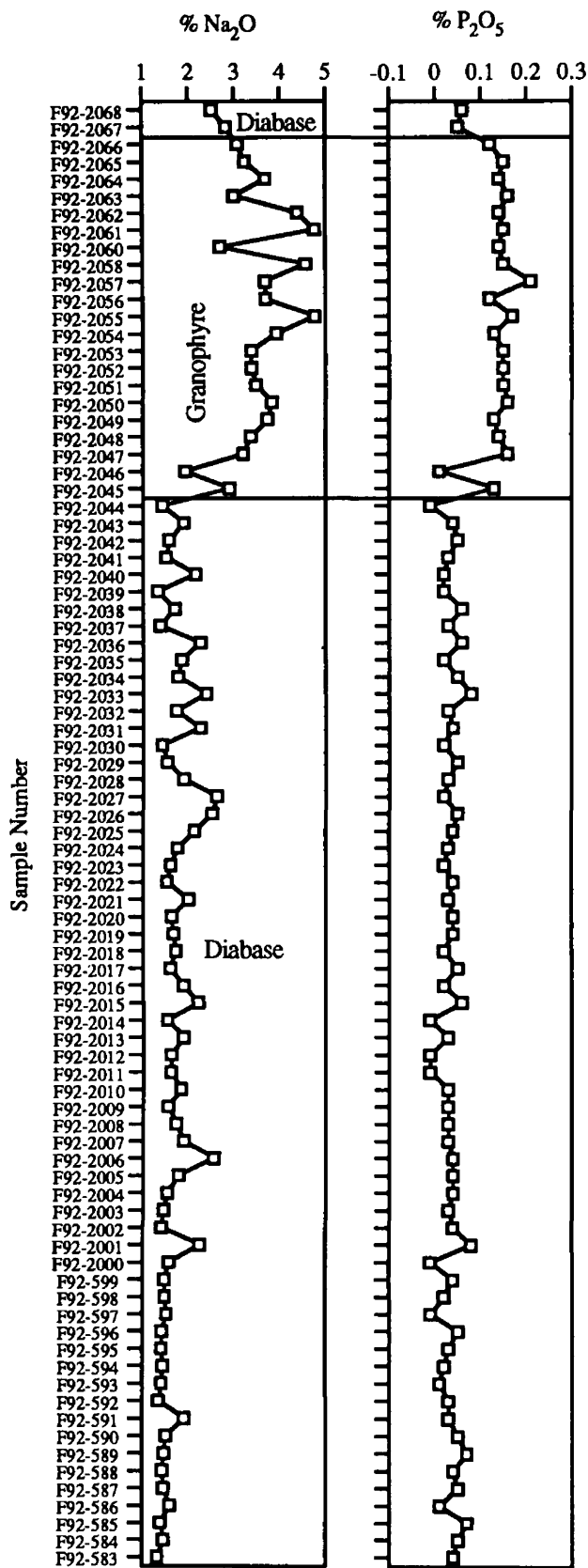
Figure 42 continued.
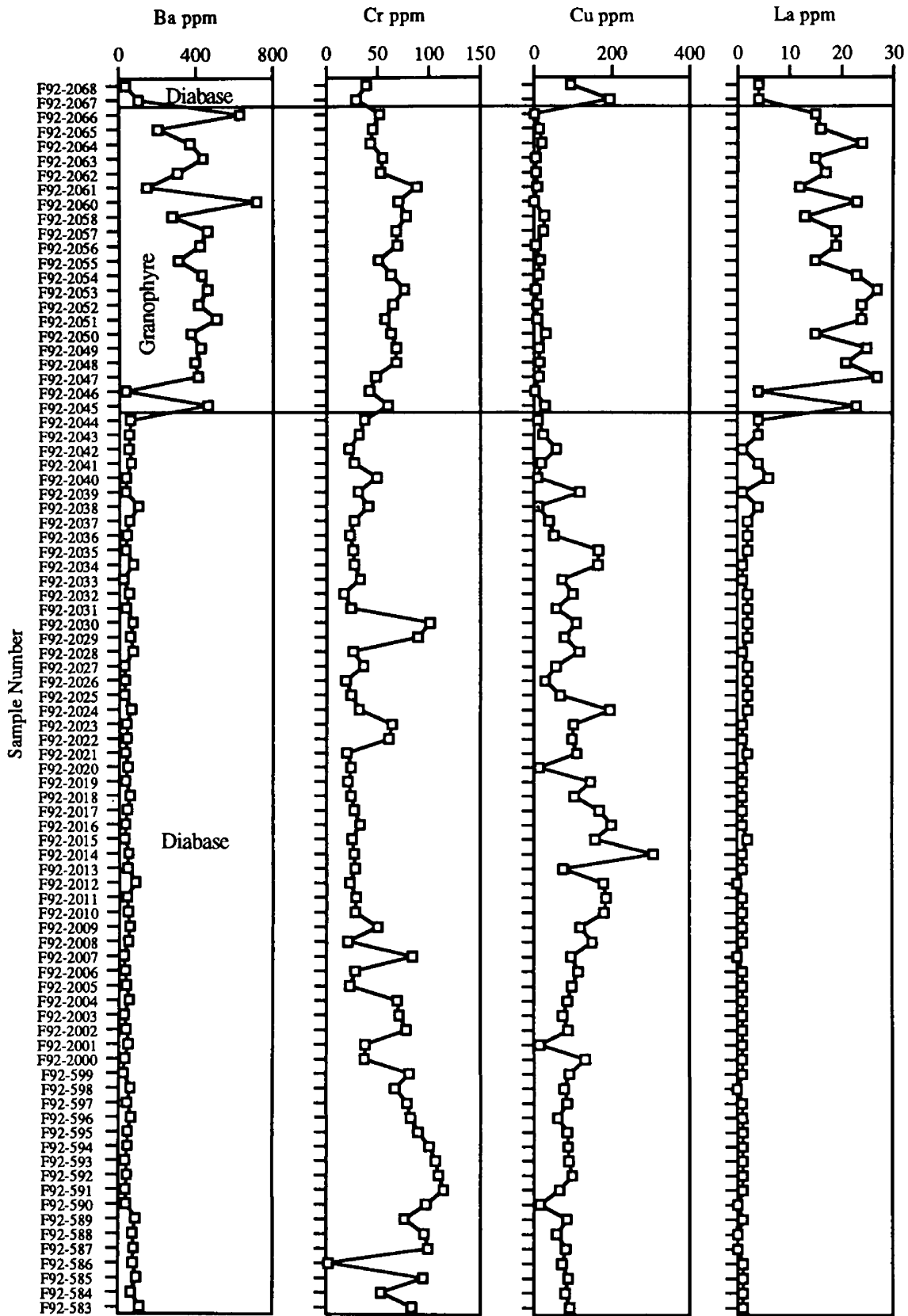
Figure 43. Trace-element profiles upward through the Plains Sill at the Seepay Ridge Section. Continuous samples taken over ~4 meter intervals.
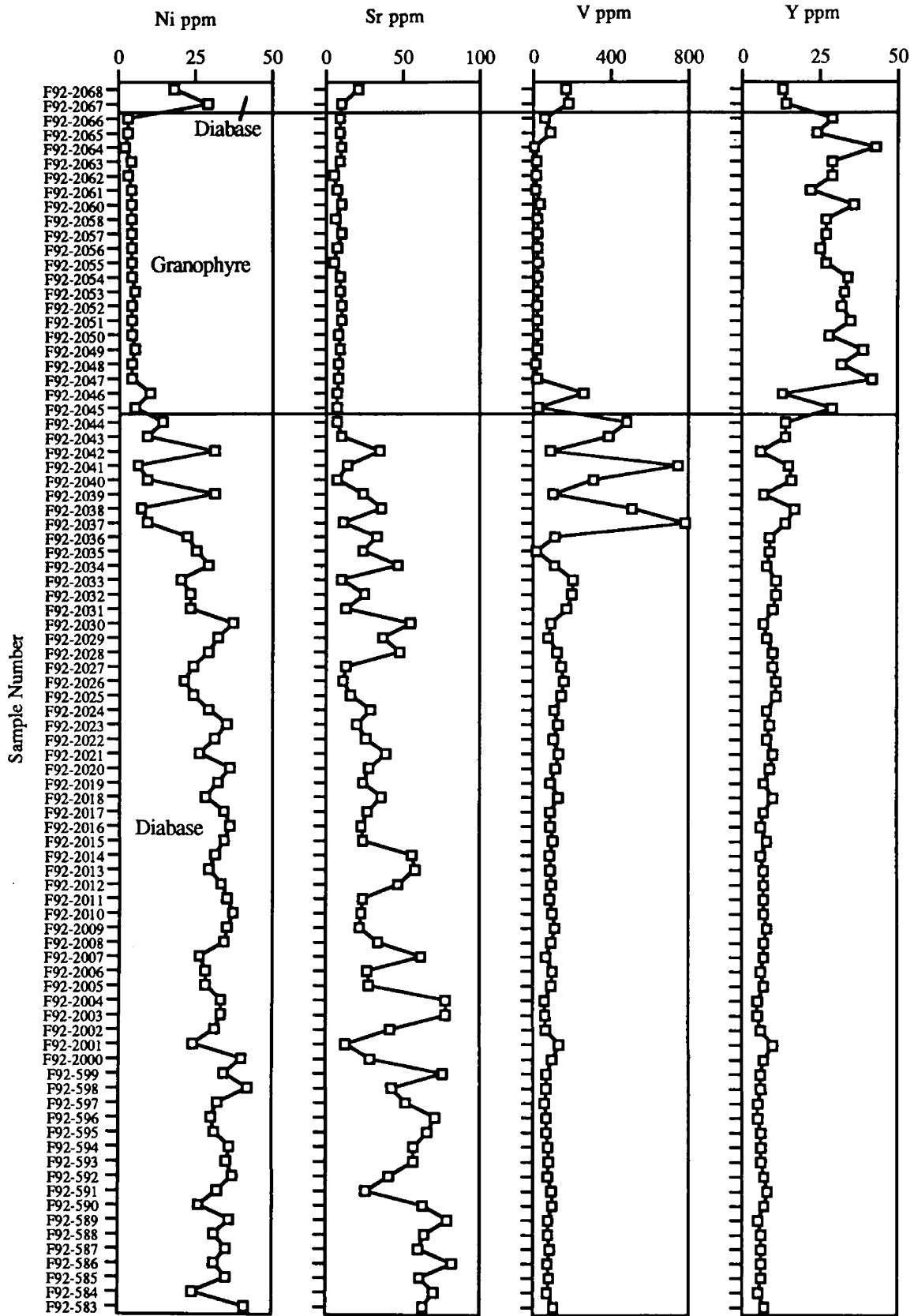
Figure 43 continued.
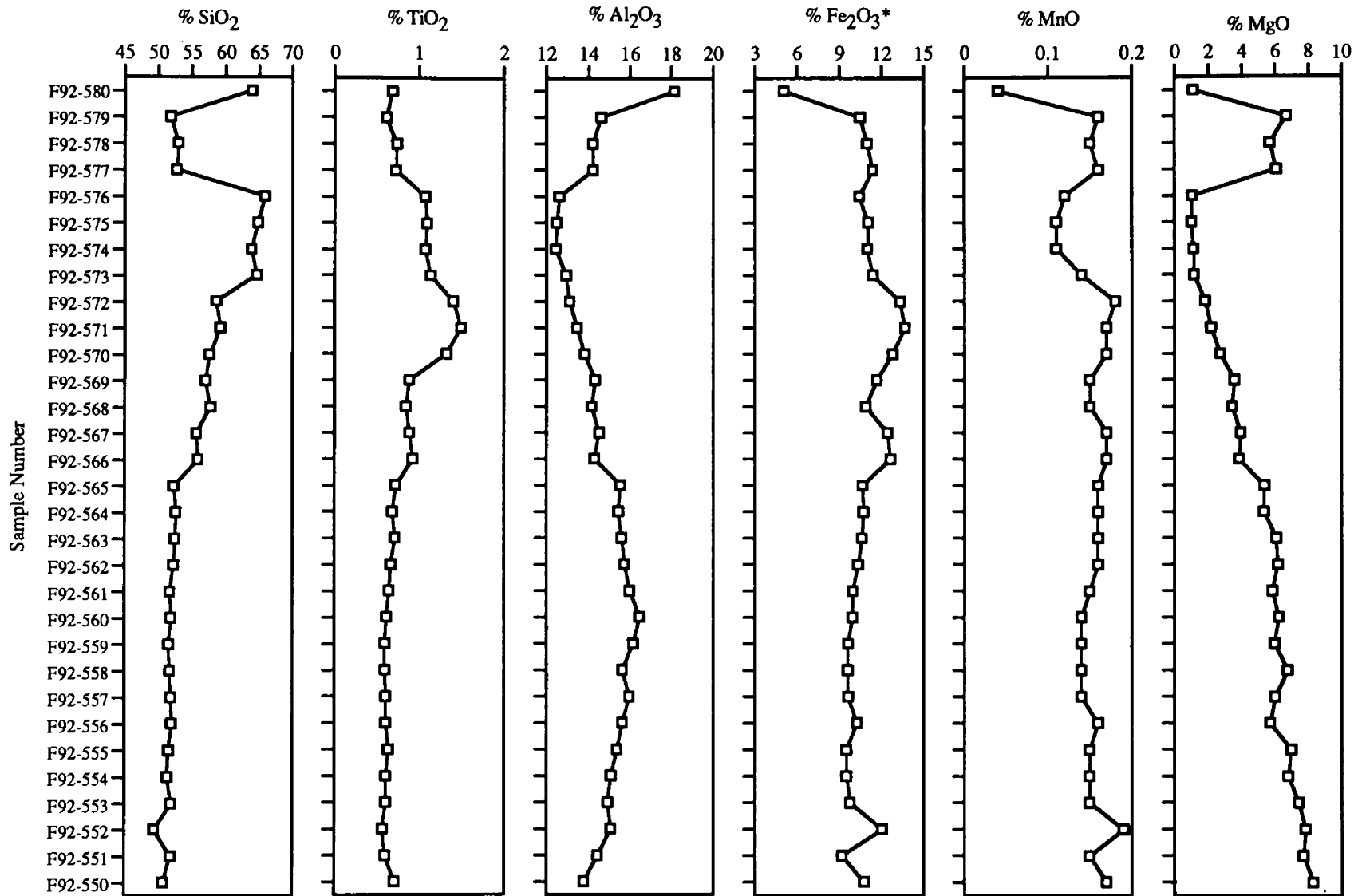
Figure 44. Major-oxide profiles upward through the Paradise Sill. Continuous samples taken over ~6 meter intervals.
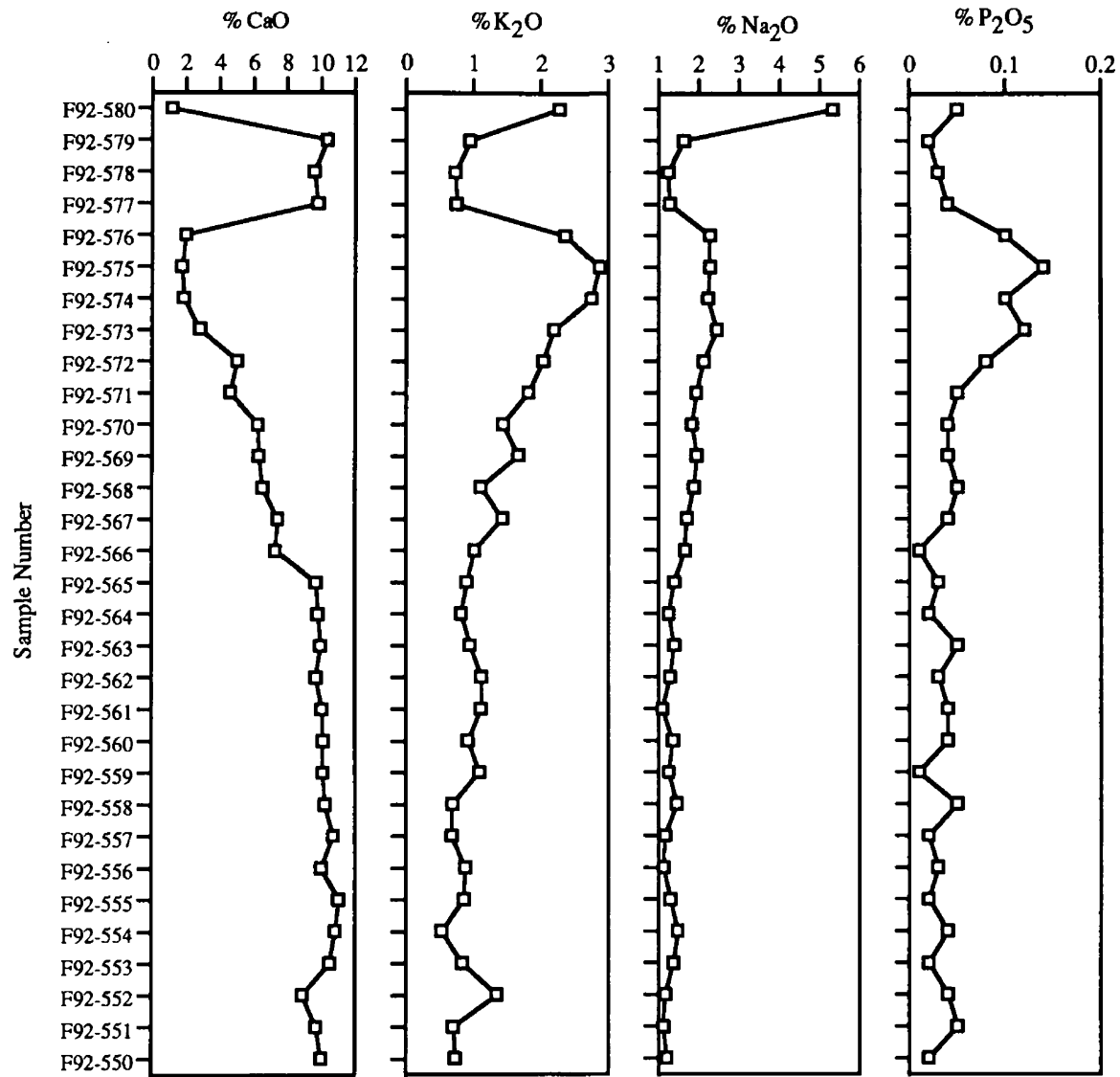
Figure 44 continued.
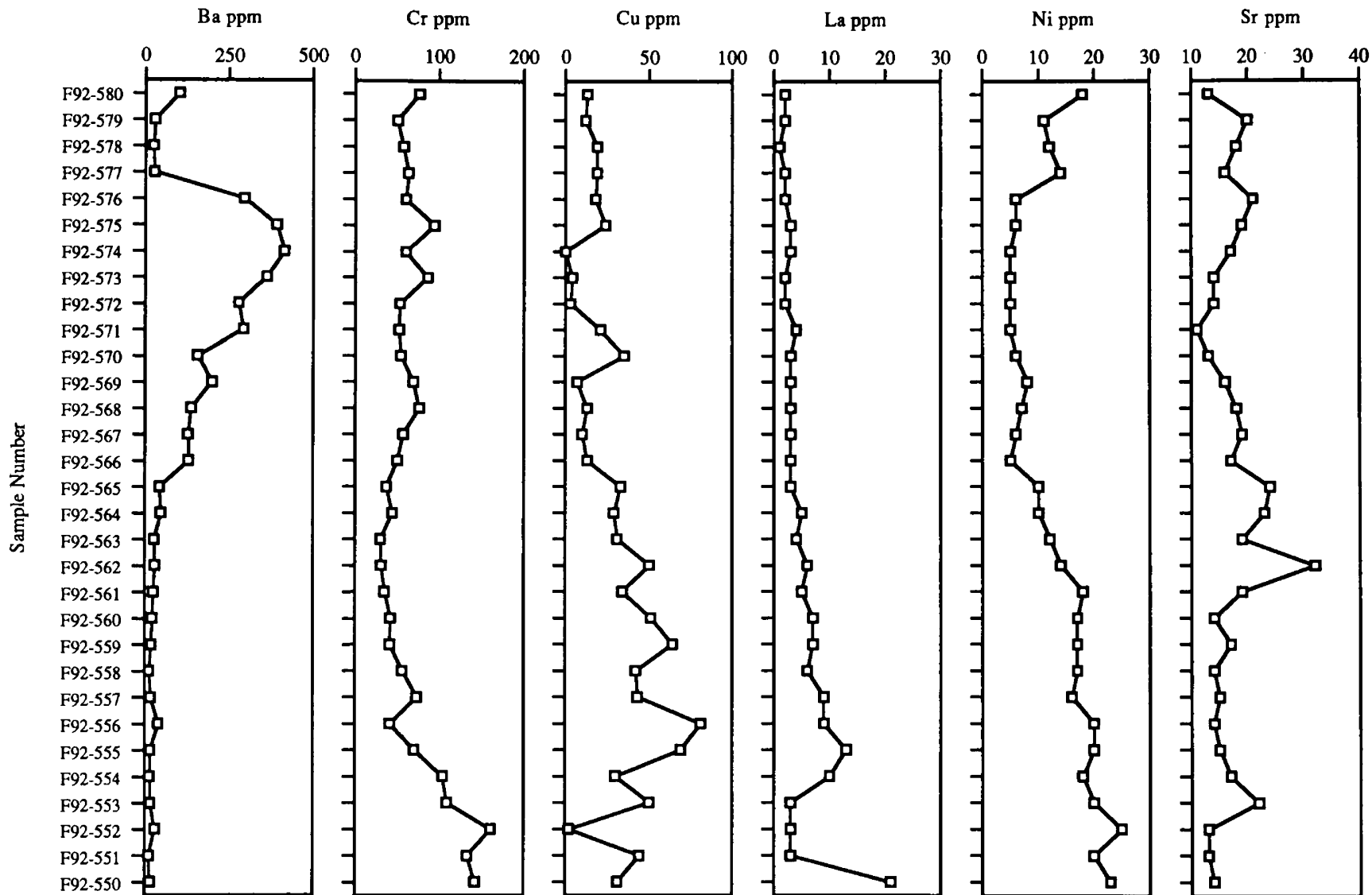
Figure 45. Trace-element profiles upward through the Paradise Sill. Continuous samples taken over ~6 meter intervals.
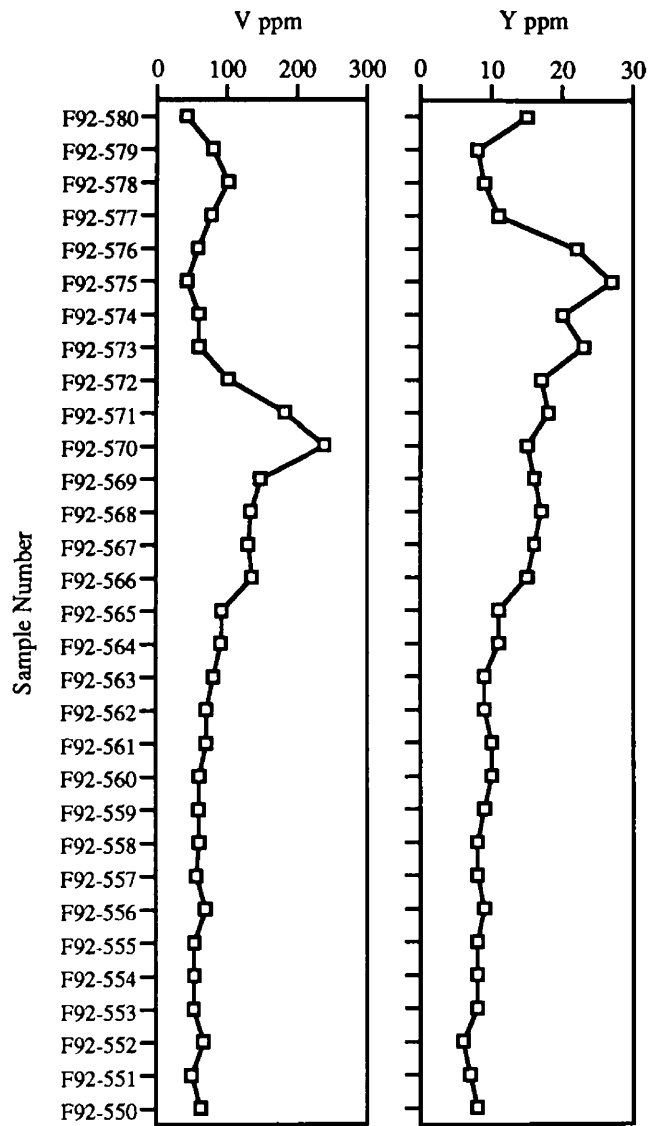
Figure 45 continued.

Sample	SiO2	TiO2	Al2O3	FeO*	MnO	MgO	CaO	Na2O	K2O	P2O5
B.S. II	72.00	0.59	15.19	3.90	0.07	1.46	0.49	4.07	2.14	0.10
B.S. I	73.59	0.53	13.23	3.69	0.07	1.29	1.79	4.78	0.94	0.09
72701	52.92	0.79	14.78	10.22	0.19	8.00	10.93	1.65	0.45	0.07
72702	52.93	0.78	14.72	10.03	0.18	8.05	11.25	1.64	0.34	0.07
72703	53.00	0.77	14.89	9.60	0.17	8.02	11.32	1.66	0.50	0.07
72704	53.10	0.75	14.75	9.39	0.17	8.17	11.51	1.67	0.42	0.07
72705	53.08	0.75	14.73	9.41	0.17	8.18	11.61	1.56	0.45	0.07
72706	52.95	0.74	14.75	9.74	0.17	8.21	11.28	1.61	0.47	0.07
72707	52.64	0.75	15.62	9.98	0.17	7.54	11.01	1.58	0.64	0.07
72708	52.47	0.75	15.90	9.89	0.17	7.32	11.06	1.82	0.54	0.07
72709	52.55	0.77	15.98	9.94	0.16	6.98	11.20	1.80	0.55	0.07
72710	52.97	0.96	15.40	11.17	0.18	6.06	10.62	1.85	0.69	0.09
72711	53.22	0.89	15.17	10.58	0.17	6.77	10.84	1.71	0.57	0.08
72712	53.58	0.98	14.83	11.23	0.18	6.26	10.37	1.80	0.67	0.09
72713	53.93	1.02	14.68	11.60	0.19	6.11	9.97	1.79	0.62	0.10
72714	53.08	0.93	16.47	10.65	0.17	5.52	10.67	1.79	0.64	0.09
72715	53.52	1.05	15.50	11.78	0.18	5.30	9.90	1.99	0.68	0.10
72716	53.47	1.04	15.74	12.34	0.19	5.22	9.25	1.97	0.68	0.11
72717	53.81	1.01	15.98	12.21	0.18	5.22	8.81	1.86	0.84	0.10
72718	53.39	0.98	15.94	12.30	0.19	5.38	9.02	2.06	0.65	0.10
72719	54.56	0.97	15.65	12.04	0.19	5.24	8.38	1.97	0.92	0.09
72720	54.47	1.04	15.08	12.17	0.20	5.31	9.07	2.00	0.57	0.10
72721	55.29	1.18	14.76	11.95	0.19	4.83	8.56	2.24	0.91	0.10
72722	53.97	1.05	15.50	11.40	0.18	5.41	9.62	2.21	0.55	0.10
72723	69.90	1.04	13.51	6.79	0.07	1.14	0.79	3.61	2.96	0.19
72724	69.39	0.99	13.66	7.03	0.11	0.96	1.26	3.49	2.94	0.17
72725	69.73	0.96	13.61	7.00	0.10	0.94	1.01	3.76	2.73	0.16
72726	69.44	0.97	13.44	7.13	0.11	0.93	1.45	3.67	2.70	0.16
72727	68.66	0.99	13.52	7.91	0.11	1.02	1.33	3.32	2.96	0.17
72728	69.60	0.92	13.39	7.17	0.11	0.87	1.43	3.46	2.90	0.16
72729	69.17	0.96	13.62	7.17	0.11	1.03	1.29	3.63	2.85	0.17

Table 4. XRF major-oxide data for the Plains Sill at the Three Lakes Peak section. All analyses performed by Washingtor State University's GeoAnalytical Laboratory.

Sample	SiO2	TiO2	Al2O3	FeO*	MnO	MgO	CaO	Na2O	K2O	P2O5
72730	69.72	0.96	13.46	7.18	0.08	1.06	0.83	3.61	2.95	0.16
72731	69.87	0.94	13.41	7.07	0.10	0.93	1.03	3.51	2.98	0.16
72732	69.80	0.95	13.55	6.71	0.10	0.98	1.15	3.65	2.93	0.17
72733	70.63	0.87	13.35	6.66	0.08	0.85	0.61	3.69	3.10	0.15
72734	70.33	0.89	13.35	6.84	0.10	0.96	0.84	3.59	2.94	0.15
72735	69.66	0.93	13.49	7.07	0.10	1.01	1.06	3.57	2.95	0.16
72736	70.26	0.92	13.40	6.89	0.09	1.08	0.79	3.42	2.99	0.15
72737	70.76	0.90	13.42	6.38	0.09	0.93	0.77	3.58	3.02	0.14
72738	69.19	0.76	15.31	5.64	0.08	1.42	0.80	2.78	3.92	0.11
72739	70.50	0.76	14.42	5.84	0.07	1.18	0.61	3.12	3.37	0.13
72740	69.80	0.66	15.77	5.14	0.07	1.48	0.51	2.25	4.22	0.10
72741	69.70	0.66	15.82	5.12	0.06	1.40	0.52	2.46	4.16	0.10
72742	69.56	0.66	15.89	5.09	0.06	1.45	0.55	2.35	4.28	0.09
72743	69.73	0.65	15.77	5.11	0.06	1.48	0.50	2.32	4.27	0.09
72744	69.17	0.67	16.05	5.15	0.07	1.52	0.61	2.33	4.34	0.09
72745	69.96	0.66	15.82	4.86	0.07	1.47	0.57	2.33	4.19	0.09
72746	69.33	0.68	15.95	5.08	0.07	1.52	0.55	2.42	4.31	0.09
72747	69.30	0.68	16.06	5.03	0.07	1.50	0.60	2.34	4.33	0.09
72748	68.50	0.74	16.29	5.31	0.08	1.52	0.82	2.51	4.12	0.10
72749	67.87	0.79	15.65	6.23	0.10	1.70	1.09	2.59	3.88	0.10
72750	68.32	0.73	16.69	5.33	0.07	1.42	0.64	2.35	4.34	0.11
72751	68.58	0.70	17.19	5.11	0.06	1.30	0.41	1.90	4.64	0.10
72752	69.33	0.67	16.80	4.69	0.06	1.40	0.45	2.16	4.35	0.10
72753	69.54	0.67	16.69	4.79	0.06	1.39	0.45	2.20	4.12	0.09
72754	69.61	0.67	16.78	4.78	0.06	1.31	0.56	2.02	4.11	0.10
72755	78.58	0.45	11.80	3.30	0.04	0.98	0.39	2.12	2.23	0.10
72756	77.60	0.47	12.29	3.71	0.05	1.03	0.32	1.98	2.50	0.06

Table 4 continued.

Sample	Ba	Ce	Cr	Cu	Ga	La	Nb	Ni	Pb	Rb	Sc	Sr	Th	V	Y	Zn	Zr
B.S. II	392	75	37	15	18	40	14.6	21	12	89	10	74	12	53	32	54	215
B.S. I	175	66	33	8	15	31	13.7	15	11	44	5	86	9	49	34	74	220
72701	59	32	255	54	16	0	5.4	78	4	18	41	94	2	255	19	115	69
72702	27	21	246	73	16	3	4.8	76	3	13	47	102	2	253	18	102	68
72703	77	14	243	99	12	17	6	77	5	22	47	95	3	253	19	91	66
72704	45	34	242	84	18	0	5.3	79	5	18	44	96	3	254	18	88	66
72705	64	21	250	102	11	19	5.1	80	2	21	41	96	1	234	18	82	65
72706	99	17	241	92	13	4	5.7	79	4	22	42	92	4	250	17	86	65
72707	94	24	170	111	17	21	5.3	70	6	31	42	95	2	238	18	99	67
72708	56	25	157	111	14	7	5.6	68	4	23	41	100	1	234	18	90	65
72709	84	9	141	99	15	15	4.2	67	5	23	39	105	1	257	19	95	70
72710	105	33	50	178	19	28	6.5	58	3	31	41	102	1	296	22	102	81
72711	92	21	115	137	18	12	5.4	64	4	24	45	99	1	270	23	100	77
72712	85	17	87	138	15	13	5.6	52	9	30	42	92	3	301	23	102	82
72713	85	28	75	114	16	10	6.8	51	1	25	44	92	1	299	24	107	88
72714	118	24	52	119	18	20	6.5	51	5	26	41	123	2	272	22	92	79
72715	95	21	24	137	16	6	7.2	49	2	26	41	105	0	307	26	102	92
72716	120	22	29	169	21	16	6.8	33	2	30	42	109	5	309	24	108	93
72717	110	28	28	140	21	9	6.6	32	5	43	41	110	4	294	24	111	89
72718	95	30	35	82	17	18	7	29	6	30	44	112	6	299	23	111	89
72719	128	17	48	35	21	6	7.1	13	4	51	43	122	3	306	23	111	95
72720	92	41	38	85	17	5	6.7	30	5	21	47	109	3	311	26	110	96
72721	175	39	21	98	18	14	7.2	34	7	33	44	111	3	292	28	108	106
72722	86	16	23	105	20	12	7	37	4	19	41	115	3	308	24	104	89
72723	626	27	32	5	17	0	16	10	5	104	23	57	10	59	29	70	230
72724	733	90	19	10	20	39	16.9	5	7	103	30	87	11	54	45	117	234
72725	574	75	10	19	18	46	17.3	7	5	99	26	78	13	49	43	119	236
72726	606	81	15	11	22	32	16.9	6	9	104	31	110	14	59	47	117	240
72727	621	80	14	11	21	49	17.5	7	8	119	26	96	11	65	47	118	238
72728	617	80	12	12	21	31	15.6	7	10	117	26	105	13	55	49	110	244
72729	631	82	12	15	19	39	17.4	5	7	116	27	96	13	65	47	122	237

Table 5. Trace element geochemistry (ppm) for the Plains Sill at the Three Lakes Peak Trail section. All analyses performed by XRF at Washington State University's GeoAnalytical Laboratory.

Sample	Ba	Ce	Cr	Cu	Ga	La	Nb	Ni	Pb	Rb	Sc	Sr	Th	V	Y	Zn	Zr
72730	693	74	15	8	20	36	17.1	4	2	111	22	78	14	69	44	79	241
72731	722	80	11	19	22	26	16.8	4	7	114	22	91	12	52	46	108	241
72732	627	70	9	6	18	43	16.8	7	2	121	28	93	12	66	46	94	238
72733	785	81	14	10	19	44	16.7	6	5	110	23	71	10	50	46	71	249
72734	856	58	11	15	20	36	15.6	5	9	99	27	74	13	65	48	106	242
72735	840	72	14	11	20	36	16.5	6	4	105	25	86	11	53	46	88	238
72736	836	66	12	12	21	37	16.8	5	4	103	22	71	13	60	44	72	243
72737	840	88	9	12	23	36	17.1	7	6	103	24	80	12	48	46	67	245
72738	860	81	33	10	18	42	15.9	11	17	134	21	86	11	86	39	62	223
72739	810	80	20	38	19	34	15.1	11	22	114	16	73	12	60	43	67	240
72740	1010	77	43	6	20	33	15.7	19	8	153	16	57	11	74	37	62	224
72741	1011	78	38	12	22	31	16.7	18	8	147	18	61	15	75	36	58	222
72742	1111	69	41	11	22	38	16.5	17	7	149	13	59	14	75	36	57	223
72743	1139	62	43	6	21	40	16	17	9	148	18	56	14	70	37	61	220
72744	1182	81	45	18	19	41	16.3	15	7	146	18	63	12	74	37	55	221
72745	1123	78	42	6	23	35	16.7	18	9	145	13	60	11	75	40	59	219
72746	1153	68	43	9	22	47	15.9	20	7	145	14	57	13	78	37	63	218
72747	1129	71	43	10	19	26	16.1	16	9	149	8	61	11	83	35	62	215
72748	1123	79	47	11	20	32	15.6	21	7	143	4	69	12	94	35	63	209
72750	1121	71	45	9	25	40	16.2	22	6	151	4	54	13	103	34	54	209
72751	1083	73	49	13	20	19	17.2	25	3	164	7	39	15	82	35	40	211
72752	1025	67	44	8	23	41	15.9	22	4	160	11	40	14	72	35	43	212
72753	938	68	47	6	22	43	16.1	25	5	153	16	36	14	69	35	43	216
72754	850	86	52	9	22	38	16.7	25	7	150	14	39	17	79	34	37	217
72755	411	59	35	6	14	28	12.6	17	5	89	4	25	11	48	27	28	211
72756	434	73	38	9	14	35	13.9	21	5	94	5	23	10	47	28	26	204

Table 5 continued.

Sample	SiO2	TiO2	Al2O3	FeO*	MnO	MgO	CaO	Na2O	K2O	P2O5
71501	67.62	0.63	17.82	3.41	0.03	0.87	0.47	3.02	6.04	0.08
71502	74.48	0.53	14.18	2.82	0.03	0.84	0.36	2.44	4.26	0.06
71503	53.91	0.89	14.33	9.89	0.19	7.65	10.72	1.82	0.51	0.09
71504	53.12	0.82	14.58	10.76	0.20	7.41	10.64	1.82	0.57	0.08
71505	53.62	0.88	14.68	10.66	0.20	6.90	10.58	1.92	0.47	0.09
71506	53.72	0.89	14.42	10.82	0.18	6.79	10.57	1.79	0.72	0.09
71507	53.49	0.80	14.76	10.85	0.17	6.65	10.59	1.91	0.68	0.09
71508	53.28	0.95	14.72	11.51	0.19	6.21	10.49	1.92	0.64	0.09
71509	53.05	0.91	15.14	11.21	0.21	6.31	10.58	2.04	0.45	0.10
71901	53.18	0.95	14.60	11.26	0.18	6.61	10.63	1.89	0.59	0.10
71902	58.15	1.68	12.89	14.23	0.23	2.75	6.13	2.97	0.78	0.19
71903	64.51	1.34	12.75	11.43	0.17	1.22	3.72	3.12	1.46	0.28
71904	66.56	1.21	12.32	11.11	0.13	0.84	2.73	3.00	1.81	0.27
71905	68.97	0.97	12.14	9.67	0.13	0.60	1.84	3.53	1.87	0.28
71909	68.71	0.95	12.05	9.34	0.11	0.51	2.98	3.40	1.66	0.29
72003	69.95	0.90	12.14	8.96	0.10	0.46	2.23	3.20	1.82	0.23
72007	70.48	0.86	11.99	9.20	0.14	0.40	1.03	3.47	2.18	0.26
72011	71.05	0.89	12.19	8.38	0.11	0.41	1.20	3.48	2.07	0.22
72015	70.93	0.90	12.39	7.94	0.06	0.58	1.35	3.63	2.01	0.22
72016	70.64	0.87	11.96	8.79	0.10	0.47	1.60	3.42	1.91	0.25
72017	54.32	0.72	14.90	9.35	0.19	7.20	10.81	1.90	0.54	0.07
72018	53.54	0.97	14.19	11.20	0.21	6.85	10.91	1.80	0.25	0.09
72019	65.97	0.74	19.13	5.59	0.07	1.40	0.35	1.04	5.61	0.10
72020	68.17	0.69	18.06	4.76	0.06	1.22	0.41	1.41	5.13	0.07

Table 6. XRF major-oxide data for the Plains Sill at the Clear Creek section. All analyses performed by Washington State University's GeoAnalytical Laboratory.

Sample	Ba	Ce	Cr	Cu	Ga	La	Nb	Ni	Pb	Rb	Sc	Sr	Th	V	Y	Zn	Zr
71501	1405	49	50	8	25	26	16.6	25	13	176	13	108	17	65	30	22	208
71502	1230	32	36	10	16	31	15.4	20	2	119	7	76	16	46	30	22	285
71503	94	20	204	137	13	8	5.5	73	6	23	48	109	3	272	20	98	74
71504	162	23	160	75	16	18	5.3	70	5	25	43	108	2	268	20	108	76
71505	98	34	90	93	14	14	5.3	61	4	18	43	103	3	273	22	107	79
71506	145	28	49	**161**	15	8	5.7	64	1	34	47	110	4	292	21	81	81
71507	139	6	33	**161**	15	25	5.7	66	3	33	41	102	1	272	19	77	72
71508	146	17	27	**157**	15	21	6.3	55	6	28	43	115	2	307	22	93	82
71509	106	27	20	138	16	7	6.1	54	4	17	39	121	2	312	21	**144**	78
71901	115	24	54	149	16	13	5.6	58	2	27	47	108	4	333	22	103	77
71902	171	52	11	30	18	16	11.6	0	9	29	41	88	5	279	41	**292**	159
71903	383	75	5	8	20	25	15.5	4	37	53	29	125	9	58	57	**428**	218
71904	431	79	10	5	21	40	16.6	0	42	64	30	127	7	35	58	**295**	246
71905	517	81	3	6	17	33	17.8	0	50	72	24	123	10	4	61	**189**	258
71909	341	71	9	5	17	24	18.0	2	11	51	25	141	8	4	61	67	250
72003	410	63	6	7	18	34	17.9	4	18	58	22	163	11	1	64	**193**	280
72007	550	87	6	11	18	37	18.6	2	14	81	15	113	11	14	58	**130**	283
72011	595	70	6	17	21	38	18.3	1	11	76	17	132	9	15	55	**124**	269
72015	484	81	8	12	20	14	17.3	4	13	69	18	134	10	14	48	**126**	256
72016	556	76	6	34	22	40	17.7	4	15	73	16	131	11	14	59	**131**	274
72017	81	9	96	133	15	12	5.8	60	13	25	47	111	1	253	19	96	72
72018	38	32	115	0	17	6	5.5	55	6	4	47	93	2	295	24	**138**	79
72019	1213	34	61	20	24	9	17.7	21	32	199	15	36	17	80	27	100	200
72020	1311	64	54	12	27	38	16.9	22	36	187	11	71	17	76	26	**175**	212

Table 7. Trace element geochemistry (ppm) for the Plains Sill at the Clear Creek section. All analyses performed by XRF at Washington State University's GeoAnalytical Laboratory. Values in excess of 120% of WSU's highest standard are shown in bold.

Sample	SiO2	TiO2	Al2O3	Fe2O3*	MnO	MgO	CaO	Na2O	K2O	P2O5
F92-583	52.21	0.90	14.37	12.08	0.19	7.17	10.29	1.33	0.38	0.04
F92-584	50.62	0.73	17.03	9.86	0.15	5.98	11.74	1.46	0.25	0.05
F92-585	50.80	0.77	14.94	10.73	0.17	7.85	10.89	1.39	0.48	0.07
F92-586	51.31	0.77	15.21	10.69	0.17	8.11	11.06	1.59	0.26	0.01
F92-587	50.48	0.79	14.81	10.88	0.17	7.63	10.76	1.46	0.38	0.05
F92-588	51.55	0.75	15.09	10.62	0.16	7.66	10.96	1.43	0.39	0.04
F92-589	52.38	0.71	15.55	9.80	0.15	8.00	11.29	1.47	0.31	0.07
F92-590	45.80	0.89	14.73	12.25	0.20	8.30	11.18	1.51	0.19	0.05
F92-591	51.39	0.83	13.69	12.03	0.20	8.25	10.20	1.91	0.23	0.03
F92-592	51.42	0.76	14.08	10.48	0.16	7.96	10.40	1.35	0.62	0.03
F92-593	50.50	0.77	14.38	10.56	0.17	8.03	10.50	1.41	0.47	0.01
F92-594	51.30	0.76	14.69	10.13	0.16	7.81	10.47	1.44	0.44	0.02
F92-595	51.13	0.70	15.06	10.19	0.16	7.84	11.24.	1.41	0.40	0.03
F92-596	50.90	0.67	14.96	10.17	0.16	8.23	11.20	1.42	0.33	0.05
F92-597	50.65	0.66	15.48	9.59	0.14	7.67	10.79	1.52	0.59	-0.01
F92-598	50.72	0.73	15.96	10.14	0.16	7.83	10.49	1.48	0.59	0.02
F92-599	50.83	0.69	15.13	10.32	0.16	8.21	11.09	1.47	0.32	0.04
F92-2000	50.62	0.81	16.56	11.07	0.15	6.00	10.15	1.57	0.87	-0.01
F92-2001	51.78	1.16	15.18	12.24	0.22	5.61	9.54	2.24	0.31	0.08
F92-2002	51.04	0.70	14.89	10.40	0.16	7.76	10.89	1.40	0.54	0.04
F92-2003	51.06	0.69	15.22	9.89	0.16	8.25	11.25	1.44	0.28	0.03
F92-2004	51.02	0.66	15.27	9.86	0.16	8.24	11.44	1.53	0.14	0.04
F92-2005	51.41	0.86	15.32	11.16	0.17	6.41	9.63	1.77	0.62	0.04
F92-2006	49.82	0.88	17.80	11.43	0.16	4.83	10.44	2.54	0.31	0.04
F92-2007	51.15	0.61	14.91	10.28	0.16	7.15	10.68	1.88	0.35	0.03
F92-2008	50.93	0.79	15.24	11.50	0.17	6.58	9.76	1.72	0.70	0.03
F92-2009	51.76	1.00	14.19	12.38	0.21	6.85	10.08	1.54	0.71	0.03
F92-2010	50.14	0.83	16.80	10.56	0.18	5.33	9.68	1.82	0.62	0.03
F92-2011	49.91	0.81	16.71	10.38	0.15	5.98	9.76	1.60	0.87	-0.01
F92-2012	51.46	0.82	15.12	11.69	0.17	6.28	9.38	1.61	0.84	-0.01
F92-2013	50.70	0.80	16.87	11.12	0.18	5.97	10.41	1.87	0.24	0.03
F92-2014	50.36	0.78	16.89	11.48	0.17	5.94	10.35	1.52	0.33	-0.01

Table 8. ICP major-oxide data for the Plains Sill at the Seepay Ridge Section. All analyses by Bondar-Clegg. Data used with permission of the Confederated Salish-Kootenai Tribes.

Sample	SiO2	TiO2	Al2O3	Fe2O3*	MnO	MgO	CaO	Na2O	K2O	P2O5
F92-2015	50.93	0.83	16.85	10.37	0.15	5.61	9.63	2.20	0.55	0.06
F92-2016	50.79	0.78	16.10	10.52	0.15	5.97	9.70	1.88	0.61	0.02
F92-2017	54.05	0.74	14.32	10.76	0.16	6.03	9.59	1.59	0.51	0.05
F92-2018	52.22	0.97	14.32	12.67	0.18	5.95	9.87	1.71	0.50	0.02
F92-2019	51.21	0.80	15.32	11.74	0.16	6.76	9.63	1.66	0.88	0.04
F92-2020	51.81	0.86	14.10	12.86	0.19	6.81	9.60	1.62	0.67	0.04
F92-2021	52.16	0.99	14.01	12.46	0.17	6.04	9.70	1.99	0.34	0.03
F92-2022	50.60	0.88	14.05	12.03	0.19	7.15	10.28	1.52	0.70	0.04
F92-2023	50.48	0.96	13.72	12.34	0.18	6.71	10.00	1.60	0.55	0.02
F92-2024	51.45	0.82	15.60	11.46	0.15	5.73	9.35	1.75	0.82	0.03
F92-2025	52.02	1.10	13.89	13.30	0.19	5.52	9.33	2.12	0.28	0.04
F92-2026	51.41	1.18	14.45	13.57	0.21	5.55	8.99	2.51	0.24	0.05
F92-2027	52.74	1.14	13.74	12.36	0.20	5.73	8.91	2.61	0.29	0.02
F92-2028	52.31	0.97	15.12	12.46	0.18	6.01	9.96	1.88	0.35	0.03
F92-2029	51.46	0.80	14.13	10.87	0.17	7.63	10.44	1.53	0.49	0.05
F92-2030	51.98	0.85	13.78	11.40	0.18	7.93	10.36	1.41	0.35	0.02
F92-2031	51.57	1.08	13.61	13.78	0.23	5.66	9.15	2.25	0.31	0.04
F92-2032	50.56	1.11	13.51	14.54	0.20	5.70	9.61	1.73	0.49	0.03
F92-2033	53.87	1.39	13.06	12.66	0.17	4.74	8.82	2.38	0.37	0.08
F92-2034	51.34	0.85	15.18	12.03	0.17	5.85	9.57	1.76	0.64	0.05
F92-2035	51.68	0.94	15.33	12.38	0.17	5.42	9.32	1.84	0.68	0.02
F92-2036	52.36	0.80	15.22	11.53	0.17	5.78	9.25	2.25	0.16	0.06
F92-2037	49.95	2.15	12.29	20.61	0.27	4.19	8.18	1.38	0.42	0.03
F92-2038	53.89	2.16	12.15	16.28	0.28	3.02	8.18	1.69	0.25	0.06
F92-2039	50.09	0.73	15.53	13.72	0.20	6.70	8.96	1.32	0.29	0.02
F92-2040	52.81	1.93	14.70	16.15	0.24	3.12	7.24	2.15	0.33	0.02
F92-2041	49.71	2.32	12.87	19.70	0.30	4.24	8.19	1.50	0.31	0.03
F92-2042	50.60	0.76	16.18	10.97	0.17	7.13	9.81	1.57	0.57	0.05
F92-2043	51.50	1.98	14.44	16.92	0.26	3.24	7.52	1.89	0.31	0.04
F92-2044	48.83	2.22	14.24	18.91	0.30	3.91	7.73	1.42	0.26	-0.01
F92-2045	68.77	0.87	12.40	8.67	0.10	0.74	0.75	2.89	2.87	0.13
F92-2046	50.50	2.10	14.88	17.96	0.28	3.36	7.53	1.92	0.28	0.01
F92-2047	69.41	0.83	12.56	8.05	0.10	0.70	0.68	3.19	2.74	0.16

Table 8 continued.

Sample	SiO2	TiO2	Al2O3	Fe2O3*	MnO	MgO	CaO	Na2O	K2O	P2O5
F92-2048	71.38	0.68	12.39	6.53	0.09	0.67	0.86	3.36	1.99	0.14
F92-2049	68.57	0.85	12.47	7.75	0.11	0.84	0.90	3.73	2.27	0.13
F92-2050	69.09	0.81	12.05	7.52	0.10	0.84	0.80	3.82	1.95	0.16
F92-2051	68.40	0.85	12.60	8.06	0.09	0.74	1.00	3.47	2.01	0.15
F92-2052	68.96	0.86	12.60	8.09	0.11	0.79	0.85	3.37	2.49	0.15
F92-2053	68.77	0.90	12.70	8.65	0.10	0.81	0.97	3.37	2.58	0.15
F92-2054	69.16	0.92	12.67	8.45	0.11	0.92	1.02	3.92	2.30	0.13
F92-2055	71.88	0.89	13.03	6.91	0.10	0.81	0.61	4.76	1.86	0.17
F92-2056	69.41	0.81	12.24	7.48	0.11	0.78	0.78	3.68	2.12	0.12
F92-2057	69.38	0.89	12.63	7.46	0.14	0.80	0.97	3.67	2.19	0.21
F92-2058	71.66	0.88	12.68	6.61	0.09	0.78	0.85	4.56	1.59	0.15
F92-2060	63.90	0.90	12.78	11.82	0.10	1.43	0.83	2.69	3.23	0.14
F92-2061	74.60	0.78	12.07	3.71	0.10	0.41	0.84	4.75	0.86	0.15
F92-2062	73.29	0.78	12.55	6.34	0.10	0.74	0.74	4.38	1.53	0.14
F92-2063	69.47	0.77	12.58	7.59	0.08	0.81	1.11	2.99	2.43	0.16
F92-2064	72.06	0.66	12.12	6.57	0.07	0.51	0.74	3.68	1.95	0.14
F92-2065	64.35	1.64	13.22	10.69	0.14	1.62	3.76	3.23	1.09	0.15
F92-2066	64.42	1.64	12.94	11.52	0.17	1.28	0.99	3.07	2.73	0.12
F92-2067	53.15	1.34	13.86	13.91	0.20	4.97	7.55	2.82	0.25	0.05
F92-2068	55.27	1.41	13.54	14.48	0.21	4.60	7.88	2.51	0.04	0.06

Table 8 continued.

Sample	Ba	Cr	Cu	La	Ni	Sr	V	Y
F92-583	111	83	92	1	41	63	103	7
F92-584	66	53	79	1	24	70	70	5
F92-585	93	94	87	1	35	61	81	6
F92-586	75	2	71	1	31	82	73	6
F92-587	79	99	81	0	35	60	85	6
F92-588	73	95	58	0	31	64	75	6
F92-589	89	76	84	1	36	79	75	5
F92-590	40	97	15	0	26	63	97	7
F92-591	36	114	65	1	32	26	94	8
F92-592	44	109	98	1	37	41	74	7
F92-593	35	106	89	1	35	57	79	6
F92-594	46	100	87	1	36	57	75	6
F92-595	46	89	85	1	31	66	67	6
F92-596	65	82	61	1	30	71	67	5
F92-597	43	79	85	1	32	52	58	5
F92-598	60	67	77	0	42	43	66	6
F92-599	23	81	90	1	34	76	67	6
F92-2000	31	37	131	1	40	29	96	7
F92-2001	48	38	14	1	24	13	132	10
F92-2002	37	78	88	1	31	42	63	6
F92-2003	27	71	74	1	33	78	62	5
F92-2004	52	69	86	1	33	78	59	5
F92-2005	37	23	97	1	28	28	93	7
F92-2006	31	28	114	1	28	27	100	6
F92-2007	23	84	95	0	26	62	66	7
F92-2008	46	21	150	1	34	34	93	7
F92-2009	53	50	119	1	35	22	113	8
F92-2010	45	28	181	1	37	23	99	7
F92-2011	39	29	186	1	35	24	85	7
F92-2012	82	23	179	0	33	47	93	7
F92-2013	42	28	75	1	29	58	88	7
F92-2014	49	27	308	1	31	56	85	6
F92-2015	29	25	157	2	34	24	102	8
F92-2016	33	33	200	1	36	23	87	6
F92-2017	42	27	168	1	34	27	87	7
F92-2018	56	24	104	1	28	36	129	10
F92-2019	33	21	146	1	32	24	88	7
F92-2020	45	24	13	1	36	28	115	9
F92-2021	32	20	110	2	26	39	132	10
F92-2022	40	61	98	1	31	26	104	8
F92-2023	37	64	102	1	35	20	128	9
F92-2024	62	32	196	2	29	29	108	8
F92-2025	25	24	67	2	24	16	146	11
F92-2026	29	19	28	2	21	11	158	11
F92-2027	25	36	56	2	24	13	145	10
F92-2028	70	26	116	1	29	48	124	10
F92-2029	56	89	78	2	32	37	77	8
F92-2030	68	101	109	2	37	55	92	7
F92-2031	35	24	57	2	23	13	173	10
F92-2032	50	17	100	2	23	25	200	11
F92-2033	20	33	72	1	20	10	205	11
F92-2034	71	27	164	1	29	47	111	8

Table 9. ICP trace-element data (ppm) for the Plains Sill at the Seepay Ridge Section. All samples analyzed by Bondar-Clegg. Data used with permission of the Confederated Salish-Kootenai Tribes.

Sample	Ba	Cr	Cu	La	Nl	Sr	V	Y
F92-2035	33	26	166	2	25	24	16	9
F92-2036	39	23	51	2	22	33	113	9
F92-2037	52	27	38	2	9	11	785	14
F92-2038	98	41	11	4	7	36	510	17
F92-2039	33	31	118	1	31	24	102	7
F92-2040	35	49	9	6	9	7	311	16
F92-2041	60	27	18	4	6	14	748	15
F92-2042	48	22	57	1	31	35	88	6
F92-2043	51	32	23	4	9	10	388	14
F92-2044	56	37	10	4	14	7	483	14
F92-2045	460	60	27	23	5	7	25	29
F92-2046	33	42	2	4	10	7	261	13
F92-2047	408	48	12	27	4	8	19	42
F92-2048	393	68	14	21	4	8	11	32
F92-2049	423	68	12	25	5	9	19	39
F92-2050	372	63	30	15	4	8	21	28
F92-2051	505	57	8	24	4	10	20	35
F92-2052	411	65	8	24	4	10	20	32
F92-2053	459	76	4	27	5	9	21	33
F92-2054	429	63	11	23	4	9	21	34
F92-2055	307	51	16	15	4	5	22	27
F92-2056	419	69	4	19	4	7	19	25
F92-2057	458	68	24	19	4	10	20	27
F92-2058	275	78	26	13	4	6	19	27
F92-2060	714	70	0	23	4	10	34	36
F92-2061	144	88	8	12	4	7	10	22
F92-2062	303	53	5	17	3	5	13	29
F92-2063	435	55	4	15	4	9	17	29
F92-2064	368	43	20	24	2	10	4	43
F92-2065	201	45	13	16	3	9	88	24
F92-2066	626	52	1	15	3	9	58	29
F92-2067	101	29	194	4	29	10	180	14
F92-2068	34	39	94	4	18	21	167	13

Table 9 continued.

Sample	SIO2	TIO2	Al2O3	FeO*	MnO	MgO	CaO	Na2O	K2O	P2O5
F92-550	50.73	0.70	13.75	10.76	0.17	8.25	9.97	1.21	0.73	0.02
F92-551	51.81	0.59	14.41	9.19	0.15	7.67	9.67	1.12	0.70	0.05
F92-552	49.40	0.56	15.05	12.03	0.19	7.80	8.86	1.17	1.35	0.04
F92-553	51.90	0.60	14.90	9.75	0.15	7.39	10.48	1.37	0.83	0.02
F92-554	51.32	0.60	15.06	9.51	0.15	6.77	10.81	1.48	0.53	0.04
F92-555	51.57	0.63	15.35	9.50	0.15	6.95	11.02	1.30	0.86	0.02
F92-556	52.00	0.60	15.61	10.25	0.16	5.70	9.98	1.13	0.88	0.03
F92-557	51.88	0.60	15.94	9.61	0.14	6.01	10.69	1.17	0.68	0.02
F92-558	51.69	0.59	15.61	9.58	0.14	6.74	10.21	1.46	0.69	0.05
F92-559	51.56	0.59	16.12	9.60	0.14	5.96	10.08	1.26	1.09	0.01
F92-560	51.90	0.61	16.44	9.92	0.14	6.21	10.10	1.36	0.92	0.04
F92-561	51.69	0.64	15.95	9.95	0.15	5.83	10.03	1.10	1.11	0.04
F92-562	52.27	0.66	15.71	10.32	0.16	6.16	9.68	1.29	1.12	0.03
F92-563	52.46	0.71	15.57	10.59	0.16	6.06	9.95	1.39	0.95	0.05
F92-564	52.62	0.68	15.41	10.69	0.16	5.33	9.81	1.26	0.82	0.02
F92-565	52.30	0.72	15.52	10.63	0.16	5.35	9.69	1.39	0.90	0.03
F92-566	55.90	0.92	14.27	12.62	0.17	3.84	7.27	1.66	1.02	0.01
F92-567	55.68	0.88	14.50	12.41	0.17	3.93	7.41	1.71	1.43	0.04
F92-568	57.75	0.84	14.13	10.87	0.15	3.42	6.51	1.88	1.11	0.05
F92-569	57.05	0.88	14.30	11.66	0.15	3.57	6.30	1.95	1.67	0.04
F92-570	57.63	1.32	13.81	12.78	0.17	2.72	6.24	1.83	1.44	0.04
F92-571	59.21	1.49	13.45	13.68	0.17	2.16	4.60	1.94	1.82	0.05
F92-572	58.62	1.40	13.09	13.31	0.18	1.81	5.02	2.12	2.03	0.08
F92-573	64.65	1.13	12.92	11.37	0.14	1.15	2.82	2.45	2.19	0.12
F92-574	63.85	1.07	12.42	10.97	0.11	1.12	1.88	2.23	2.75	0.10
F92-575	64.83	1.09	12.47	11.03	0.11	1.00	1.76	2.28	2.87	0.14
F92-576	65.88	1.07	12.60	10.40	0.12	1.03	2.00	2.28	2.36	0.10
F92-577	52.70	0.72	14.21	11.36	0.16	6.06	9.79	1.28	0.75	0.04
F92-578	52.93	0.73	14.19	10.96	0.15	5.68	9.58	1.25	0.73	0.03
F92-579	51.81	0.61	14.60	10.45	0.16	6.64	10.35	1.63	0.95	0.02
F92-580	63.91	0.68	18.12	5.06	0.04	1.11	1.17	5.33	2.27	0.05
F92-581	63.98	0.68	18.38	5.59	0.04	1.19	0.50	2.49	4.47	0.04

Table 10. ICP major-oxide data for the Paradise Sill. All analyses by Bondar Clegg. Data used with permission of the Confederated Salish-Kootenai Tribes.

Sample	Ba	Cr	Cu	La	Ni	Sr	V	Y
F92-550	15	142	31	2	23	14	63	8
F92-551	12	133	44	2	20	13	50	7
F92-552	29	161	2	1	25	13	67	6
F92-553	16	109	50	2	20	22	53	8
F92-554	14	104	30	2	18	17	54	8
F92-555	16	70	69	3	20	15	54	8
F92-556	40	41	81	3	20	14	70	9
F92-557	17	73	43	2	16	15	57	8
F92-558	13	56	42	2	17	14	61	8
F92-559	19	41	64	4	17	17	60	9
F92-560	22	42	51	3	17	14	61	10
F92-561	25	35	34	3	18	19	71	10
F92-562	29	31	50	3	14	32	71	9
F92-563	27	30	31	3	12	19	81	9
F92-564	47	44	29	3	10	23	92	11
F92-565	43	37	33	3	10	24	93	11
F92-566	130	50	13	5	5	17	136	15
F92-567	128	57	10	4	6	19	131	16
F92-568	137	76	13	6	7	18	134	17
F92-569	199	69	7	5	8	16	148	16
F92-570	157	54	35	7	6	13	239	15
F92-571	292	52	21	7	5	11	182	18
F92-572	278	53	3	6	5	14	102	17
F92-573	362	86	4	9	5	14	60	23
F92-574	414	60	0	9	5	17	60	20
F92-575	391	94	24	13	6	19	43	27
F92-576	295	60	18	10	6	21	59	22
F92-577	27	63	19	3	14	16	78	11
F92-578	24	57	19	3	12	18	102	9
F92-579	28	50	12	3	11	20	80	8
F92-580	101	76	13	21	18	13	42	15
F92-581	124	66	0	29	22	6	25	15

Table 11. ICP trace-element data (ppm) for the Paradise Sill. All samples analyzed by Bondar-Clegg. Data used with permission of the Confederated Salish-Kootenai Tribes.

Sample	60227	60228	60229	60230
SiO2	54.92	56.37	54.44	52.94
TiO2	0.735	0.825	0.632	0.533
Al2O3	14.31	14.55	15.35	15.83
FeO*	9.65	9.55	9.74	8.13
MnO	0.198	0.196	0.183	0.167
MgO	6.74	6.02	6.56	7.47
CaO	11.13	10.16	10.19	12.34
Na2O	1.23	1.45	1.48	1.14
K2O	0.37	0.57	0.84	0.5
P2O5	0.069	0.09	0.056	0.054
Ba	40	105	109	54
Ce	38	32	26	22
Cr	146	67	34	252
Cu	5	14	30	52
Ga	17	20	17	16
La	19	13	37	26
Nb	6.2	5.5	6	5
Ni	18	12	7	32
Pb	8	6	9	13
Rb	7	20	32	24
Sc	52	45	48	49
Sr	101	92	99	110
Th	3	2	4	3
V	260	287	256	224
Y	22	24	20	16
Zn	107	101	82	82
Zr	75	83	70	55

Table 12. XRF major-oxide and trace-element data from four samples taken toward the bottom of the Paradise Sill. All analyses performed at Washington State University's GeoAnalytical Laboratory.

References

Anderson, G. M. and Burnham, C. W., 1965, The solubility of quartz in supercritical water: American Journal of Science, v. 263, p. 494-511.

Augustithus, S. S., 1982a, On the metamorphic-metasomatic origin of the granophyres of the layered ultrabasic complexes of Ezhimala, Payyanur, Cannanore District, Kerala, India and of Langberg, Bushveld, Transvaal, South Africa, in Drescher-Kaden, F. K. and Augustithus, S. S. eds., Transformists' Petrology: Athens, Theophrastus Publications S. A., p. 231-291.

Augustithus, S. S., 1982b, Some aspects of chromite remobilization, in Drescher-Kaden, F. K. and Augustithus, S. S. eds., Transformists' Petrology: Athens, Theophrastus Publications S. A., p. 231-291.

Bischoff, J. L. and Dickson, F. W., 1975, Seawater-basalt interaction at 200°C and 500 bars: Implications for origin of sea-floor heavy-metal deposits and regulation of seawater chemistry: Earth and Planetary Science Letters, v. 25, p. 385-397.

Bishop, D. T., 1974, Petrology and geochemistry of the Purcell Sills, in Boundary County, Idaho: in Belt Symposium volume 2: Idaho Bureau of Mines and Geology, Special Publication, p. 15-66.

Blackadar, R. G., 1956, Differentiation and assimilation in the Logan Sills, Lake Superior District, Ontario: American Journal of Science, v. 254, p. 623-645.

Boberg, W. W., 1985, Geological and geophysical review of results of the Arco 1 Paul Gibbs Well, Flathead County, Montana: Geological Society News Bulletin, v. 30, p. 3.

Bruiyn, H. D., 1975, Phenocryst analysis: A technique for determining the origin of granophyre in the Bushveld Complex: Transactions of the Geological Society of South Africa, v. 78, p. 185-190.

Buckley, S. N. and Sears, J. W., 1992, Evidence for emplacement of mafic sills into wet sediments in the Prichard Formation, Middle Proterozoic Belt Supergroup, Perma area, Western Montana: Geological Society of America, Abstracts with Programs, v. 24, p. 4-5.

Buckley, S. N. and Sears, J. W., 1993, Shallow emplacement of sills into wet Belt Supergroup sediments at Perma, Western Montana: Belt Symposium III, Abstracts with Programs, Whitefish Montana.

Burnham, C. W., 1975, Water and magmas: a mixing model: Geochimica et Cosmochimica Acta, v. 39, p. 1077-1084.

Burnam, C. W. and Jahns, R. H., 1962, A method for determining the solubility of water in silicate melts: American Journal of Science, v. 260, p. 721-745.

Burwash, R. A., 1993, Overview of Belt geochronology and problems of dating the Belt-Purcell Supergroup, Belt Symposium III, Abstracts with Programs, Whitefish Montana.

Coleman, R. G. and Donato, M. M., 1979, Oceanic plagiogranite revisited, *in* F. Barker ed., *Trondhjemites, Dacites and Related Rocks*: New York, Elsevier Scientific Publishing Company, p. 149-168.

Cressman, E. R., 1985, The Prichard Formation of the lower part of the Belt Supergroup (Middle Proterozoic), near Plains, Sanders County, Montana: United States Geological Survey Bulletin 1553, p. 64.

Cressman, E. R., 1989, Reconnaissance stratigraphy of the Prichard Formation (Middle Proterozoic) and the early development of the Belt Basin, Washington, Idaho and Montana: United States Geological Survey Professional Paper 1490, p. 80.

Currie, K. L., 1968, On the solubility of albite in supercritical water in the range 400 to 600 degrees C and 750 to 3500 bars: American Journal of Science, v. 266, p. 321-341.

Einsele, G., 1985, Basaltic sill-sediment complexes in young spreading centers: Genesis and significance: Geology, v. 13, p. 249-252.

Ernst, W. G., 1960, Diabase-granophyre relations in the Endion Sill, Duluth, Minnesota: Journal of Petrology, v. 1, p. 286-303.

Fahlquist, L. and Popp, R. K., 1987, The effect of sodium chloride on nickel solubility in supercritical hydrothermal fluids: Geological Society of America, Abstracts with Programs, v. 19, p. 151.

Faure, G., 1986, Principles of isotope geology. John Wiley and Sons, New York, 589 p.

Garcia, M. O., 1978, Criteria for the identification of ancient volcanic arcs: Earth-Science Reviews, v. 14, p. 147-165.

Ghent, E. D., Stout, M. Z. and Parrish, R. R., 1988, Determination of metamorphic pressure-temperature-time (P-T-t) paths, *in* Nisbet, E. G. and Fowler, C. M. R. eds., *Heat, metamorphism and tectonics*, Mineralogical Association of Canada Short Course 14, p. 155-188.

Hamilton, D. L., Burnham, C. W. and Osborn, E. F., 1964, The solubility of water and effects on oxygen fugacity and water content on crystallization in mafic magmas: Journal of Petrology, v. 5, part 1, p. 21-39.

Harrison, J. E., Cressman, E. R. and Kleinkopf, M. D., 1985, Regional structure, the Atlantic Richfield-Marathon Oil No. 1 Gibbs Borehole, and hydrocarbon resource potential west of the Rocky Mountain Trench in northwestern Montana: United States Geological Survey Open-File Report, 8 p.

129

Hawkes, L., 1929, On a partially fused quartz-feldspar rock and on glomero-granular texture: The Mineralogical Magazine and Journal of the Mineralogical Society, v. 22, p. 163-173.

Helz, R. T., 1973, Phase relations of basalts in their melting range at $P(H_2O)=5Kb$ as a function of oxygen fugacity: Journal of Petrology, v. 14, p. 249-302.

Helz, R. T., 1982, Phase relations and compositions of amphiboles produced in studies of the melting behavior of rocks, in Veblen, D. R. and Ribbe, P. H. eds., Amphiboles: Petrology and experimental phase relations: Mineralogical Society of America Reviews in Mineralogy, v. 9B, p. 279-353.

Hotz, P. E., 1953, Petrology of granophyre in diabase near Dillsburg, Pennsylvania: Bulletin of the Geoloical Society of America, v. 64, p. 675-704.

Höy, T., 1989, The age, chemistry, and tectonic setting of the Middle Proterozoic Moyie Sills, Purcell Supergroup, Southeastern British Columbia: Canadian Journal of Earth Sciences, v. 26, p. 2305-2317.

Humphris, S. E. and Thompson, G., 1978a, Hydrothermal alteration of oceanic basalts by seawater: Geochimica and Cosmochimica Acta, v. 42, p.

Humphris, S. E. and Thompson, G., 1978b, Trace element mobility during hydrothermal alteration of oceanic basalts: Geochimica and Cosmochimica Acta, v. 42, p. 127-146.

Hunt, J. M., 1979, Petroleum Geochemistry and Geology. W. H. Freeman and Company, San Francisco, 617 p.

Hyndman, D. W., 1985, Petrology of Igneous and Metamorphic Rocks. McGraw-Hill, Inc., New York, 786 p.

Irvine, T. N. and Baragar, W. R. A., 1971, A guide to chemical classification of the common volcanic rocks: Canadian Journal of Earth Sciences, v. 8, p. 523-547.

Jaeger, J. C., 1968, Cooling and solidification of igneous rocks, in Hess, H. H. and Poldervaart, A. eds., Basalts: The Poldervaart treatise on rocks of basaltic composition v. 2, Interscience Publishers, New York, p. 503-536.

Jahns, R. H. and Burnham, C. W., 1969, Experimental studies of pegmatite genesis: I. A model for the derivation and crystallization of granitic pegmatites: Economic Geology, v. 64, p. 843-864.

Jensen, L.S., 1976, A new cation plot for classifying subalkalic volcanic rocks: Ontario Division of Mines, Miscellaneous Paper 66.

Kalsbeek, F. and Jepsen, H. F., 1983, The Midsommerso Dolerites and associated intrusions in the Proterozoic Platform of Eastern North Greenland - a study of the interaction bewteen intrusive basic magma and sialic crust: Journal of Petrology, v. 24, p. 605-634.

Kokelaar, B. P., 1982, Fluidization of wet sediments during the emplacement and coolng of various igneous bodies: Journal of the Geological Society, London, v. 139, p. 21-33.

Krynaux, J. R., Hunter, D. R. and Wilson, A. H., 1988, Emplacement of sills into wet sediments at Grunehogna, western Dronning Maud Land, Antarctica: Journal of the Geological Society, London, v. 145, p. 1019-1032.

Liou, J. G., Kuniyoshi, S. and Ito, K., 1974, Experimental studies of the phase relations between greenschist and amphibolite in a basaltic system: American Journal of Earth Sciences, v. 274, p. 613-632.

Lytwyn, J. N. and Casey, J. F., 1995, The geochemistry of postkinematic mafic dike swarms and subophiolitic metabasites, Pozanti-Karsanti ophiolite, Turkey: Evidence for ridge subduction: Geological Society of America Bulletin, v. 107, p. 830-850.

McBirney, A. R. and Nakamura, Y., 1974, Immiscibility in the late-stage magmas of the Skaergaard intrusion: Carnegie Institute of Washington Year Book 73, for 1973-1974, p. 348-352.

McBirney, A. R., 1975, Differentiation of the Skaergaard intrusion, Nature, v. 253, p. 691-694.

Meglen, J. F., 1975, Geology of the Perma area, Sanders County, Montana: Unpublished Master's Thesis, University of Oklahoma, 80 p.

Miyashiro, A., 1968, Metamorphism of mafic rocks, in Hess, H. H. and Poldervaart, A. eds., Basalts: The Poldervaart treatise on rocks of basaltic composition v. 2, Interscience Publishers, New York, p. 799-834.

Morton, J. L., Holmes, M. L. and Koski, R. A., 1987, Volcanism and massive sulfide formation at a sedimented spreading center, Escanaba Trough, Gorda Ridge, Northeast Pacific Ocean: Geophysical Research Letters, v. 14, p. 769-772.

Mudge, M. R., 1968, Depth control of some concordant intrusions: Geological Society of America Bulletin, v. 79, p. 315-332.

Obradovich, J. D. and Peterman, Z. E., 1968, Geochronology of the Belt Series, Montana: Canadian Journal of Earth Sciences, v. 5, p. 737-747.

Pearce, J. A. and Cann, J. R., 1973, Tectonic setting of basic volcanic rocks determined using trace element analyses: Earth and Planetary Science Letters, v. 19, p. 290-300.

Pearce, T. H., Gorman, B. E. and Birkett, T. C., 1975, The $TiO_2-K_2O-P_2O_5$ diagram: a method of discriminating between oceanic and non-oceanic basalts: Earth and Planetary Science Letters, v. 24, p. 419-426.

Philpotts, A. R., 1976, Silicate liquid immiscibility: its probable extent and petrogenetic significance: American Journal of Science, v. 276, p. 1147-1177.

Philpotts, A. R., 1979, Silicate liquid immiscibility in tholeiitic basalts: Journal of
Petrology, v. 20, p. 99-118.

Philpotts, A. R., 1982, Compositions of immiscible liquids in volcanic rocks:
Contributions to Mineralogy and Petrology, v. 80, p. 201-218.

Philpotts, A. R., 1990, Principles of igneous and metamorphic petrology: Prentice
Hall, Englewood Cliffs, New Jersey, 498 p.

Poldervaart, A., 1956, Zircon in Rocks. 2. Igneous Rocks: American Journal of
Science, v. 254, p. 521-554.

Roedder, E., 1979, Silicate liquid immiscibility in magmas, in Yoder, H. S. ed., *The
evolution of igneous rocks, fiftieth anniversary perspectives*, Princeton
University Press, Princeton, N.J., 588 p.

Sasaki, A. and Smith, D., 1979, Sulfur isotopic evidence of diabase-granophyre-
sedimentary rocks interaction, Sierra Ancha, Central Arizona: Geochemical
Journal, v. 13, p. 227-229.

Sears, J. W. and Price, R. A., 1978, The Siberian connection: a case for Precambrian
separation of the North America and Siberian Cratons: Geology, v. 6,
p. 267-270.

Sears, J. W., 1992, Relationship of the Perma Sills to the Prichard Formation,
Southwest Flathead Reservation: Report to Tribal geologist, Confederated
Salish-Kootenai Tribes, Pablo, MT, 30 p.

Sears, J. W. and Buckley, S. N., 1992, Dynamic model for emplacement of mafic sills
and collapse of the Middle Proterozoic Belt Basin at the Prichard E-F boundary:
Geological Society of America, Abstracts with Programs, v. 24, p. 61.

Sears, J. W. and others, 1994, Mid-Continent Rift analog for the Middle Proterozoic
Belt Basin, Geological Society of America, Abstracts with Programs, v. 26,
p. 62.

Smith, D. and Silver, L. T., 1975, Potassic granophyre associated with Precambrian
diabase, Sierra Ancha, Central Arizona: Geological Society of America Bulletin,
v. 86, p. 503-513.

Spear, F. S., 1981, An experimental study of hornblende stability and compositional
variability in amphibolite: American Journal of Science, v. 281, p. 697-734.

Turner, R. J. W., Hoy, T., Leitch, C. H. B. and Anderson, D., 1992, Guide to the
tectonic, stratigraphic and magmatic setting of the Middle Proterozoic stratiform
sediment-hosted Sullivan Zn-Pb deposit, southeastern British Columbia: British
Columbia Geological Survey Contribution No. 11, Sullivan-Aldridge Project
Information Circular 1992-23, 53 p.

Walker, F., 1958, The pegamtitic differentiates of basic sheets: American Journal of
Science, v. 251, p. 41-60.

Walraven, F., 1985, Genetic aspects of the granophyric rocks of the Bushveld Complex: Economic Geology, v. 80, p. 1166-1180.

Walther, J. V. and Woodland, A. B., 1993, Experimental determination and interpretation of the solubility of the assemblage microcline, muscovite, and quartz in supercritical H_2O: Geochimica et Cosmochimica Acta, v. 57, p. 2431-2437.

Wasserburg, G. J., 1958, The solubility of quartz in supercritical water as a function of pressure: Geology, v. 66, p. 559-578.

Winchester, J. A. and Floyd, P. A., 1977, Geochemical discrimination of different magma series and their differentiation products using immobile elements: Chemical Geology, v. 29, p. 325-343.

Winston, D., Woods, M., and Byer, G.B., 1984, The case for an intracratonic Belt-Purcell basin: tectonic, stratigraphic and stable isotope considerations: Montana Geological Society 1984 field conference, p. 103-118.

Wones, D. R. and Gilbert, M. C., 1982, Amphiboles in the igneous environment, *in* Veblen, D. R. and Ribbe, P. H. eds., *Amphiboles: Petrology and experimental phase relations*: Mineralogical Society of America Reviews in Mineralogy, v. 9B, p. 355-383.

Wooden, J. L., Vitaliano, C. J., Koehler, S. W. and Ragland, P. C., 1978, The late Precambrian mafic dikes of the southern Tobacco Root Mountains, Montana: geochemistry, Rb-Sr geochronology and relationship to Belt tectonics: Canadian Journal of Earth Sciences, v. 15, p. 467-479.

Woodland, A. B. and Walther, J. V., 1987, Experimental determination of the solubility of the assemblage paragonite, albite, and quartx in supercritical H_2O: Geochimica et Cosmochimica Acta, v. 51, p. 365-372.

Zartmann, R. E., Peterman, Z. E., Obradovich, J. D., Gallego, M. D. and Bishop, D. T., 1982, Age of the Crossport C Sill near Eastport Idaho: Idaho Bureau of Mines and Geology Bulletin, v. 24, p. 61-69.